UNIVERSITY OF OKLAHOMA

GRADUATE COLLEGE

CARBON NANOTUBE ENHANCED LITHIUM ION COMPOSITE CATHODES

A DISSERTATION

SUBMITTED TO THE GRADUATE FACULTY

in partial fulfillment of the requirements for the

Degree of

DOCTOR OF PHILOSOPHY

By

WESLEY DANIEL TENNYSON
Norman, Oklahoma
2014

CARBON NANOTUBE ENHANCED LITHIUM ION COMPOSITE CATHODES

A DISSERTATION APPROVED FOR THE
COLLEGE OF ENGINEERING

BY

Dr. Daniel E. Resasco, Chair

Dr. Daniel T. Glatzhofer

Dr. Jeffery H. Harwell Sr.

Dr. Rolf E. Jentoft

Dr. Mrinal C. Saha

Dedication

In memory of my father, whose humility and service were inspirational.

ACKNOWLEDGMENTS

First and foremost, I have to thank the post doctorial students that worked with me and began my training in this field of study, Dr. Rachel Nash and Dr. Chris Burba. Without them we would have had no basis for beginning this work. I have had the pleasure to work with many bright and insightful minds as colleagues and understudies. In no particular order, Jonathan Compos, Jimmy Brown, Nhung Duong, Marina Nascimento, Jacklyn Roberts, Fauzia Ahmed, Hugo Alvaregna Oliveira, Joshua Henderson, and Rose Medill all contributed with their generous work and questions.

Some say if you cannot enjoy the journey do not take the trip. I can thank my dear friends Chris Lewis, Needa Virani, Kelsey Potter, Alana Denning, Danielle Baker, Christina Owen, Kristen Knight, Sam Bush, Jessica Funk, and Austin Miller for keeping me sane and making this "trip" well worth the time and effort.

I should thank Nick Briggs for being one of the best lab coordinators I have yet known. His communication and style of handling problems minimized interpersonal issues and moved our lab forward on so many occasions. Keep up the fight, Nick, against the tide of unlabeled samples! I should thank Alan Miles and his many students for the numerous conversations and assistance on all the bizarre problems that come up when doing research.

Both SWeNT and The Oklahoma Center for the Advancement of Science & Technology through the ONAP program made this work possible by providing the financial support to ask the question. From SWeNT I should thank Ricardo, Tan, and Wanda for all their efforts in finding and making interesting CNTs for us to study.

All of the faculty of the engineering college I have interacted with have been excellent and knowledgeable beyond their years. I need to thank Dr. Schmidtke for access to the EIS, Dr. Grady for his unique perspective on composites and access to the hot press and ball milling, and Dr. Glatzhoffer for having the insight to suggest "I go back to go forward".

Thank you, Dr. Resasco, for giving me a chance to re-enter graduate school to unlearn some bad habits and to grow anew as a leader and a scientist.

And finally a thank you to Toyota for asking someone,

who asked someone, who asked someone,

who asked me,

to solve a problem.

TABLE OF CONTENTS

LIST OF TABLES

LIST OF FIGURES

ABSTRACT

Batteries are sought that can deliver high energy density and high power density over thousands of cycles, with minimum environmental impact and cost. Invariably no one material can achieve all of these requirements. Lithium Iron Phosphate (LFP) satisfies most of these requirements reasonably well with the exception of power density. Two coincident methods have been utilized to increase the power capability and cycle life of battery cathodes by reducing the electrode resistance to the reaction site and increasing the diffusion coefficient for ions and electrons. Electrode resistance is typically reduced by a combination of surface coatings and carbon additives in the composites. Recent work has demonstrated that spray deposition with PVdF as binder increases the cathode capacity resilience over extended cycling.[1] Likewise, incorporation of carbon nanotubes (CNT) has demonstrated decreased cathode fade over many life cycles as well.[2-3] Since capacity fade has been experimentally connected to loss of electrode contact, it stands to reason that a battery made with a process that optimizes the binder contact and utilizes a resilient and highly conductive carbon additive would have extended capacity life, with the potential added benefit of higher energy density from a small inactive material content in the cathode.[4] In this work, we investigate the properties of the CNT, the processing of CNTs in cathode films made using slurry and spray deposition techniques with $LiFePO_4$ as the cathode material, and the synthesis of the materials with CNTs. We demonstrate that with an optimized processing method composites with minimal inactive material (10%) can perform with rate capabilities comparable to 20% carbon black (25% inactive material) without capacity fade.

Preface

I have tried to include as many salient topics as possible in this work without it becoming unmanageable. I hope that the perspective that I bring will be both unique and useful to students and scientists working on batteries. There are many related topics that influence this subject that I have not covered principal among these are electrolytes and anodes. I encourage the reader to explore these areas as well since the rate of change in the field of energy storage has increased in recent years. There are many advances and new techniques published every month. This is a vibrant and exciting time to study batteries.

As with any good book on a subject, we must have organization. For those that are looking for introductory material on batteries chapter one should prove most interesting. On the other hand, for those that just want an executive summary look to chapter six. Chapter two develops the foundation of conductivity in composites in order to understand the composite formulation in chapter three. The CNTs measurements and properties as they pertain to battery composites are investigated in chapter four. An alternative method for incorporating CNTs into the battery material growth is discussed in chapter five.

Chapter 1. Introduction to Batteries

1.1 Energy Storage

Some say civilization began in order to purse making beer and all the merriment that comes with it. Others might argue this was really an attempt to make something clean to drink. Nevertheless, the mastering of fermentation made possible new realities in society. Thus, it is with energy storage; the ability to make and store energy for later use has revolutionized our way of life. This is especially important as we look to the future due to the ecological impacts of our energy use. The ability to store energy for later use allows us to select the source, whether it is renewable, inexpensive, slow in production, or based on a contract. Regardless of our motivation, energy storage mediums that can hold massive amounts of energy and deliver them quickly make possible new and exciting technologies.

Batteries have enabled portable devices since their inception. Some notable technologies include metal detectors,[a] smart phones, and fully electric vehicles. At the cell level, batteries are just a pair of electrodes called an anode and cathode with a separator (electronic insulator) soaked with electrolyte between them. The electrolyte saturates the electrodes and the separator, which allows ion conduction. Energy is stored by combing a pair of redox reactions at the cathode and anode. The standard cell is made by wrapping these layers up and packing them into a can, Figure 1.1. The names cathode and anode refer to the respective reactions that occur at the electrodes when a battery is under discharge. In electrochemistry, the cathode is the electrode where the reduction occurs ($M^{3+} \rightarrow M^{2+}$), and the anode refers to the electrode where

[a] Alexander Graham Bell invented the metal detector to search for a bullet in President James Garfield.

oxidation occurs ($M^{2+} \rightarrow M^{3+}$). When charging rechargeable batteries the oxidation and reduction locations actually flip. Thus, as a convention to reduce confusion, during discharging the anode refers to the negative terminal and cathode the positive terminal.

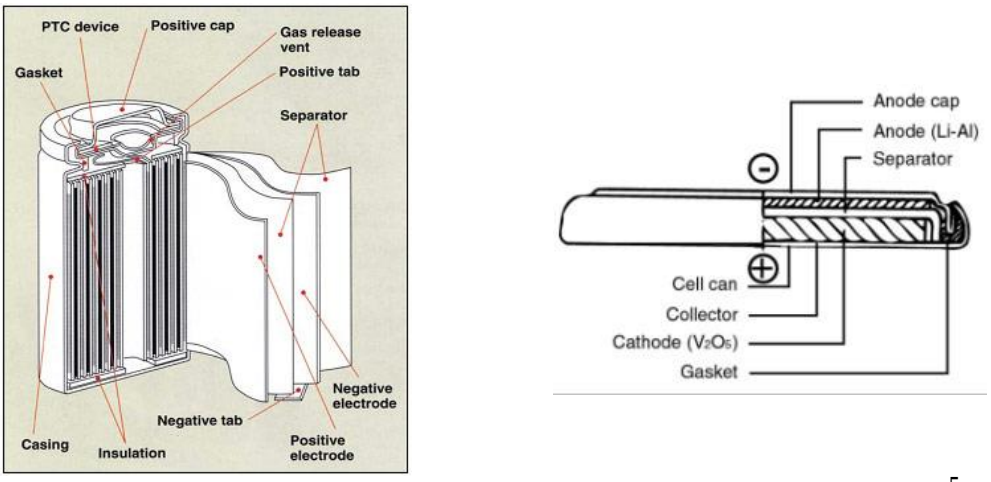

Figure 1.1. A cross-section view of a cylinder and a coin cell battery.[5]

There are basically two classes of materials that can be used as battery materials: those that undergo a crystal structure change and those that incorporate ions by intercalation. Lead acid is the classic example of a battery material that acts by undergoing a phase change, where on the cathode metallic Lead is oxidized by the sulfuric acid to form Lead sulfate and on the anode Lead oxide is reduced to form Lead sulfate and water. These materials typically can produce very high current densities but suffer from corrosion at their electrodes that limits their life. Intercalation compounds, such a Lithium Iron Phosphate, on the other hand have the same crystal structure between charged and discharged states but with different unit cell volumes. Due to their stable nature, they typically are very durable batteries and will be useful for many thousands of cycles. The problem with these materials is they

tend to have poor power performance since getting the Lithium in and out completely tends to be very difficult unless one uses very small current densities.

The problem now is to find solutions that can solve the electrochemical, phase, transport, and kinetic problems at every length scale, Figure 1.2; the redox reaction occurs between an Fe and a Li (at the atomic scale), the Lithium intercalation through a material causes a phase change (at the 100 nm scale), the current path is along the interfaces between the particles (at the 100 μm scale), and finally the package must manage the heat generated (at the device scale).

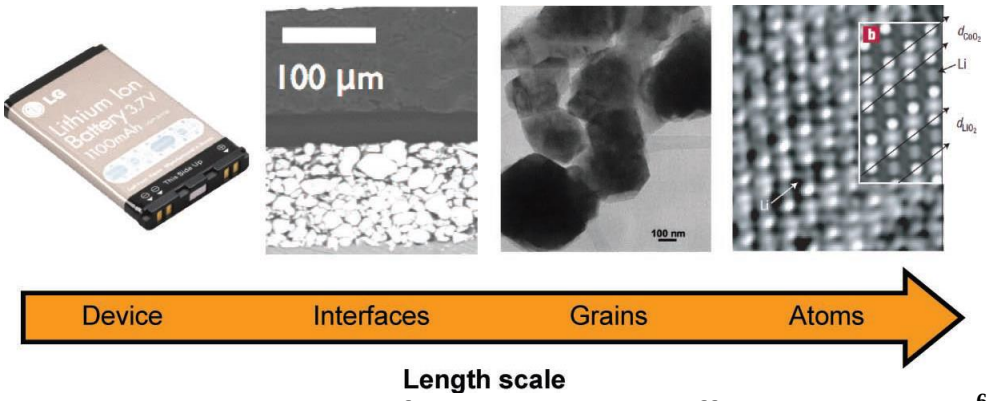

Figure 1.2. The components of a prismatic cell at different length scales.[6]

1.1.1 Lithium Iron Phosphate

When under charging conditions the Lithium Iron Phosphate (LFP) cathode is oxidized (Fe^{2+} ⇨ Fe^{3+} in $LiFePO_4$) and the anode is reduced. The electrolyte shuttles the Li^+ ions across the separator film (which is not electrically conductive). After charging, when the external circuit is completed (discharged) the lithium stored in the anode is transported across the separator and reduces the cathode and an electron leaves the anode and completes the circuit through the load. Each half reaction (Equations 1.1 and 1.2.) occurs at each electrode to produce or consume a pair, one electron and one Li^+ ion.

$$LiFePO_4 \leftrightarrow Li_{1-x}FePO_4 + x\,Li^+ + x\,e^- \qquad \text{Equation 1.1.}$$

$$x\,Li^+ + x\,e^- + 6\,C \leftrightarrow Li_xC_6 \qquad \text{Equation 1.2.}$$

The V_{OC} is determined by the difference of the chemical potentials at the anode and cathode reaction sites, Equation 1.3. Under a current load we can further define cell polarization (η) as a deviation from V_{OC}, Equation 1.4. The metal group need not be only iron, but it is plentiful and cheap. The chemical potentials vary depending on the metal, starting oxidation state, and the final state given in Table 1.1.

$$eV_{OC} = \mu_A - \mu_C \leq E_g \qquad \text{Equation 1.3.}$$

$$\eta = V_{OC} - V \qquad \text{Equation 1.4.}$$

Table 1.1 Chemical Redox Reactions of Selected Metals.[7] [b]

Cathode Reactions	Potential (V)
$V^{2+} + e \leftrightarrow V^+$	-1.18
$V^{3+} + e \leftrightarrow V^{2+}$	-0.26
$Cr^{2+} + e \leftrightarrow Cr^+$	-0.09
$Cr^{3+} + e \leftrightarrow Cr^{2+}$	-0.42
$Mn^{2+} + e \leftrightarrow Mn^+$	-1.18
$Mn^{3+} + e \leftrightarrow Mn^{2+}$	1.49
$Fe^{2+} + e \leftrightarrow Fe^+$	-0.44
$Fe^{3+} + e \leftrightarrow Fe^{2+}$	0.77
$Co^{2+} + e \leftrightarrow Co^+$	-0.28
$Co^{3+} + e \leftrightarrow Co^{2+}$	1.82
$Ni^{2+} + e \leftrightarrow Ni^+$	-0.26
$Cu^{2+} + e \leftrightarrow Cu^+$	0.34
Anode Reactions	
$Li^+ + e \leftrightarrow Li$ (s)	-3.0401
$Li^+ + e \leftrightarrow LiC$	-2.9

LFP is particularly stable due to its olivine crystal structure, Figure 1.3. The tetrahedral bonds of the phosphate groups stabilize the structure. This advantage allows LFP to cycle for many thousands of cycles without severe capacity loss. Not all cathodes in use exhibit this capability. Lithium cobalt cells ($LiCoO_2$) undergo a

[b] Potentials are versus the standard carbon electrode

more severe phase change when charging and discharging, thus there is the possibility of Lithium Oxide formation if the rate is too high. This is problematic because this will cause cell expansion and can lead to the failure of the cell.

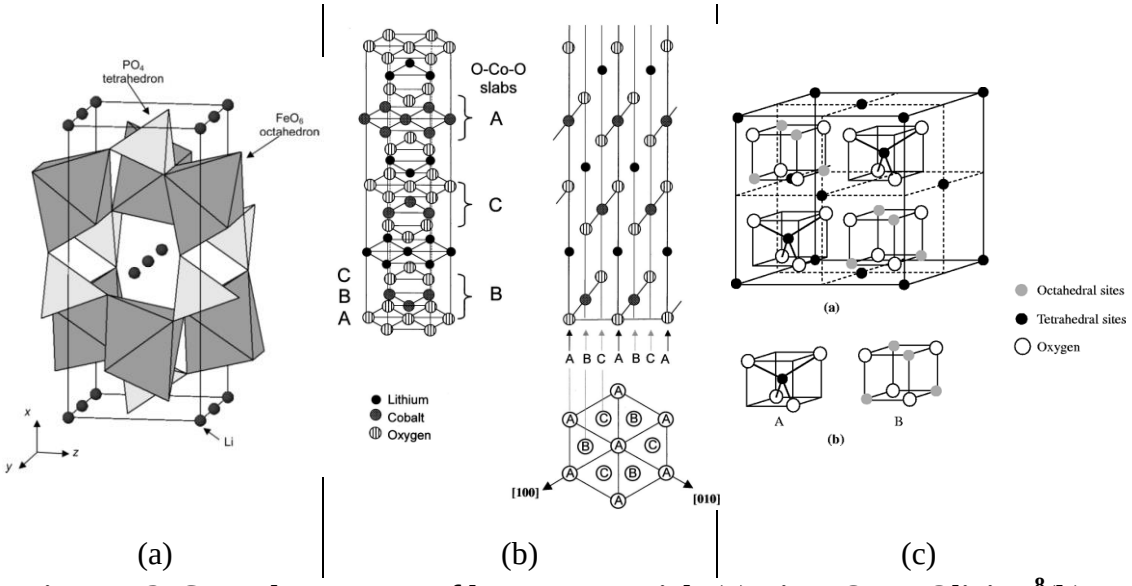

(a) (b) (c)

Figure 1.3. Crystal structures of battery materials (a) $LiFePO_4$ an Olivine,[8](b) $LiCoO_2$ a Layered Oxide,[9] and (c) $LiMn_2O_4$ a Spinel.[10]

1.2 Energy Density

Energy density is the amount of usable energy that can be stored in a material per unit mass. Table 1.2 list the properties of some of the more common and up and coming battery materials. The theoretical energy densities of any material can be calculated if the redox reaction potential is known. It is simply a matter of stoichiometry to calculate the capacity. For example, $LiFePO_4$ (or LFP) has a theoretical charge capacity of 170 mAh/g merely based on the molecular weight of the material, Eq. 1.6.

$$\text{Energy Density} = \frac{\text{E}\times\text{I}\times t}{mass} = \frac{\text{E}\times\text{Q}}{mass} \qquad \text{Equation 1.5}$$

$$\frac{1\ mol\ \text{LiFePO}_4}{157.75\ \text{g}}\ \frac{1\ mol\ e^-}{1\ mol\ \text{LiFePO}_4}\ \frac{96487\ \text{C}}{1\ mol\ e^-}\ \frac{1\ \text{Amp s}}{1\ \text{C}}\ \frac{1\ \text{h}}{3600\ \text{s}} = 170\ \text{mAh/g} \qquad \text{Equation 1.6}$$

This is actually a useful method to understand what kind of energy densities can be expected from the best possible batteries. Materials with high redox potentials and low molecular mass should give the highest energy density; Li-O_2 and Li-S are good examples of this. It should also be pointed out that capacity fade is a major concern. Many battery crystal structures break down with full utilization of the anion (Li+), e.g. in $LiCoO_2$ only about half the Lithium can be extracted before a phase change occurs that destroys the reversibility. In other words, if the battery is discharged too completely, the battery is destroyed. Other materials, which do not rely on the anion for the crystal structure, such as $LiFePO_4$ a so-called intercalation cathode, can deliver nearly all of their capacity without a structural phase change. Thus depending on the cathode type the capacity may be dependent on the power density, which is the topic of the next section.

Table 1.2. Energy Density of Battery Materials.

Cathodes[11]	Redox Potential (V vs Li^+/Li)	Realized Capacity (mAh/g)	Theoretical energy density (W·h/kg)	Current life (cycles)
$LiCoO_2$ $½C_6Li + Li_{0.5}CoO_2 + e^- \leftrightarrow 3C+LiCoO_2$	3.8 – 3.9	137	387	500
$LiFePO_4$ $C_6Li + FePO_4 + e^- \leftrightarrow C_6 + LiFePO_4$	3.4	170	578	>5000
NASICON $Li_3M_2(PO_4)_3$ M = Fe (Fe^{2+}/Fe^{3+})	2.7-3.0	190	475	100
Li-O_2 (aqueous) $2Li + ½O_2 + H_2O + 2e^- \leftrightarrow 2LiOH$	3.2		3,582	~10
Li-S $2Li + S + 2e^- \leftrightarrow Li_2S$	2.2		2,567	~100
Anodes				
Natural Graphite	0.5	340		
Silicon	0.5 – 1	4200		
LTO	1.55	170		

Finally, it should be mentioned that there is an upper limit on magnitude of the redox potentials, see Table 1.2. We do not currently have electrolytes that are stable above 5V vs Li^+. In fact, the current electrolytes are not particularly stable with the currently available high voltage cathodes. Normally part of the electrolytes will decompose on a fresh anode and cathode surfaces and form a solid electrolyte interfaces (SEI). If the reaction potential is too extreme this interphase may not be stable and the electrolyte may continue to react with the surface during cycling use resulting in capacity fade and cell degradation. Some have suggested that this interface is better named an interphase since this is where the de-solvation, solvation occurs. With this limitation on increasing the redox potential on individual cells decreasing the mass of the battery seems the best way to improve battery energy density.

It is common practice to report the energy density only in terms of the active material content. This can be problematic when there are large fractions of other materials. In order to be consistent, the general convention g for grams of active material will be used. When referring to the whole cathode mass g* will the indicated. For example, in a work by Goodenough *et al*[12] LFP with different conductive polymers seems to indicate the LFP/16% Ppy-ED is best, Figure 1.4. After correcting for the inactive content, the capacities are much more similar, except at very high C-rates.

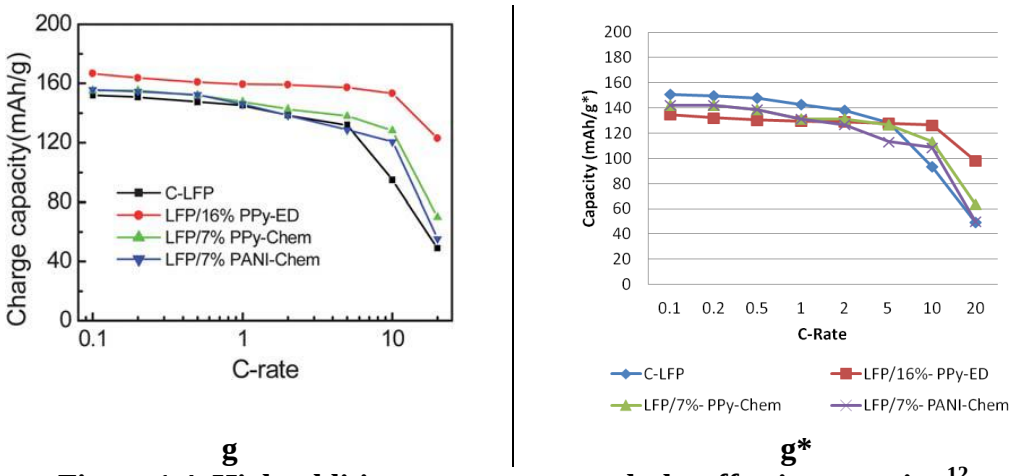

g **g***

Figure 1.4. High additive content can mask the effective capacity.[12]

1.3 Power Density

Power density or specific power is the amount of energy per unit time a battery can deliver. We have three extrinsic parameters that we can adjust to increase power density: E the cell voltage, I the current delivered, or g the mass of the material, Eq. 1.7. While power density appears directly proportional to energy density, that is not the case. Unit analysis does not reveal the transport limitation within the materials. Thus a critically important question is, "What is the rate limiting step?" Since there are two current carriers it can be hard to distinguish which pathway limits the reaction more. Let us consider a simple model to outline the problem and potential remedies.

$$\text{Power Density} = \frac{\text{E}\times\text{I}}{mass} = \frac{\text{E}\times\text{Q}}{mass \times time} \qquad \text{Equation 1.7}$$

A simple model to begin to understand the component cell potential would include the internal resistance (R_i), activation energy polarization (η_{ct}), and the concentration polarizations (η_c) at both electrodes (anode and cathode, respectively, a and c in eq. 1.8). Although this is a very simple model the three major aspects of power production with batteries are included: the cost of moving electrons

(resistance), the cost of moving the ions (concentration polarization), and the energy stored as a new phase in the material (activation energy).

$$E = E_o - [(\eta_{\mathrm{ct}})_a + (\eta_{\mathrm{ct}})_c] - [(\eta_c)_a + (\eta_c)_c] - iR_i = i\mathrm{R} \qquad \text{Equation 1.8}$$

Using Kirchhoff's circuit laws, we can determine the maximum power the cell can transfer to a load. The maximum power transfer occurs when the impedances of the battery and load match, hence the name impedance matching. This is not the maximum power it could potentially produce since above that current the internal resistance dominates. It is clear, then that decreasing internal resistance is one of the most direct routes to increasing power density.

Essentially, increasing the power density comes down to reducing the kinetic barriers to ion or electron transport. Both of these take very different routes in the battery system, but at the end points, they arrive at the same location. So now the question is, "What can be done about the kinetic barriers?" For electron transport it is a straightforward answer; reduce the resistance. For ion transport, the answer is likely one of the following: reduce the path length the ions have to diffuse, increase the diffusivity of the solid, or increase the effective rate of solvation at the interface. Some have suggested that lithium diffusion is primarily rate limited by the surface states, that is the rate of the solvation process is determined by the states available at the interface where the organic electrolyte is decoupled from the Li^+ ion..[13]

One needs to remember that there are many different interfaces within the cells with electrolytes that tend to be quite reactive in air thus studying these interfaces is not always straightforward. For example, Lithium carbonate was thought

to be a main component of the SEI layer, but now it appears that it is present only after exposure to air.[14]

Using the resistance and the capacity from Table 1.2 we can now estimate the potential energy density at any given C-rate, eq. 1.9. This holds so long as the resistance is constant during the discharge of the cell. Unfortunately, R_B is not constant with respect to the state of charge or with respect to the C-rate.

$$Energy\ Density = \left(1 - \frac{R_B}{V_{OC}}(\text{C-rate})\text{Capacity}\right) U_{Max} \qquad \text{Equation 1.9}$$

At low current densities, the battery materials undergo a phase change from charged to uncharged (or vise-versa) without severe internal polarization. Additionally, parts of the battery cell that are less well connected to the electrode (say they have a more resistive path) are allowed to equilibrate with the rest of the cell and thus contribute to the produced power. At higher current rates, side effects can be driven by fast changing chemical potentials, concentration gradients in the electrolyte, kinetic limitations of the ion transport, or simple ohmic heating due to the high electron flux. These side effects could include side reactions: decomposition of the electrolyte, non-uniform diffusion or polarization of the battery material, or physical cracking of the battery particles due to differences in the unit cell volume across the particle. Nearly all of these problems can contribute to reduction in usable capacity. Furthermore, particle degradation or any damage to the electrode connections contributes to capacity fade. This is irreversible. Clearly it is advantageous to avoid these problems, thus it is no wonder that nearly all battery types perform best under low current density conditions.

1.4 Life Expectancy

A good battery will not only produce the voltage and currents needed but will also last a long time. Obtaining good durability is still a major concern, since so many things can go wrong with high chemical potentials, intense heat, and long required shelf-life. The contact with the particles, the resilience of the film, and the transport of the electrolyte all must be maintained for batteries to last a long time.

In order for the particles in the composite to contribute, they must be connected electrically to the electrode. Since the volume of the charged and discharged states can vary by as much as 7%[c] there is significant stress both within and between particles formed and released between the discharged and charged stages. Particle cracking under this stress has been identified as one mechanism through which battery capacity fades. As the particles crack, parts of them lose contact to the electrode and become inactive in the battery composite.

The severe volume change between charged and discharged states can also cause cracks in the film and separate large areas of the electrode from other areas. This can lead to internal polarization or worse, delamination, where whole sections of the composite become disconnected from the electrode. A binder polymer, e.g. PVdF, is typically used to stabilize the electrodes at a loading of between 5% and 10%.

Although the decomposition of the electrolyte on the interfaces of the battery electrodes has long been a controversial subject it is well established now that a protective layer is required to protect the electrodes from reacting with the electrolyte. This is typically done using a natively formed layer from the electrolyte (e.g. $LiPF_6$/ethylene carbonate) or a carbon coating. Cracking in this layer will result in

[c] Based on unit cell volume change, see Table 2.2.

irreversible capacity loss upon charging the cell. In addition to reducing the battery efficiency, the loss of the electrolyte increases the electrolyte polarization.

If the electrolyte has a sufficiently large enough over potential, lithiation on the surfaces of the materials can begin to occur. Large formations called dendrites can form and breach the electrically insulating barriers between the anode and cathode. Shorting of a battery in this way can result in a very serious runaway effect.[15]

These are some of the principal ways that batteries can fail. Poor diffusion can also contribute to battery capacity fade and will be discussed in the next chapter.

1.5 The Way Forward

Increasing the cathode conductivity of high energy density battery materials has been a major focus for many groups for some time. Carbon coatings, conductive polymers, isovalent substitution, particle size reduction, and conductive additives have all been investigated to increase the energy available at higher specific currents.[16] Among the conductive additives, materials able to the deliver the highest current densities with the smallest impact on the composite weight will be the most advantageous, CNTs appear to fit this criteria well. CNTs, have been incorporated into battery systems by multiple groups,[17-19] and reviewed by Liu *et al*,[20] in fact CNT pastes as conductive additives are already commercially available.

While most of these works found that nanotubes decreased the reactance (cathode resistance), improved the energy density (a smaller fraction of additive is required for the same conductivity), stabilized discharge capacity, and increased the energy available at higher current densities, these advantages were realized within formulations and with methods that did not fully utilize the CNT. The reasons for

these advantages have been attributed to the formation of distributed networks of CNTs formed within the electrode composite.[21] The local current density at each battery particle can be reduced by directly connecting all the particles in the cathode to the distributed network.

Of particular importance is the method for dispersing and separating the individual CNTs. Stirring alone is not energetic enough to overcome the Van der Waals attraction between bundles of nanotubes.[22,23] Bundles of CNTs are particularly troublesome for two reasons; they reduce the total surface area coverage per gram of additive, and bundles of tubes are much less conductive than single tubes.[24] Ball milling is the most common mixing technique for battery materials, as it can reduce aggregate particle size and thoroughly mix materials. Unfortunately, ball milling mixes by physical impact, which will dramatically reduce the CNT length.[25,26] Since the percolation threshold is inversely proportional to length of the CNTs mixing methods that preserve high aspect ratios, such as shear mixing or ultrasonication, are more likely to produce highly conductive composites.[27]

In summary, batteries are an enabling technology, enabling mobile technologies and electric vehicles. Improvements in battery technologies make possible new realities and new technologies. Higher energy dense and high power density capable devices are needed to power the next generation of electric vehicles. The specific energy is determined by the redox reaction couples between the anode and cathode and the mass of the unit cell. Decreasing the inactive material present is the most direct method to improving the energy density of battery materials today. Carbon nanotubes can be incorporated into composites at lower concentrations than

carbon black to obtain a highly conducting material. This work addresses the methods and problems associated with mixing CNTs into composites. CNTs can be incorporated mechanically using mixing tools or at an early stage during the growth of the $LiFePO_4$. Both of these routes are investigated in this work.

Chapter 2. Conductivity in a Composite

2.1 Transport in Batteries

Let us consider the transport steps that the electrons and Li-ions must undergo to charge a Li-Ion battery. Potentially any of these steps could be the rate limiting step by either a diffusion limitation or a kinetic rate limitation.[28]

Adsorption Model of Lithium exchange

(1) When charging a battery, work is done to apply a potential on the cathode vs. the anode. The electron density on the cathode electrode drops, shifting the Fermi level down.

(2) Once there is a large enough potential difference the iron is oxidized from Fe^{3+} to Fe^{2+} and an electron Lithium ion pair is released.

(3) The electron is then driven by the field potential through the composite to the electrode (Al backing) and then on to the anode.

(4) The Lithium diffuses to the surface, driven by the potential and phase gradient while flow is mitigated by defect sites and neighboring Li attraction.

(5) Once at the surface (or in SEI layer if present) the Li can partially solvate.

(6) (Optional) Lithium then transports along the surface to a preferable site.

(7) It can then fully solvate and diffuse into the bulk to contribute to the electrolyte.

(8) Once in the electrolyte the applied field then drags the Li to the anode.

(9) Li^+ then de-solvates in the SEI layer at the anode surface.

(10) (Optional) After partial desolvation it can surface transport to a preferable insertion site.

(11) The Li^+ then diffuses into anode to balance the charge attraction and mechanical stress in the anode.

There is still some argument about where the electron and Lithium interact. The adsorption or ad atom model as presented above places the exchange at the metal site. The exchange could also occur in the solid electrolyte interface (SEI) layer.

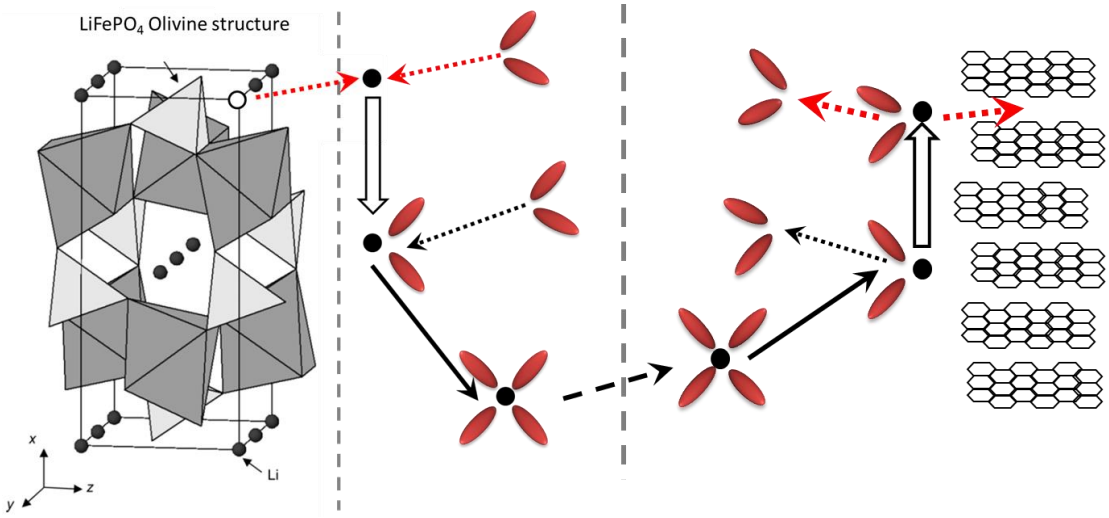

Figure 2.1 Schematic representation of the Li^+ adsorption mechanisms.

SEI Model of Lithium exchange

(1) Lithium transport in an electrolyte

(2) Lithium-ion migration through the SEI film

(3) Charge-transfer through the electrode/electrolyte interface

(4) Lithium-ion diffusion in an electrode

(5) Accumulation-consumption of the Li in the electrode, a phase transition

(6) Electron transport in an electrode and at an electrode/current collector interface

This solution has two issues, although it matches the data well in EIS experiments. It glosses over the desolvation required to get a Lithium ion from the electrolyte. Secondly, a Lithium-electron pair under an applied field would separate, or if bound tightly (3 eV) the electrostatic field would be significantly shielded and the pair would not have as large of a driving force to intercalate. This is another issue with theories that merely match the data but do not yield any physical understanding. A theory is only as good as its predictions. Circuit element models developed later in this chapter suffer from this problem since their physical meaning is obscured.

Table 2.1 Li-ion conductivity and diffusivity of battery materials.[29]

Material	ρ (S/cm)	D_{Li} (cm^2/s)
$LiCoO_2$	10^{-4}	10^{-7} to 10^{-14}
$LiMn_2O_4$	10^{-6}	10^{-8} to 10^{-11}
$LiFePO_4$	10^{-9}	10^{-9} to 10^{-15}

The wide range of diffusion rates reported is most likely due to the anisotropy of the Li-diffusion in these materials. Lithium transports most readily down channels in the {010} direction. Thus, crystal volume and orientation can have an inordinate effect on the diffusion rate. Control of the crystal growth to express these plains predominately on the surfaces has produced some very high rate capable cathodes.[30] Now we have one more issue: many batteries with high energy content are insulators, LFP is a prime example. An alternative view of these materials with ultra-low electron conductivity compared to their ionic conductivity is that they are semiconductors where the dominant charge carriers are the ion (Li^+). This inversion of the typical charge carrier (ion instead of electron or hole) would in fact be the case if the activation energy were higher for electrons than Li-ions. Due to the anisotropy of the Lithium diffusion, it appears that this may only be the case in one crystal orientation (010).

2.2 Electron Conductivity

Battery composites consist of two phases (at least). To understand the transport of electrons through these materials one must consider both the meso-scale and nano-scale that the electron current will encounter.

2.2.1 Meso-Scale

With a continuous conductive additive, electrons obey Ohm's law, Eq. 2.1. Now we have to determine the conductivity of a composite with a highly conductive phase and a highly insulating phase. Levi and Aurbach[31] developed a model of this particle intercalation in porous systems, and found that the admittances can be added together as an averaged sum, given in Eq. 2.2 where Z is admittance and θ is the fraction of additive material. Since the real part of the admittance, the conductivity, of the cathode materials is typically five or more orders of magnitude smaller than the additive, conductivity of the composite will be dominated by the additive, so long as enough is present ($\theta > \delta$). Where δ is the percolation threshold, which will be discussed in the section 2.6. The cathode material particle size distribution should also be considered. While a narrow distribution is easy to model, a wide distribution requires more careful analysis, see Levi and Aurbach.[31]

$$E = I\,R \qquad \text{Equation 2.1}$$

$$\frac{1}{Z_{mix}} = \frac{\theta}{Z_{add}} + \frac{1-\theta}{Z_{cath}} \qquad \text{Equation 2.2}$$

In the electrode the Lithium-ion, electron, and iron site must all meet in order for the reduction (or oxidation) to occur thus allowing for the storage (and use) of energy to occur. The path of the electron may include parallel and routes in series. The effective resistance of these interconnections is additive. The shorter these connections are, the lower the potential drop due to Ohmic losses and the lower the heat generation will be in the composite.

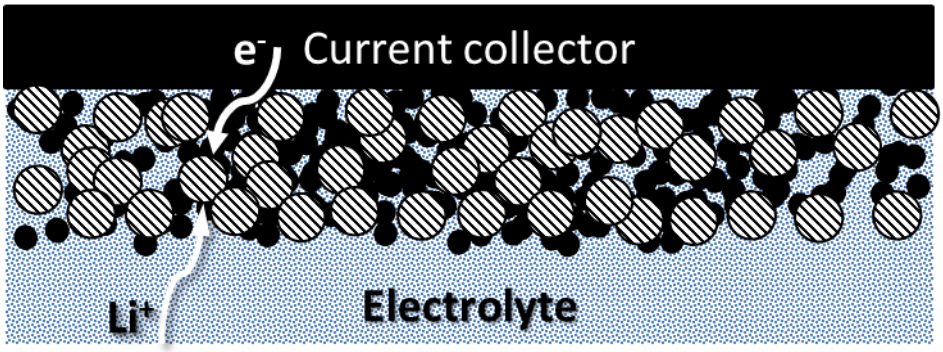

Figure 2.2. Schematic view of a porous electrode with electrochemically active particles (white-stripped) and conductive additive (black).

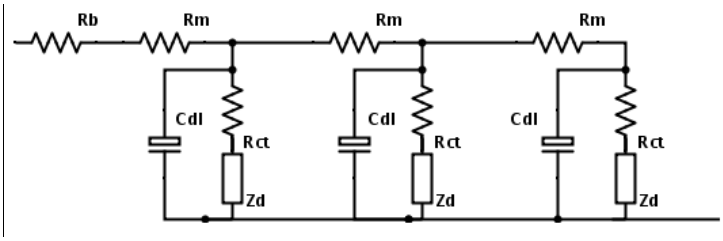

Figure 2.3. Circuit diagram of a transmission line model of a battery composite.

The porous electrode can be modeled as a transition line network, where the circuit model is given in Figure 2.3. Each particle is modeled as a single battery element with capacitance, internal resistance, and impedance. The capacity of the battery is determined by the number of connected elements. The potential drop to electrode for each element is the sum of all Rm to the electrode. The impedance of this model is given in eq. 2.3. Although the attribution of the resistive elements in this model is straightforward, the competing ideas outlined above indicated widely different meanings for the capacitive and impedance fits found from these models.[32]

$$Z(s) = \sqrt{R_m/(s\,C_{dl} + \frac{1}{R_{ct}+Z_d(s)})}\,coth\left[\sqrt{R_m/(s\,C_{dl} + \frac{1}{R_{ct}+Z_d(s)})}\right] \qquad \text{Equation 2.3}$$

A distributed network where each element may be connected in any combination of series or parallel better represents the composite.[33] If any of these connections were to fail then the capacity of the battery would fade.

2.2.2 Nano Scale

Now suppose there were a small gap of width d in the conductive network. Electrons can tunnel across the gap so long as d is small. The conductivity is exponentially related to the strength of the near field, which is determined by the work function of the material. Effectively, there is a characteristic length that conduction will occur, Equation 2.4. This is determined by the work function of the material (Φ) and the mass of the tunneling electron (m). This demonstrates the localization of the current flows from the conductive network. The most effective network should completely cover the battery material, and be continuous and durable.

$$\sigma \propto \exp\left(-\frac{\sqrt{2m\Phi}}{\hbar}d\right) \qquad \text{Equation 2.4}$$

Local probe measurements of electrode contacts on working batteries have shown that surfaces evolve with the electrode potential. Surface roughness and dendrites form and erode during discharging and charging cycles. Stress from volume changes due to Lithiation can crack the particles and also the conductive films on their surfaces.[34] These problems can be mitigated by either increasing the number of routes to the electrochemically active site, or by increasing the durability. Thus in order to test new materials, a large fraction of conductive material is generally used to mitigate the electrode contact decay. Good reviews of these effects with respect to batteries can be found in the works by Sastry[29] and Goodenough.[35]

2.3 Ionic Conductivity: Diffusion

Diffusion describes the movement of atoms, in this case Lithium ions. When there is no force on the ions, Fick's first law applies, as given in equation 2.5; *D* is the diffusion coefficient (cm^2 per second), *N* is the volume concentration (atoms per

cm^2), and y is the distance (cm). The flux density (the ionic current) is directly proportional to the concentration gradient.

$$J = -D\frac{\partial N}{\partial y} \qquad \text{Equation 2.5}$$

Now in batteries, during charging conditions and discharging, there is an applied field, either external or internal. The force on a charged particle is given in Equation 2.6, where Zq is the charge, E is the local electric field, v is the drift velocity, α is the factor of proportionality, and m^* is the effective mass. Additionally drift velocity and mobility in the steady state are typically defined by Equation 2.7, where μ is the mobility (cm^2 per volt-second).

$$F = Z\,q\,E = m^*\frac{dv}{dt} + \alpha\,v \qquad \text{Equation 2.6}$$

$$v_d = \frac{Z\,q\,E}{\alpha} = \mu\,E \qquad \text{Equation 2.7}$$

At the cathode (anode) interface of the battery the electrolyte concentration is depleted during discharging (charging) and creates a region with reduced electrolyte concentration. If the electrolyte mobility is limited, possibly due to very low temperatures, this can contribute to cell polarization. Sever polarization can enhance the rate of dendrite growth and dendrites can internally short a battery in a catastrophic manner. Generally speaking, the ionic diffusivity of the liquid electrolytes far exceeds that of the cathode materials. Thus only in extreme conditions is this a concern.

Generally, in a crystal lattice the diffusion rate for electrons is much higher than ions. This can create a space charge separation between the positively charged ions and the electrons. If the electron flux, equation 2.8, is merely due to the applied

field, which is a steady state condition, where *n* is the electron concentration, then one can derive an effective diffusion rate.[36]

$$J_n = 0 = -D_n \frac{\partial n}{\partial x} - \mu_n \, n \, E \qquad \text{Equation 2.8}$$

$$J = -D \frac{\partial N}{\partial x} - \mu \, N \left(-\frac{kT}{q} \frac{1}{n} \frac{\partial n}{\partial x}\right) = -D \left(1 + \frac{N}{n} \frac{\partial n}{\partial N}\right) \frac{\partial N}{\partial x} \qquad \text{Equation 2.9}$$

$$D_{eff} = D \left(1 + \frac{N}{n} \frac{\partial n}{\partial N}\right) \qquad \text{Equation 2.10}$$

Diffusion in the cathode as derived above assumes no energy barrier to the movement of ions and that is, there is no contribution from the lattice to the localization of the ions. If there is an interaction, then diffusion can then progress either by interstitial or substitutional diffusion, as in Figure 2.4. This assumes, of course that there is insufficient energy for the ions to exchange with the metal sites, Fe. Generally, this is the case. One should recognize that these mechanisms can represent two extremes for the cathode; when a battery is depleted of Lithium (charged) the interstitial diffusion dominates and when a material is lithiated (discharged) the substitutional mechanics dominates. This is an important distinction since different kinetics can be revealed at different depths of discharge. In Equations 2.11 and 2.12 E_m is the activation energy for moving an ion in a dilute medium and E_d is the activation energy for moving a vacancy.

Figure 2.4. Diffusion by interstitial (left) or substitutional (right) mechanism.

$$D = D_o\, e^{-E_m/kT} \qquad \text{Equation 2.11}$$

$$D = D_o\, e^{-(E_m+E_d)/kT} \qquad \text{Equation 2.12}$$

2.4 The Influence of Strain on Conduction

The unit cell volume increases as the $FePO_4$ is lithiated to $LiFePO_4$. Table 2.2 gives the fundamental cell parameters. This stress has a measureable impact on the cell polarization and is one of the sources of irreversible capacity loss as the stressed regions have hysteresis and, if not relaxed, can cause defects that block regions from charging and discharging. These stress effects can be mitigated by using small charging currents. In fact, exceptionally small charge and discharge currents need to be used to avoid stress issues, C/20 or even C/100.

Table 2.2. Lattice Constants for $LiFePO_4$ and $FePO_4$. [37,38]

	a (Å)	b (Å)	c (Å)	volume (Å)^3
$FePO_4$	9.8	5.7	4.78	271.7
$LiFePO_4$	10.3	6.0	4.68	289

A consequence of stress is the possibility of particle crack formation and even cleaving. One can use the Griffith Theory to estimate the critical particle diameter (d_c), given fracture energy (Γ), the mismatch strain, and the elastic modulus (ε), Equation 2.13.[39,40] The critical diameter is the dimension below which particles will not crack under for a given fracture energy. The fracture energy increases with the current density. Thus, cathodes designed for high power applications should have uniformly smaller particle dimensions in order to avoid cracking and cleaving. A lower limit on particle size is determined by the thickness of the SEI layer. The smallest particles will completely become part of the solid electrolyte interface. For $LiFePO_4$ d_c is 600 nm.

$$d_c = \Gamma / (Z_{max}\, Y\, \varepsilon_m^2)$$ Equation 2.13

This strain is not all bad it actually assists in the battery during de-lithiation during charging as the energy released actually promotes whole channels to empty all together. The strain will then cascade across the battery perpendicular to the exit direction {010}.[41]

2.5 Characterization of Conductivity

In order to understand battery dynamics both the electron and ionic conductivities need to be measured. Further, the mixing methods need to be evaluated in terms of their effectiveness in the composites.

2.5.1 Four Point Powder Probe

Powder conductivity cannot be measured with a basic Ohmmeter. The density and geometry of the powder must be taken into account. A powder probe, Figure 2.5, was developed to measure to compress the powders while measuring their conductivity. It consists of a stainless steel tube of ¾-inch diameter with a Teflon tube insert that is tight within the outer wall. The conductivity is calculated by Eq. 2.14.

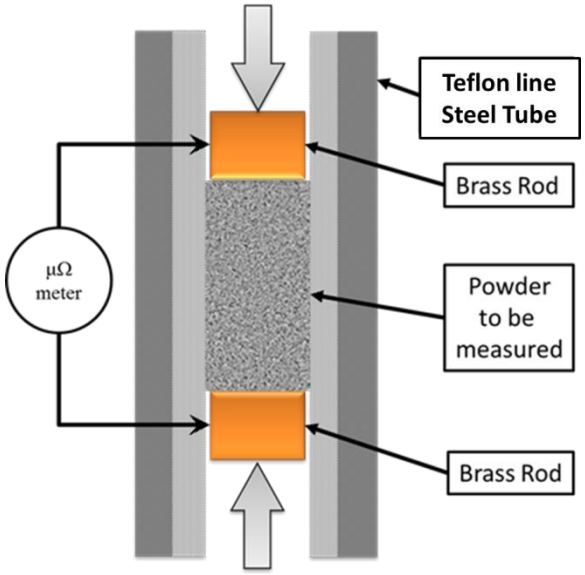

Figure 2.5. Cross Section of Powder Probe.

$$\sigma = length/(Area \times Resistance) \qquad \text{Equation 2.14}$$

The four point probe schematic is given in Figure 2.6. The voltage leads contact points are made with a separate set of wire from the current source. In this way the random contact resistances of the voltage meter is in series with the high resistance of the meter. Thus, the contact resistances (R1, R2, R3, and R4) which normally make measuring ultra-small resistances impossible are insignificant and can be ignored. In order to maintain accuracy the Ohmmeter should be calibrated with the leads in contact before each measurement and the zero volume height should be recorded before adding the powders to be measured.

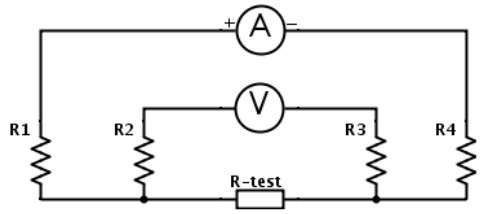

Figure 2.6. Four Point Probe Circuit Diagram.

CNT Powders were packed into the cylinder and measured under constant pressure and constant volume. It was found that the constant pressure technique

suffered from a continually dropping resistance. Most likely this is due to friction within the packed powder in the cylinder, see Figure 2.7.[52] Empirical studies have suggested that packed powder towers will settling follows a log like behavior.

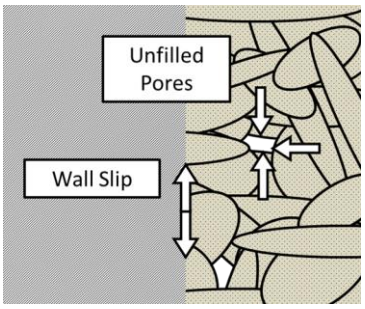

Figure 2.7. Compressed powders resist packing due to particle-particle interactions and wall slip forces.

Powders were prepared by mixing 0.01 g CNTs, 0.02g PVdF with LFP (amount varies from 0.5-0.2g) in 25-30ml NMP solvent using a ultra-sonicator (dismembrator) at 25% amplitude for 20 minutes (QSonic 500), drying the suspensions in a vacuum flask filter, and then drying them further in a vacuum oven at 80°C for 12 hours. The conductivity vs. density was then measured, using the powder conductivity probe. The probe measures powders under constant volume with a Keithly 580 micro ohmmeter. All static conductivity measurements reported here were taken at 2.1 g/cm^3.

Considering Figure 2.8, along each curve the conductivity starts small, as the contact is unreliable. As the pressure increases the unfilled pore volume decreases creating more and more internal connections. At the knee, the empty pore volume has been consumed. The movement of the knee to higher densities with the samples with more CNTs may be due to their increased "springiness" as the powders were well divided before packing and the SMW-CNTs are rigid rods with aspect ratio > 300.

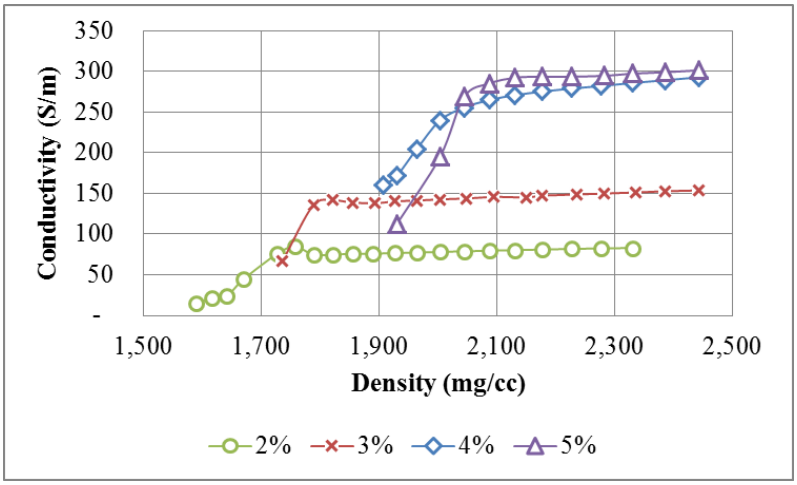

Figure 2.8. Conductivity of packed powders vs. packed density for the SMW-200 as measured by the Four Point Powder Probe.

2.5.2 Cyclic Voltammetry (CV)

A voltammagram is made by scanning the potential and recording the current. Any redox reactions will cause peaks in the current above and below the reaction potential during the up and down scans respectively. The Randles-Sevcik equation can be used determine the peak shapes and peak positions with respect to scan rate, v.[42]

$$I_{peak} = \frac{nFAC}{2.2406}\left(\frac{n\,F}{RT}\right)^{\frac{1}{2}}(D)^{\frac{1}{2}}(v)^{\frac{1}{2}}K(\Lambda,\alpha) \qquad \text{Equation 2.15}$$

The quasi-reversible peak position is represented by Eq. 2.15, where n is the electrons per reaction, F is the Faraday constant, A is the surface area, C is the concentration, R is the gas constant, T is the temperature, D is the diffusion coefficient of the Lithium ions and $K(\Lambda,\alpha)$ is the degree of irreversibility.[43]

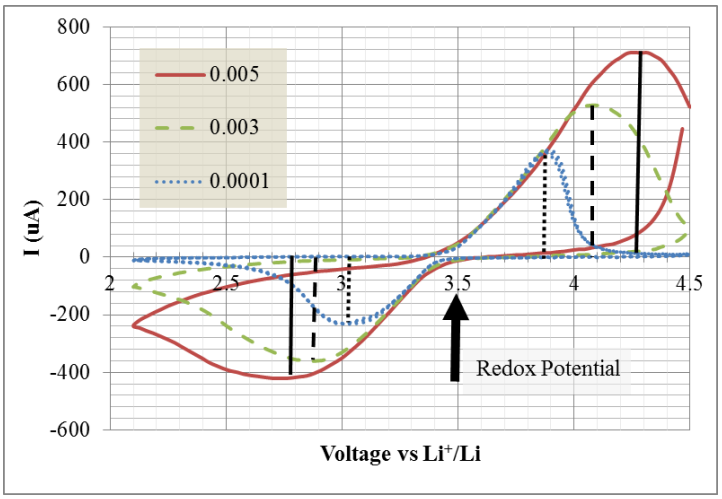

Figure 2.10. Cyclic Voltammagram of $LiFePO_4$ with 5% CNTs and 5% PVdF at various scan rates between 5 mV/second and 0.1 mV/second.

The lack of additional peaks, even at higher scan rates, indicates that there are no corrosive impurities (e.g. water) in the battery. CV can be used in this manner to identify the redox potential of side reactions, and potentially identify the impurity.

With the converse, where the voltage is held constant and the current is monitored, the Cottell equation is used to analyze the current response, Eq. 2.16. So long as there is sufficient concentration (c) in the electrolyte the current will proportional to the square root of time.

$$I = \frac{nFAc}{\pi} (D_e)^{\frac{1}{2}} (t)^{\frac{1}{2}} \qquad \text{Equation 2.16}$$

2.5.3 Electrode Impedance Spectroscopy (EIS)

A small AC voltage (5 mV) is applied to a DC offset. The phase and amplitude of the current are then measured to determine the impedance. The imaginary impedance is then plotted against the real resistance at each frequency, as in Figure 2.11. RC circuits will create semi-circles, inductors will induce loops, and resistance will shift the points to the right. Interpretation of this technique depends on the model of Lithium exchange that is used, be it the ad-atom or SEI exchange

models. Both models predict that the electron diffusion through the electrode should occur at highest frequencies. Subsequently the double layer effect due to electrolyte transport, the solvation/desolvation ion transfer, the ion diffusion through the bulk, and the crystal structure change all contribute to the impedance at lower and lower frequencies.

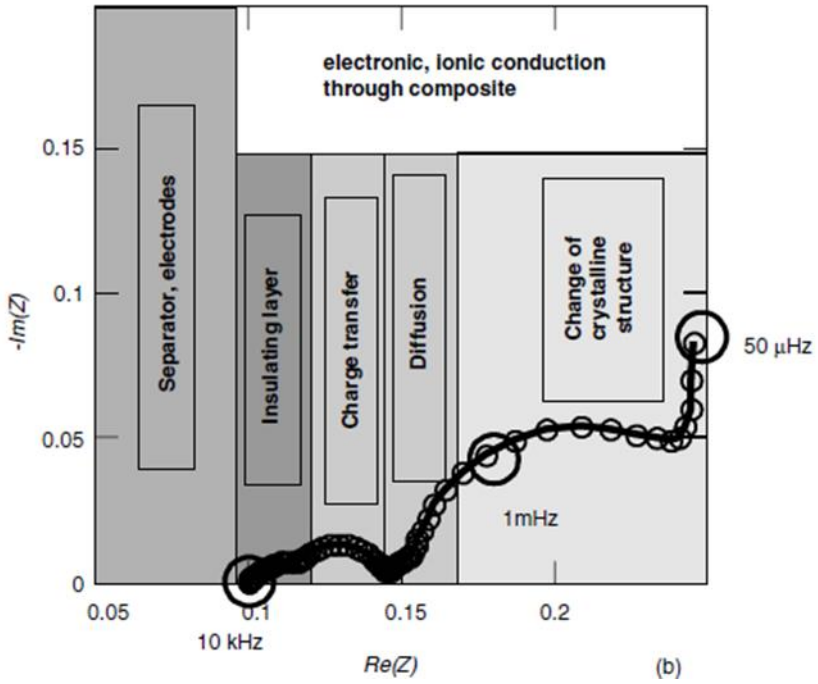

Figure 2.11. Typical impedance spectra with the SEI layer interpretation designations of each frequency region.[44]

Electro Impedance Spectroscopy (EIS) was completed with a Solatron 1287 Electrochemical Interface and a 1260 Impedance/Gain-Phase Analyzer with 5mV AC amplitude between 80 kHz to 0.01 Hz. Analysis of these was completed with the Zplot simulator from Solatron. Equivalent circuits can be built up and then simulated as in Figure 2.12.

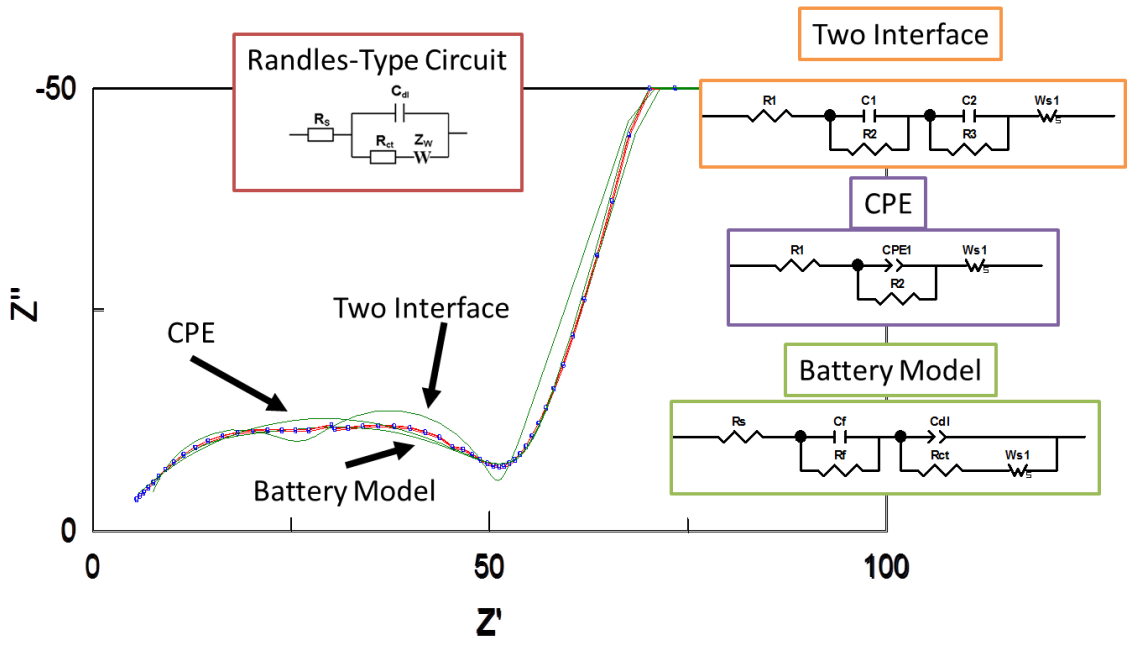

Figure 2.12. Simulation of Electrode Impedance Spectra with different battery models.

Interfaces can be modeled as RC circuits to simulate charge buildup (or depletion due to diffusion limitations). The constant phase element (CPE) is used to model porous surfaces, Equation 2.17. Where P is 1 it is identical to a capacitor, when P is zero it is identical to a resistor, and when P is ½ it creates a line on the complex plane with constant phase (θ = 45°), hence the name.

The finite length Warburg (W_S) given in Equation 2.18, is a solution to the one-dimensional diffusion equation for a single particle. The Warburg generally dominates the impedance at the lowest frequencies and causes Z" to increase quickly.

$$Z_{CPE} = 1/(T(i\,\omega)^P) \qquad \text{Equation 2.17}$$

$$W_S = \mathrm{R}\frac{\mathrm{Tanh}\left((i\,T\,\omega)^P\right)}{(i\,T\,\omega)^P} \qquad \text{Equation 2.18}$$

Connecting the circuit model parameters of the battery to the physical mechanisms is non-trivial. First there is the question of which model is the most appropriate. First principle physical models are not easily boiled down to circuit

elements. Thus, it is not perfectly clear which model is most correct from these measurements alone. Secondly, there may be multiple fitting solutions with a single model. For example, the battery model in Figure 2.12 the Warburg and electrode resistance (R_S) both have series resistance values that could exchange places. Thus, in order to find the correct fit, one must have some idea of the magnitude of the elements. Using the conductivity of the composite measured with the four point probe, we can exclude solutions that have extreme values for the electrode contact resistance (R1).

These techniques are extremely powerful, and reveal the characteristics of the transport phenomena in batteries. Takahashi *et. al.* was able to determine the activation energy for the Lithium and electron diffusion using cyclic voltammetry and electrode impedance spectroscopy, see Table 2.3.[44] The electrode resistance can be directly read off the spectra as minimum real resistance. The semi-circle diameter is equal to the resistance of the Lithium charge transfer (or solvation depending on your model).

Table 2.3. Activation Energy as determined by CV and EIS.[44]

E_{Li}	$E_{electron}$	
39	16	kJ per mol
0.4	0.16	eV per electron

2.5.4 Battery Performance

The most basic characterization of a battery is to measure the charge delivered under use. Charging and discharging the cells measures their specific energy and power densities as discussed in chapter one. The electrochemical charge and

discharge testing was completed with an Arbin Battery Tester (BT 2000). A standard test protocol was used on all batteries made. Each battery was charged at C/5 and discharged at C/10, C/5, C/2, 1C, 2C, 5C and finally C/10 for ten cycles at each rate. 1C corresponds to current that would discharge the cell in one hour with a capacity of 170mAh/g of active material. Using this test protocol, we obtain both rate capability information, Figure 2.13, and power density information, Figure 2.14.

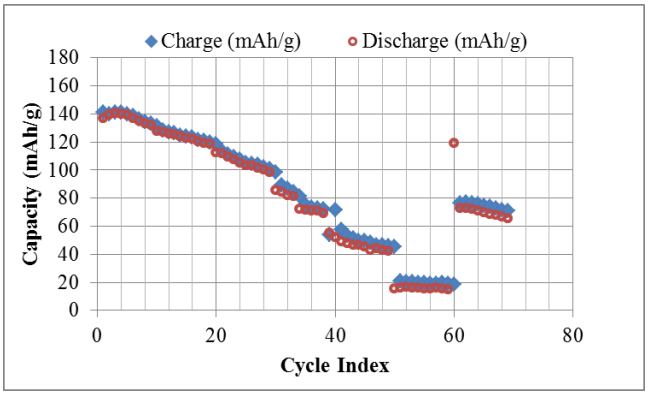

Figure 2.13. Discharge and Charge Capacity of LFP with 20% carbon black and 5% PVdF.

In this example, the battery has severe capacity fade as it is cycled. The capacity fade is exacerbated under high C-rates, but the loss continues even at the small C-rates. This is typical of electrode contact decay. Since this cell has 20% carbon black there certainly is enough material to make the composite wholly conductive. In addition, the charge capacity closely matches the discharge capacity which suggests side reactions are at a minimum (or at least reversible), such as dendrite formation or other corrosion. The discharge capacity vs cell voltage plot shows that the second C/10 has increased cell polarization at only 30 mAh/g capacity. This indicates that the available capacity of the cell is severely reduced. This may be simple due to the electrode breaking and losing contact with particles within the matrix, thus cutting off the electron current.

Most battery materials are made from more conductive material than LFP. LFP batteries typically have a higher content of binder (10%) as well. Nevertheless, this is a failure mechanism that all electrochemical cells with composite electrodes have to deal with: in other words, all batteries that do not use solid metal electrodes.

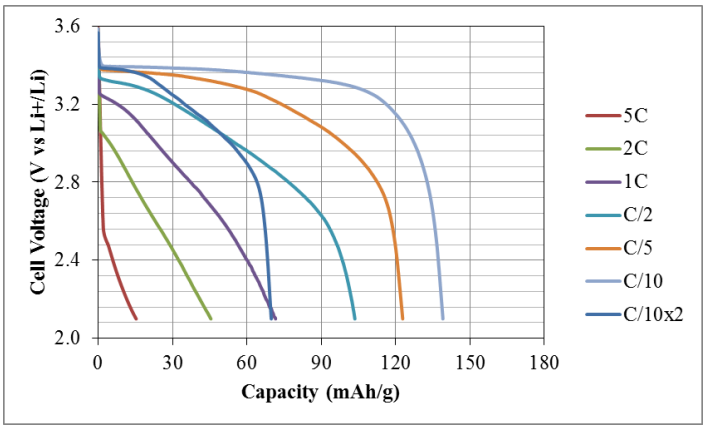

Figure 2.14. Discharge capacity vs. cell voltage for LFP with 20% carbon black and 5% PVdF.

2.6 Percolation Threshold with Nanotubes

Using both CNTs and carbon black in composites has been suggested to be the most advantageous way to increase the conductivity of a composite.[45] We know that the conductive percolation threshold for CNTs in polymer blends is typically less than 0.5%.[46] Nevertheless, batteries made with only CNTs with contents of 2% and less, exhibited poor capacity and stability. On the other hand, batteries made with at least 5% CNTs or more tend to be stable and resilient.[47] It could very well be that either the total amount of CNTs was not enough to connect each and every surface, a so called surface threshold. On the other hand, the method of dispersing the CNTs could have been inadequate for the lower CNT content batteries.

Percolation theory describes the behavior of networks of elements. Specifically the probability that they are connected across a volume, from one surface

to another. A critical density (P_C) is defined as the concentration at which the probability of a continuously connected network changes from near zero to near one.

For composites, the electrical percolation threshold is the minimum amount of conductive material needed to cause a sharp increase in the conductivity of the composite, where below that critical threshold the conductivity of a battery composite is limited by the cathode material. Recall from Table 2.1 that LFP is an basically an insulator. Above that critical threshold, the additive conductive material makes enough connections to provide a connected conductive pathway through the composite.[48] Just above the threshold, the conductivity increases rapidly following Eq. 2.19, where α is the critical exponent, typically 1.5.

$$\sigma = \sigma_{Additive}(P - P_C)^{\alpha} \quad \text{for} \quad (P - P_C) \ll P_C \qquad \text{Equation 2.19}$$

The percolation threshold in epoxy composites has been shown to vary widely depending on the processing techniques, from 0.1% for CNTs dispersed by ultrasonication, to 0.4% by shear mixing, and no percolation below 1% loading for ball milled samples.[27] These methods produce different sized agglomerates. Depending on the state of dispersion J. Li *et al.* predict that the percolation threshold can be either single CNT dominated, Equation 2.20 or agglomerate dominated, Equation 2.21, where d is the diameter of the CNTs l is the length, and ε is a parameter representing the local density of the agglomerates.

$$P_C = 27\pi d^2/(4\, l^2) \qquad \text{Equation 2.20}$$

$$P_C = V_{CNT} \,/\, V_{Total} \approx \varepsilon\, \pi/6 \qquad \text{Equation 2.21}$$

Using Equation 2.2 and assuming there is no unfilled pore volume, we can estimate the P_C for perfectly dispersed multiwalled CNTs with 10 nm diameter and

10 µm at 0.005% loading.[d] Since we have yet to find a dispersion method that can remove agglomerates completely the percolation threshold will always be larger than predicted by Eq. 2.20.

The conductivity of composites far above the percolation threshold will follow the general trend given in Eq. 2.22, where *a* depends on the aspect ratio and degree of dispersion and *b* depends on the quality of the conductive additive after dispersion, which should generally approach the conductivity of the additive, Eq. 2.23.

$$\mathrm{Log}(\sigma) = -\mathrm{a}\,P + b \qquad \text{Equation 2.22.}$$

$$\mathrm{b} = \mathrm{Log}(\sigma_{additive}) \qquad \text{Equation 2.23.}$$

2.7 Surface Threshold

While conductive additives are traditionally added to battery materials that are poor electron conductors to increase the charge that they can provide at higher currents (higher C-rates), many high energy dense materials are insulators, *e.g.* LFP. However, conductive additives are useful in conductive battery materials as well, *e.g.* $LiCoO_2$. There are two roles that are generally well understood that additives should fulfill.

1. *Reduce the Power loss due to resistive heating (Ohmic Losses)*
2. *Reduce the polarization, uniform battery particles discharge*

There is a third role that is often attributed to the binder that is to maintain interconnections when under mechanical stress. As Lithium intercalates in and out of the ceramic large volume changes occur. These stresses can be severe enough to crack particles if the stress is not uniformly distributed. Higher specific currents are the most likely cause of this problem.

[d] Densities used were 1.2 g/cm^3 for CNTs and 3.6 g/cm^3 for LFP.

This is one of the main mechanisms of battery capacity fade and failure that is not related to the electrolyte. It is also irreversible if either of the two halves of the cracked particle is not in contact with the electrode. Thus, a conductive additive should maintain contact to every particle and cracked particle.

The model that derived Eq. 2.20 assumed the CNTs were dispersed throughout the volume uniformly. However, battery composites are a combination of binders and solid crystallites. No method of mixing will place a CNT in the center of a crystal. Conductive additives are confined to the regions between particulates, the interfaces and surfaces. If the total inactive material volume is small, the percolation is not across a volume, but rather across a surface. Let us define a surface threshold:

Surface Threshold – the minimum amount of material need to make contact with every surface within a composite to form a stable and interconnected network.

Any surface not in contact with the electrode increases the diffusion length of the electrons to the redox centers near that surface. This decreases the power performance by increasing the specific currents at every other interface. With increased specific currents and longer diffusion lengths, polarization within the cells can lock out more capacity by increasing the lattice strain over short distances within the cell. The polarization or strain could be due to the layers of lithiated and de-lithiated regions induced by the ion current, or due to defects already present in the cell, *e.g*. isovalent substitutions.

The best measure of good dispersion and good contact to every surface is not conductivity but capacity from a cycled cell. The conductivity of the composite will impact the EIS initial offset resistance, and the quality of the surface coverage will

impact the specific power performance. Cells that have networks that are not resilient under strain will lose contact to surfaces and will lose capacity with progressive cycling or higher C-rates.

Chapter 3. Identifying the optimal nanotubes

3.1 Introduction

Carbon nanotubes (CNTs) have been shown to be a viable conductive additive in Li-Ion batteries.[49] By using CNTs battery life, energy, and power capability can all be improved over carbon black, the traditional conductive additive. A loading of 20% carbon black can be replaced by only 5% CNTs. In addition, many of the previous efforts found that a combination of conductive additives is the most advantageous.[50] Unfortunately, many of these efforts did not attend to the unique challenge that dispersing nanotubes presents and used non-optimal methods to disperse CNTs (e.g. ball milling).[51,52] With poor dispersion, a stable and resilient conductive network in the cathode is hard to form with CNTs alone. For example, in Figure 3.1 ball milled CNTs form larger agglomerates leaving most of the particle surface area unconnected, while ultrasonicated tubes form loose networks over the entire surface.

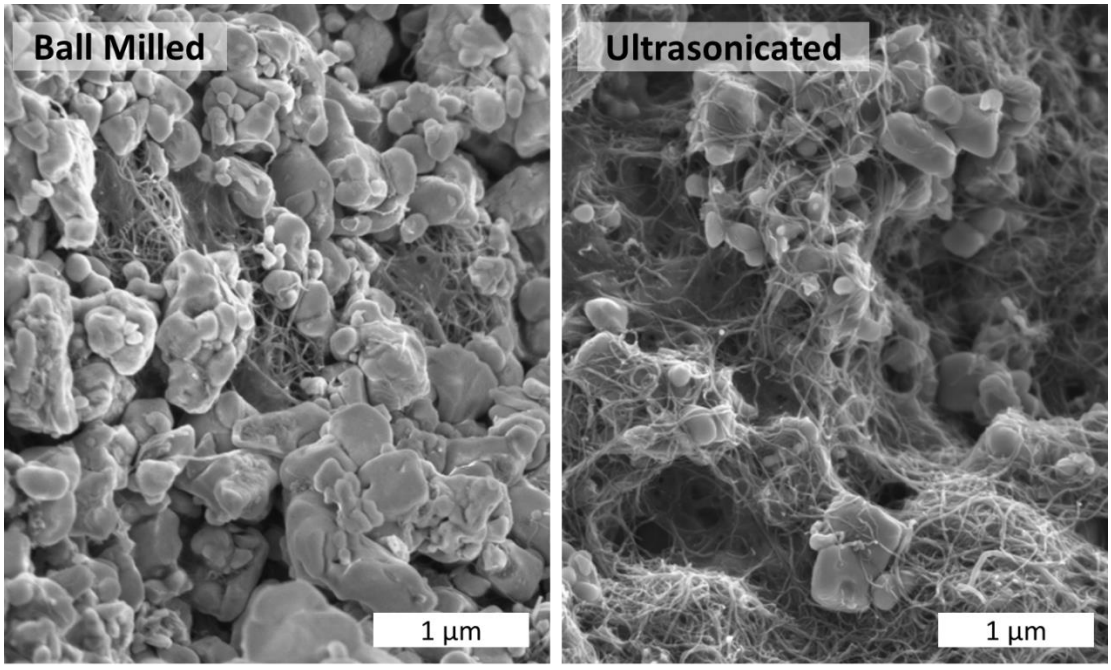

Figure 3.1. SEM micrographs of Aerosol deposited cathodes with 5% CNTs and 5% PVdF with CNTs dispersed by ball milling and ultrasonication.

3.2 Properties of Carbon Nanotubes

A nanotube is a graphene sheet that has been wrapped up into a cylinder. The angle that the sheet is wrapped at is referred to as the chiral angle. With multiple layers of graphene wrapped around the central cylinder, we have a multiwalled CNT. Single walled CNTs usually have outer diameters on the order of a nanometer while multiwalled CNTs can be much larger, from a few nanometers to tens of nanometers, depending on the number of walls.

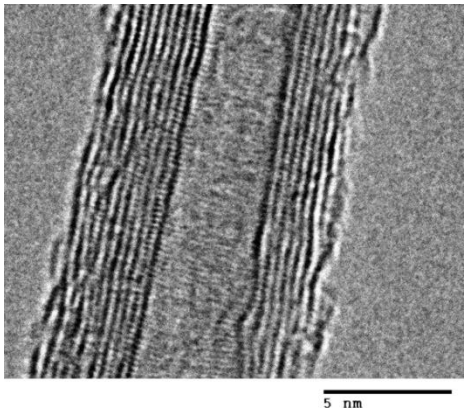

Figure 3.2 High Resolution TEM of SMW-200

Nearly everything about a carbon nanotube (CNT) is determined during growth. The catalyst, the support, the partial pressure of the carbon source, the partial pressure of any etching agents, and the temperature of the reaction all determine the conditions for the formation of the CNT. By altering these parameters, one can produce single walled or multiwalled tubes with different average diameters, numbers of walls, or length. A wide selection of CNTs can be made from a carefully controlled CVD reaction. While the growth of CNTs is outside the scope of this work, the question of the best properties for a CNT to have in a battery composite is relevant.

The best performing cathode composites published to date were made with multiwalled CNTs grown via arc-discharge.[53] Arc-discharged CNTs tend to be very

long and defect free. This should result in a CNT that is both highly conductive and easily dispersible, thus able to form highly conductive, well connected networks in a composite. Unfortunately, arc-discharge CNTs are not cost effective when scaling up to high capacity production, compared to other growth methods.[54]

As established in the previous chapter, conductivity and resilience of the network are needed to make durable and powerful batteries. Another parameter not yet considered is the cost of the CNTs. The goal of this work is to develop methods to incorporate CNTs into products. It would be a moot point if the materials were cost prohibitive. The reaction conditions of multiwalled CNTs typically increase the carbon yield dramatically over single walled CNTs. Thus, they can be as much as a hundred times cheaper per gram.

CNT physical attributes can be evaluated by: Length (100 μm to 300 μm as measured with TEM or AFM); chiral angle (measured with florescence spectroscopy or if purified UV-vis spectroscopy); defect density (measured with Raman); bend density (investigated with TEM, SEM, or XRD); and the number of walls (most easily measured by TEM). Since the inter-wall spacing is regular, the number of walls can be calculated from the outer (D) and inner (d) diameters, e.g. Figure 3.3.

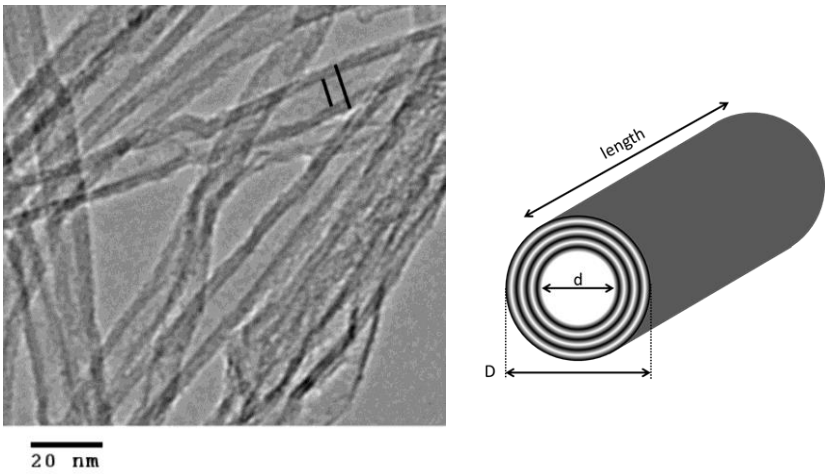

(a) (b)

Figure 3.3. (a) Transmission Electron Micrograph of SMW-200 CNTs. (b) Principle dimensions of Multiwalled Carbon Nanotubes.

3.3 Evaluating Carbon Nanotubes

Southwest Nanotechnologies kindly provided sample CNTs for evaluation in battery composites. CNTs were tested for dry powder conductivity, Figure 3.4. Single walled (SW) and multiwalled (SMW) carbon nanotubes were evaluated with the Four point Powder Probe. Typical resistances were on the order of an Ohm and as small as ¼ Ohm for a 100 mg sample with ¼ inch diameter and ½ inch height. The four point method was essential in measuring these small resistances. As expected the conductivity of SW-40G, a single walled CNT, was the highest. The SMW-200 had surprisingly high conductivity as well.

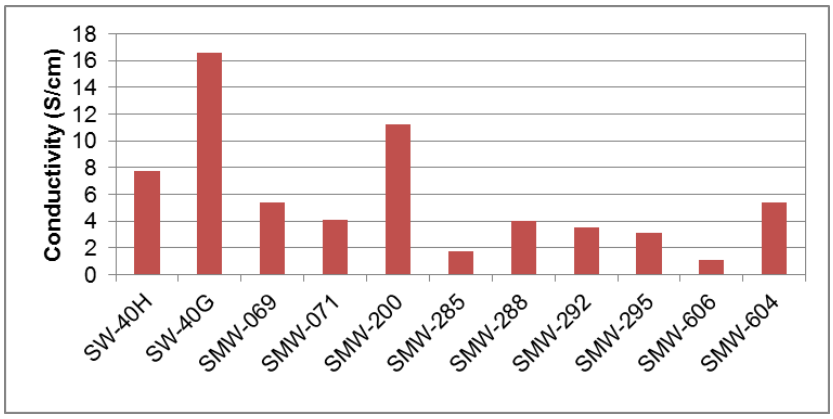

Figure 3.4. 4-Point Powder Probe Conductivity of pure CNTs as received.

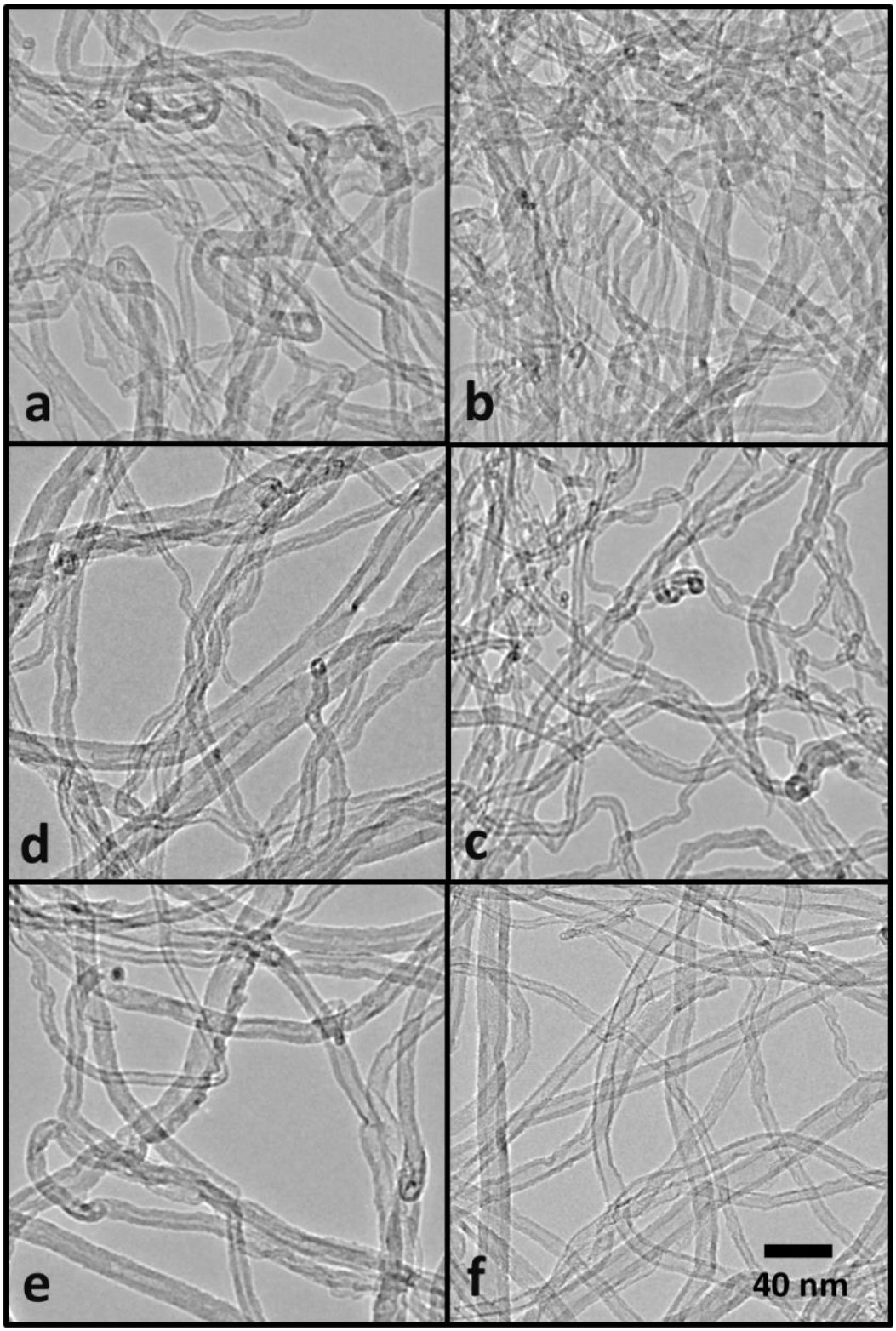

Figure 3.5. TEM micrographs of multiwalled carbon nanotubes obtained from SWeNT with designations (a) SMW-069, (b)SMW-071, (c) SMW-285, (d) SMW-288, (e) SMW-292, and (f) SMW-200.

Figures 3.5 shows transmission electron micrographs of the multiwalled CNTs evaluated with the dry powder conductivity in Figure 3.4. Several qualitative qualities can be observed: Bends, defined as a turn in a CNT with radius less than twice the diameter; defects, which are voids in the CNTs side walls; surface carbon, which is extrusions. The density of CNT bends per unit length is significantly lower for SMW-200, Table 3.1. For the CNTs in Figure 3.5 the bend density appears to be inversely correlated with conductivity. The CNTs also appear to have a rather high density of defects (SMW-285, SMW-069).

Table 3.1 Density of Bends in CNTs per 275 nm.

CNT	Bend Density	Sample Size
SMW-069	75%	24
SMW-071	35%	26
SMW-285	96%	20
SMW-288	40%	24
SMW-292	38%	13
SMW-200	10%	21

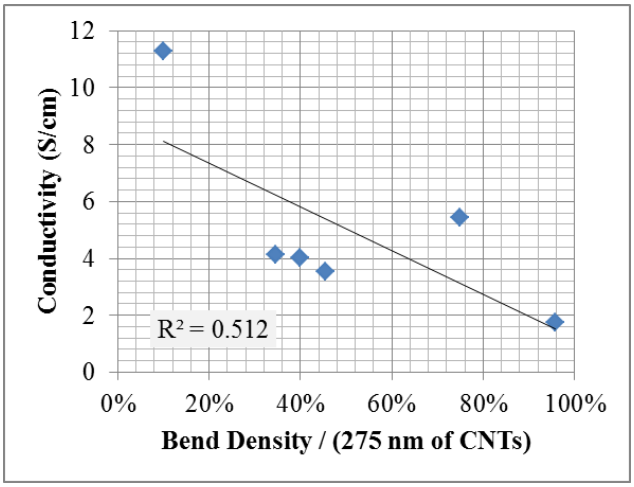

Figure 3.6. Density of bend defects per 275 nm of CNT.

The problem with TEM as a measurement tool is that it only measures one small section of the sample. For instance, a high resolution image of the SMW-200, Figure 3.2, reveals that it has few defects and very little surface carbon. However, it

only represents one single tube and does not represent the average. By measuring hundreds of tubes, a diameter distribution can be built up that better represents the sample, Figure 3.7.

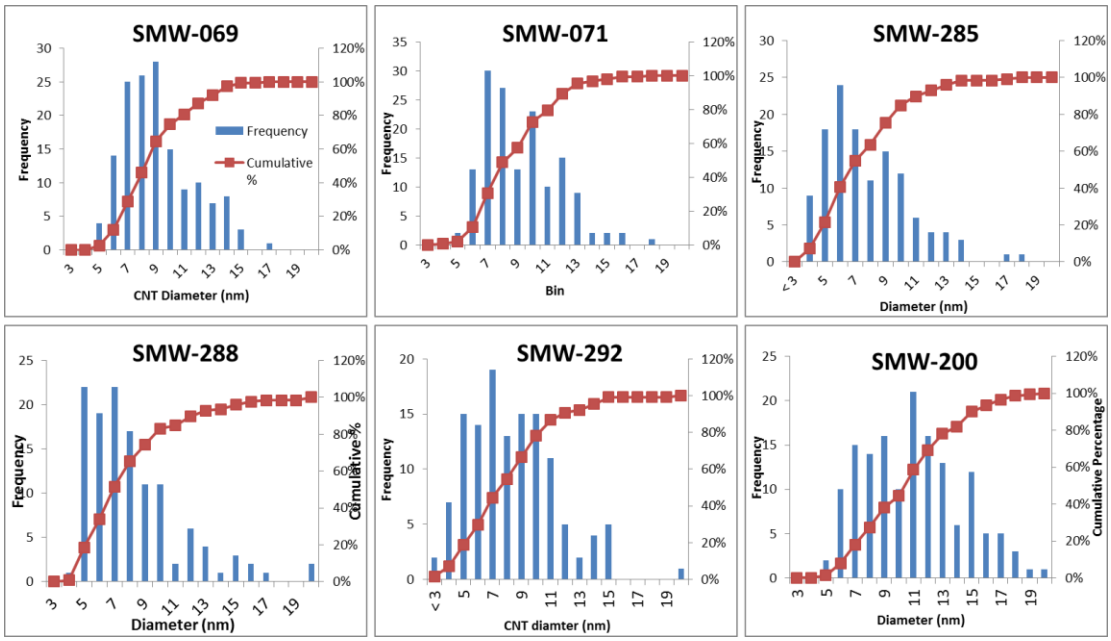

Figure 3.7. CNT diameter distributions as measured by TEM.

We can now plot the mean diameter vs. conductivity, in Figure 3.8.

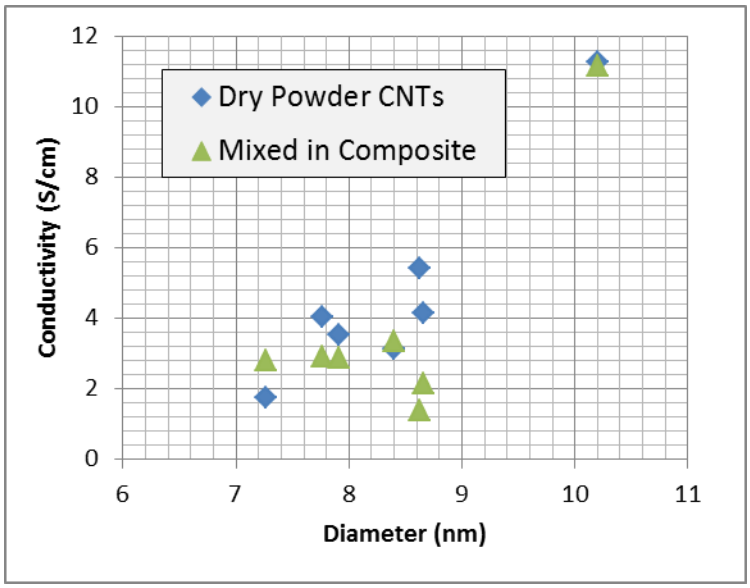

Figure 3.8. Diameter of CNTs as measured by TEM vs. 4-point conductivity.

The reduction in bend density may in fact be a by-product of an overall increase in CNT diameter between samples. The larger the diameter, the higher the number of walls, the stiffer and more pipe like the CNT will be.

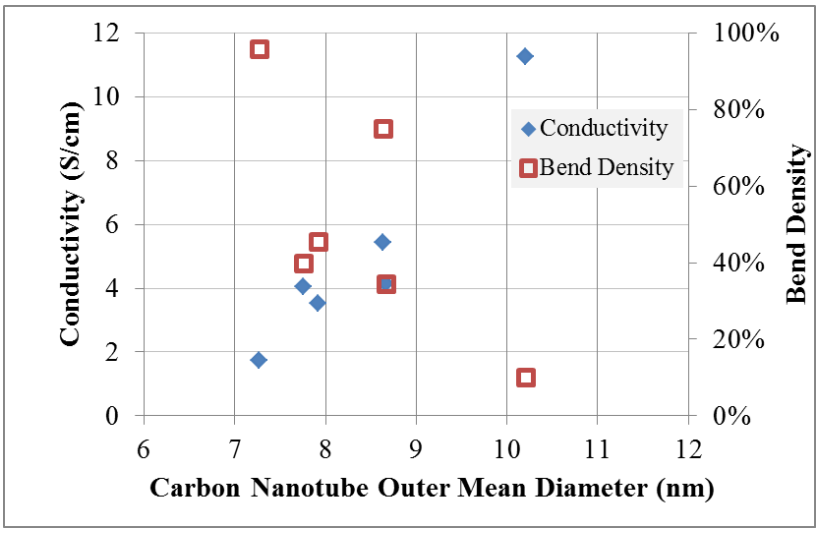

Figure 3.9. Conductivity and Bend Density vs. CNT diameter.

Based on the measurements of the dry powdered and composite conductivity the SMW-200 CNT appears to have the highest conductivity (1100 S/m), which is roughly half the conductivity of single walled CNTs. Although the average diameter for this CNT is larger there does not appear to be a trend relating conductivity and outside diameter in for the CNTs mixed into the composite, Figure 3.8. Increasing the diameter of the CNTs increases the dry powered conductivity and decreases the bend density, Figure 3.9. Thus, the bend density and the lack of CNT defects appear to be the distinctive qualities of the SMW-200 CNT.

3.4 Dispersing Carbon Nanotubes

Although understanding the intrinsic properties of a CNT is helpful in distinguishing between products of the growth reaction, this does not establish how

the CNTs will perform within a battery. We must investigate the CNTs in the composite.

LFP, PVdF, and three different kinds of CNTs were prepared as composites by wet ball milling and ultrasonication both in NMP. After the constituents are mixed, the powders are dried by vacuum flask filtration. A flask trap was used on the vacuum system vacuum line to trap the excess NMP. A 4-point powder probe conductivity measurement was then made on each sample, given in Figure 3.10. The SMW-069 10 hour ball milled increased in conductivity over sonication. The SMW-071 did not significantly change in conductivity. The SMW-200 proved the easiest to disperse with ultrasonication and produced the highest conductivity composite.

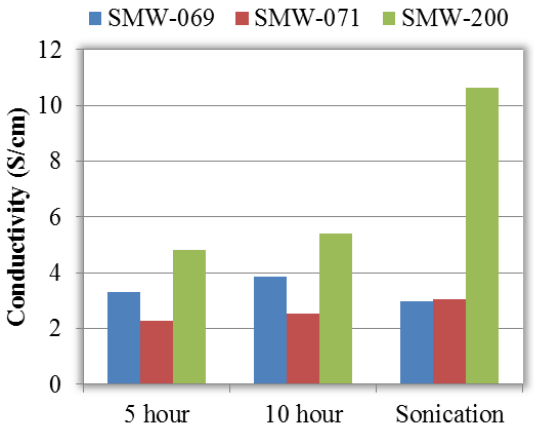

Figure 3.10. Conductivity of ball milled and sonicated composites with 5% CNTs and 5% PVdF in LFP.

We have been consistently using 5% CNTs for all of these investigations having not established the optimal loading of CNTs for battery composites. As established in chapter one, in order to maximize the specific power, the inactive fraction of material in the composite should be kept to a minimum, yet still produce a highly conductive and resilient network.

CNTs were dispersed by ultrasonication in NMP and mixed with a PVdF solution and commercial LFP. The mass ratios of the constituents included 2-5% CNTs, 5% PVdF, and the balance LFP from MTI Corp, the 4-point probe conductivities are given in Figure 3.11. Since the conductivity of LFP is 10^{-8} S/cm, all of the loadings of CNTs used are well above the percolation threshold. Almost all of the CNTs investigated increased in conductivity according to Eq. 2.17. That is, the log of conductivity (σ) increased linearly with concentration (*P*). The SMW-200 composite was nearly at its powder conductivity at 4% CNT loading.

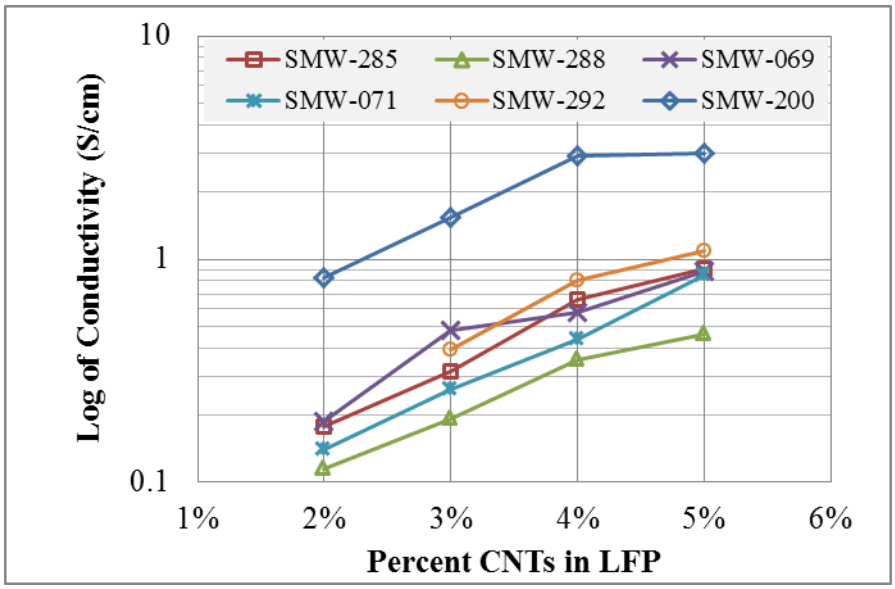

Figure 3.11. Conductivity LFP composite with various amounts of multi-walled CNTs.

3.5 Post Processing CNTs

After CNTs are made, the catalysts and supports must be removed. This is usually done with a series of baths and washes with HF to etch the support and metal catalysts away. This acid treatment can cause further defects in the CNT where imperfections already reside. One method to "heal" the CNTs is to anneal them in an anaerobic atmosphere. We investigated calcination and annealing treatments on

several CNT series in Figure 3.12. Of the three CNTs tested, only one increased in conductivity significantly, SMW-071. Although SMW-069 and SMW-288 have a significantly higher bend density than SMW-071 it is not clear why only SMW-071 increased so dramatically in conductivity.

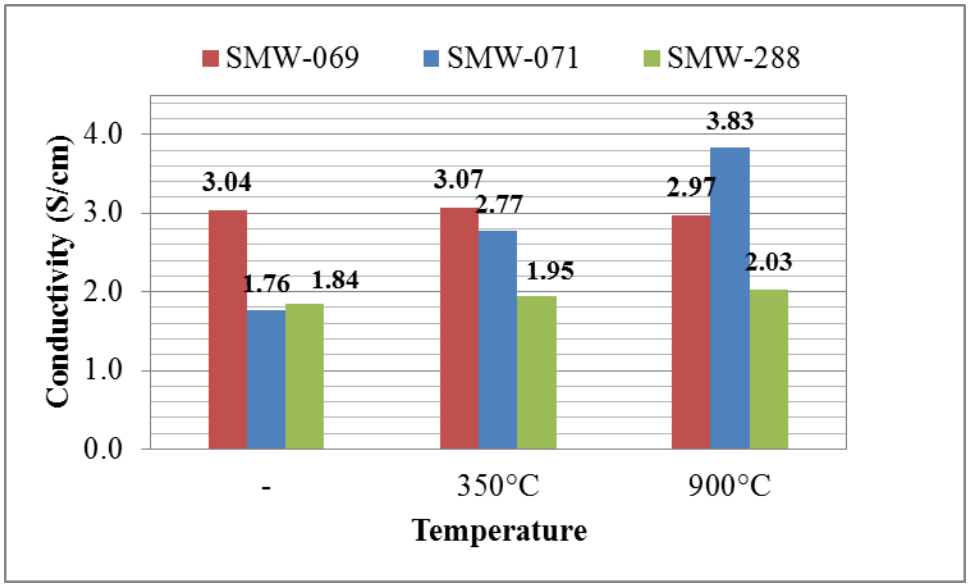

Figure 3.12. Conductivity of CNTs before and after annealing in Argon at 900°C or burning in air at 350°C.

Chapter 4. Film Formation and Processing

4.1 Introduction

Processing techniques are sought to disperse, deposit, and dry the composite materials while maintaining the high aspect ratio of the CNTs, without adding steps that would damage the cathode material. In this chapter, we investigate different mixing methods and deposition techniques. Each of these is then evaluated based on the conductivity of the composites and the electrochemical performance of the produced films.

4.2 Materials

Lithium Iron Phosphate (LFP) with average diameter of 2 μm (95% less than 21 μm) and binder (PVdF) was purchased from MTI Corporation.[e] Anhydrous n-methyl 2-prolylodone (NMP) and all other reagents were purchased from Sigma Aldrich. PVdF was prepared by dissolving 1g in 100 mL of NMP and heating the solution to 100°C for 6 hours. All CNTs in this work were multiwalled (SMW) and were graciously supplied by Southwest Nanotechnologies.

4.3 Formulation

In order to increase the specific capacity, we investigated reducing the inactive material content, either the conductive additive or the binder. PVdF was used as the binding agent; although an insulator, it is needed to stabilize the contact of the conductive additives to the active material. Any amount of PVdF in the composite will impact the cathode conductivity, as can be seen in Figure 4.1.[55] A sharp decrease

[e] A 2 μm particle diameter material are not considered high rate. Nanosized materials tend to produce the highest rate cathode material.

in conductivity is observed with even a small amount of binder added (0% vs. 0.6%) for the intermittent sonicated samples. The principle concern is that at the lowest loading of binder the films of cathode material will delaminate in the battery can.

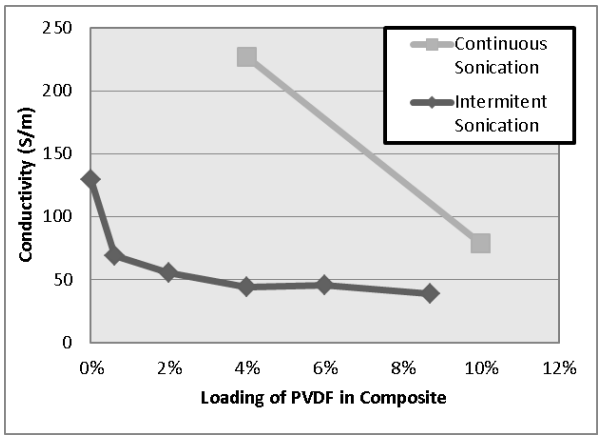

Figure 4.1 Effect of PVdF content on composite conductivity with 5% CNTs dispersed using intermittent and continuous sonication.

In order to investigate the PVdF impact we prepared batteries with the drawn down method, with binder content between 0.6% and 6% and measured their discharge capacity, Figure 4.2. Here we see that for samples with PVdF content above 4%, the initial discharge capacity represents full utilization of the cell. As the content of PVdF is reduced, the capacity and stability of the batteries diminishes. The battery with 6% PVdF has the highest capacity at 5C (85 mAh/g) and the capacity fade is minimal as it is able to return to its original capacity when at the C/10 current discharge rate.

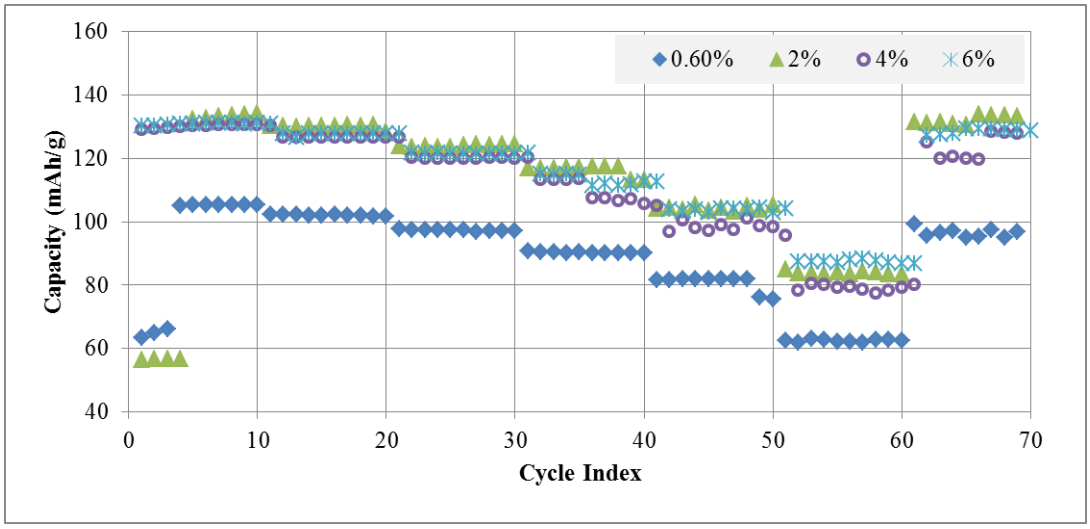

Figure 4.2. Effect of PVdF content on the electrochemical performance of half cells with 5% CNTs in composite deposited with the drawn down method.

As discussed in chapter two, in order for a composite to be conductive there needs to be enough conductive material to meet the percolation threshold. Figure 4.3 displays the discharge capacity of batteries made with CNT loading between 2% and 5%, where the CNTs were dispersed by an ultrasonic horn just prior to aerosol spray deposition. All of the batteries below 5% exhibit capacity fade that is characteristic of a loss of electrode contact for a fraction of the battery particles every cycle, although at first the battery capacity is higher with low CNT content. This suggests that the method of dispersion was effective but the 3-dimentional network is not resilient after higher current density discharge cycles. Only with 5% CNT content does the battery retain the initial capacity when returning to lower discharge current (C/10).

We know from the conductivity measurements that the amount of CNTs needed to reach percolation threshold is well below 2%. Percolation does not mean every surface is in contact with the electrode. It appears the surface threshold is between four and five percent for this composite.

We investigated the same preparation technique with carbon black, Figure 4.4, and found that the delivered capacity was poor below for the 5, and 10% loading samples. With 20% carbon black the capacity delivered was good, but the capacity fade was severe and irreversible.

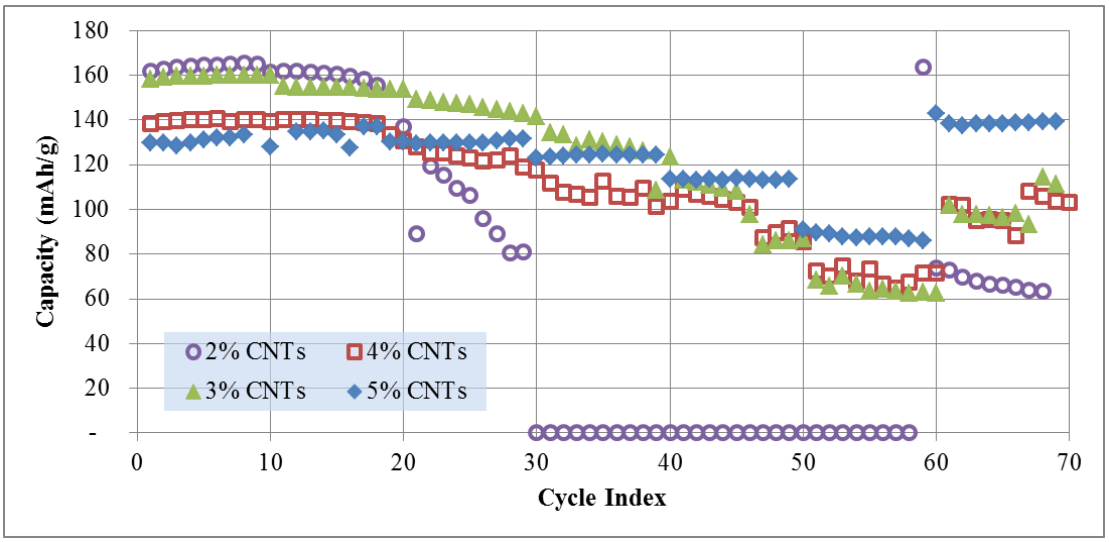

Figure 4.3. Discharge capacity of $LiFePO_4$ half cells with various CNTs loading and 5% PVdF prepared by aerosol spray deposition.

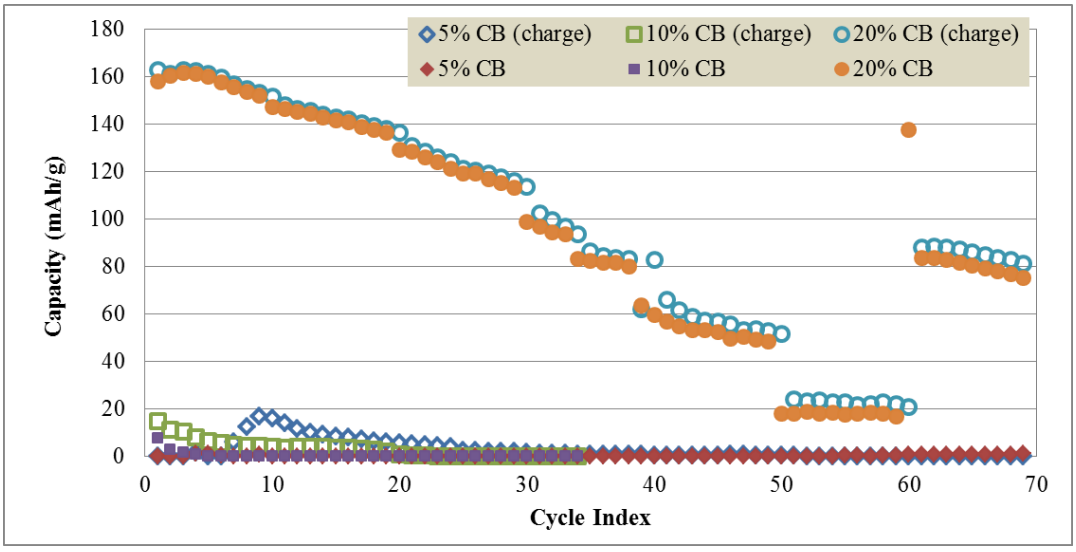

Figure 4.4. Discharge Capacity of $LiFePO_4$ with various Carbon Black loading and 5% PVdF prepared by aerosol spray deposition.

4.4 Dispersion

Flocculation, or the formation of aggregates in a fluid, is a difficult problem to deal with when trying to disperse and maintain the separation distance between long rope-like members like CNTs. If the CNTs make contact with each other they will likely form bundles, and thus reduce the concentration and reduce their own effective conductivity. When starting with a dried powder of CNTs (typically freeze dried) one should expect that the CNTs are already in bundles or at least in intimate contact.

Some sort of high energy mechanism is needed to separate the CNTs. Surfactants (surface active agents) are often used for this application by minimizing the surface energy. They keep CNTs dispersed by utilizing either charge repulsion or hindrance, depending on the end group of the surfactant molecule. Mechanical dispersion and dilution can also be utilized to separate bundles. The mechanical energy could be delivered by ball milling, mortar and pestle hand grinding, ultrasonication, or any one of numerous other techniques, see the work by J.K. Beddow for a summary of this very well developed art.[56]

In order to optimize the dispersion and reduce flocculation within the suspensions we varied the method of mixing the constituents into the mixtures. We investigated dispersing the CNTs using ball milling, intermittent ultrasonication, and continuous sonication and deposited these films by aerosol spray, Figure 4.5. For comparison, a slurry made battery with a CNTs and PVdF paste is also included. Since ultrasonication is energetic enough to cleave CNTs over time a pulsed mixing procedure might better preserve the high aspect ratio of the as produced CNTs. Unfortunately, as can be observed in Figure 4.5, continuous sonication is much more

effective at separating the CNTs before deposition via aerosol spray. On the other hand, ball milled CNTs and CNTs prepared as pastes exhibit poor performance at high C-rates. While both of these methods were able to reproduce the initial capacity after returning to smaller current densities, this indicates that the materials are well mixed, but there was a lack of good contact between the CNTs and the LFP.

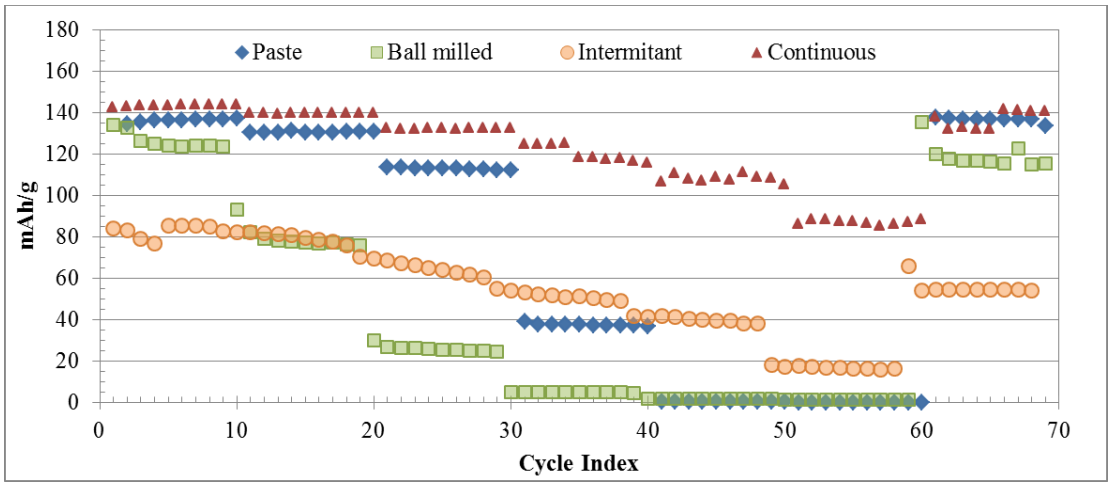

Figure 4.5. Effect of dispersion method on batteries with CNTs added as a mixed in a paste of PVdF (diamond) or an Aerosol deposition with intermittent sonication (circles), continuous sonication (triangles), or ball milling (squares).

4.5 Deposition

In order to make the batteries, the cathode film was done using two different deposition methods, one with a standard microgravure rod (wire size #22) and another with an aerosol sprayer (Paasche). In the standard microgravure rod method, the mixture of CNTs and LFP are dispersed in NMP by ultrasonication (25ml NMP for every 1g of solids). Then this suspension is dried in a vacuum flask filter, and then dried further in a vacuum oven at 80°C for 12 hours. A binder solution is prepared by mixing PVdF in NMP. The NMP is brought to just below the melting point of PVdF and mixed vigorously. The PVdF is mixed in at a 1% concentration. This viscous liquid is then added to the dry mixture of CNTs and LFP. Typically, enough is added

to obtain 5% PVdF in the final solid solution. After adding the viscous binder solution to the dry mixture, it will form a slurry paste the can be deposited on the Aluminum film easily. The microgravure rod is used to control the thickness of the film, and also to create a consistent deposition of the paste on the Aluminum film. An amount is dropped at the top of the film and the rod is rolled over the backing to distribute the material. The film is then heated with a heat gun until dry. Multiple layers can be deposited in this manner, but delamination can be a problem if the film is too dry underneath. A large fraction of material is lost in the grooves of the rod. For making 5" by 5" squares, this accounts for more than half of the prepared material.

In the aerosol sprayer method, the first step is also to sonicate the mixture of CNTs and LFP in NMP (25ml NMP for every 1g mixture). The binder solution is prepared in a similar manner to that described above. This binder solution is added to the solution of CNTs and LFP in NMP and the whole mixture is stirred at 350 rpm for another 20 minutes. This mixture is sprayed on a hot aluminum film. The aluminum backing is secured on a hot plate (160°C or 120°C on the surface unless otherwise noted.) The mixture is sprayed with 40 PSI nitrogen. Between each pass, the film was allowed to dry.

Film Deposition: Cathode films were prepared by microgravure slurry, aerosol spray, and atomizer spray, as seen in Figure 4.6. Each of these films was prepared with 5% CNTs and 5% PVdF in NMP with the commercial LFP. The atomized sprayed cathode appeared to have the most cohesion formed within the droplets as they were sprayed. The droplets on the surface were largely preserved even after compression. As such, the film had a higher tendency to crack since

material did not form strong interconnections. On the other hand, the aerosol sprayed cathode and the slurry cathode were well connected and did not form cracks.

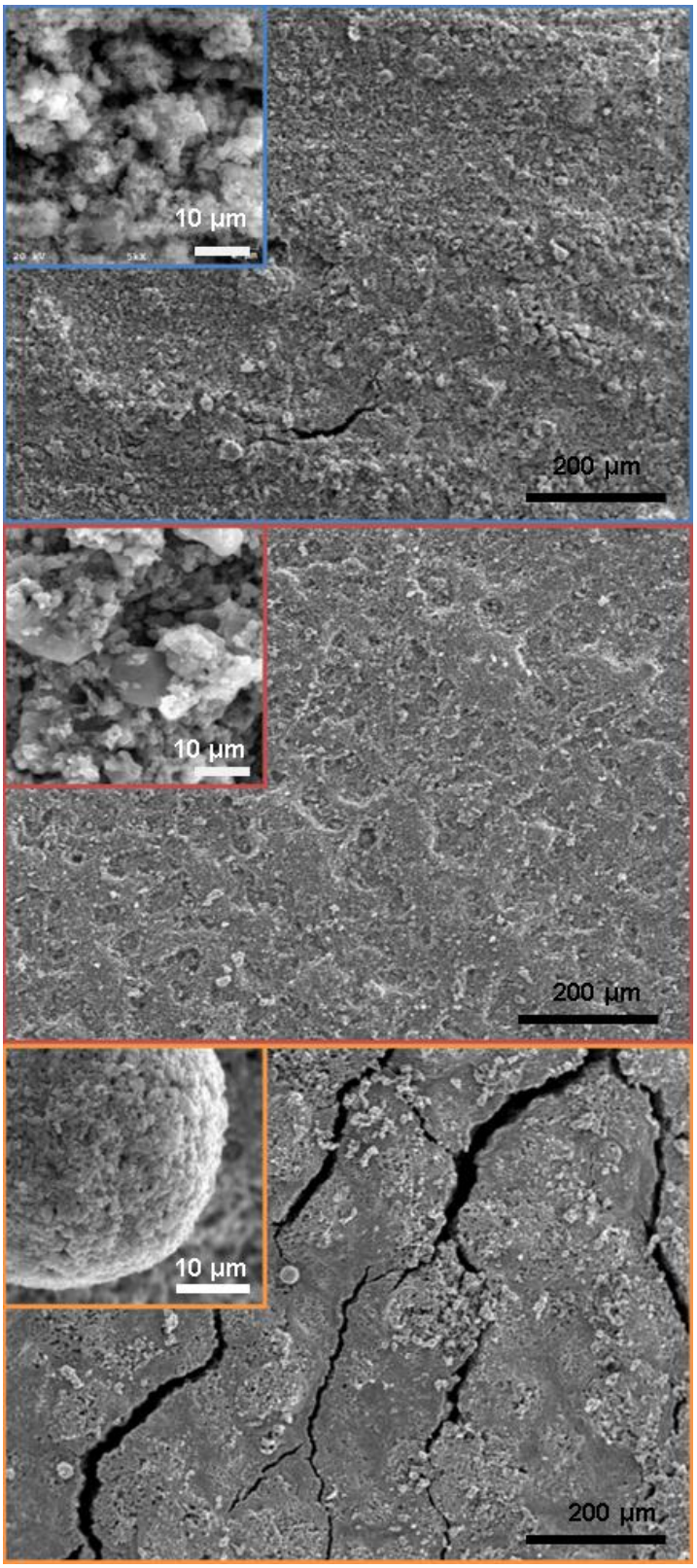

Figure 4.6. Films of LFP, CNTs and PVdF prepared by microgravure drawn down method (top), aerosol spray (middle), and atomized spray (bottom).

The spray-coated film had the best electrochemical performance, see Figure 4.7, of the three deposition methods with a capacity of 100mAh/g at 5C, followed by the slurry (85 mAh/g). Based on the SEM the aerosol cathode appears to have been more effective at dispersing the PVdF and CNTs. The atomizer sprayed cathode seems to have been too effective at coating the droplets with PVdF, which partially insulated them from the electrode.

Although spraying techniques have been suggested to be highly advantageous, the specifics of the conditions of the film deposition have not been clearly stated, the most important step in spray deposition is the removal of the solvent.[1,57] The high surface tension in small droplets will force materials to make intimate contact as the droplet size is reduced as the solvent evaporates. In the atomized sprayed cathode, the solvent is mostly removed even before the droplet lands on the surface, due to the high energy of that technique. In the slurry deposition, drying is controlled by a heat gun, and is only begun after the whole film has been deposited. Additionally, the rate of drying can occur much more slowly.

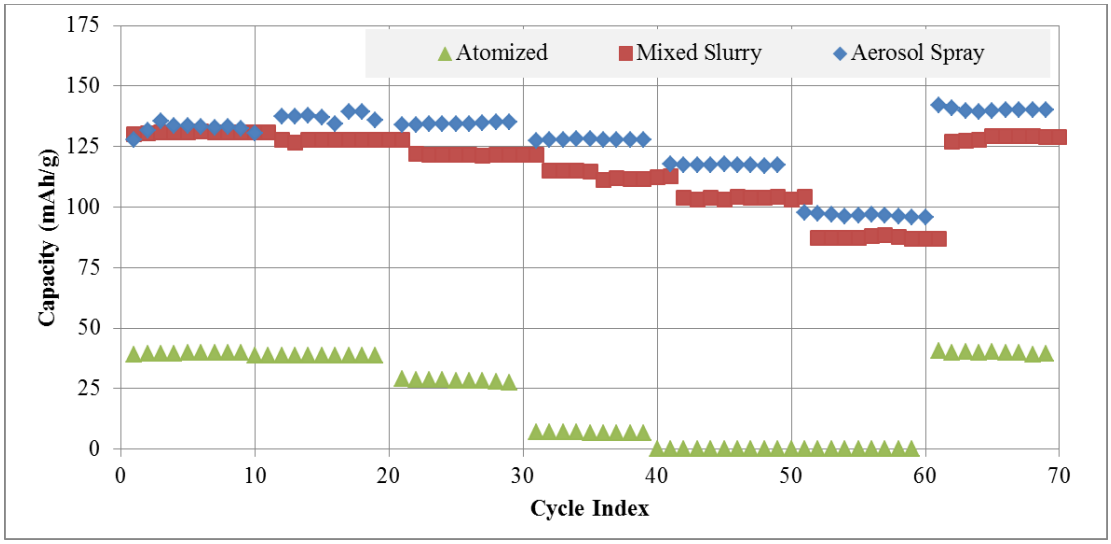

Figure 4.7. Effect of deposition techniques on the discharge capacity.

4.6 Drying

The speed of aerosol spray deposition depends on the rate at which the material can be dried once it is on the backing. This will depend on the surface area (A), the temperature of the backing (T_i), the partial pressures of the solvents present, the mass fraction of solvent to remove (X), and possibly the size of the droplets extruded out of the aerosol nozzle on the surface. The drying rate (W) is a combination of convective (Eq. 4.2) and conductive mechanisms (Eq. 4.3.). Where U is the integral coefficient of heat transmission, λ_i is the latent heat of vaporization of the liquid and k_i is the coefficient of mass transport.

$$W = \frac{S}{A}\left(-\frac{dX}{dt}\right) \qquad \text{Equation 4.1.}$$

$$W_c = k_i(X_i - X_{air}) \qquad \text{Equation 4.2.}$$

$$W_c = \mathrm{U}/\lambda_i(T_{air} - T_i) \qquad \text{Equation 4.3.}$$

The dry air flowing over the sample and the heat from the hot plate drive the solvents out of the sample into the air. During the aerosol deposition, the small droplet size will increase the rate of solvent removal before deposition onto the backing surface, due to the high surface tension. Individual small droplets on the surface will also have increase drying rates due to the surface tension. During aerosol deposition, the drying time varied between a few seconds per layer to minutes. Thus at low temperature the spraying time could exceed 4 hours.

In Figure 4.8(a), we show the discharge capacity of batteries made from films deposited with NMP as the only solvent where the hot plate setting was varied from 100°C to 200°C. All films were subsequently dried in a vacuum oven at 120°C overnight to ensure there was no residual NMP in the battery. Since NMP has a high

boiling point (202°C), the time between applications to allow the film to dry can be excessive. With the surface temperature below 100°C, the battery fails when delivering current densities of C/2 and does not recover. At higher surface temperatures the battery improved significantly but still exhibited capacity fade after delivering current densities of 1C and higher. This effect was exaggerated even further with surface temperatures above 200°C.

In order to reduce the drying time and to reduce the evaporation temperature a solvent that was compatible with PVdF and miscible with NMP was sought. Water, Isopropanol, and Ethylene cause the PVdF to coagulate. Acetone was identified as a potential candidate. Mie scattering is observed in all samples but the acetone in Figure 4.9. Acetone was added in a 1:1 ratio to NMP in the spray mixture after ultrasonication. Due to the small droplet size of the aerosol spray, the Acetone evaporates even before contact with the surface. This effectively reduces the droplet size and increases the rate of evaporation. As seen in Figure 4.8(b) the temperature of the surface during deposition impacts the discharge capacity. In particular the batteries exhibit capacity fade at both low and high temperature depositions. Finally, Acetone was added during the sonication step, Figure 4.8(c). The film deposited at a lower temperature still exhibited capacity fade at 5C, although the capacity returned when the C/10 current density returned for both batteries.

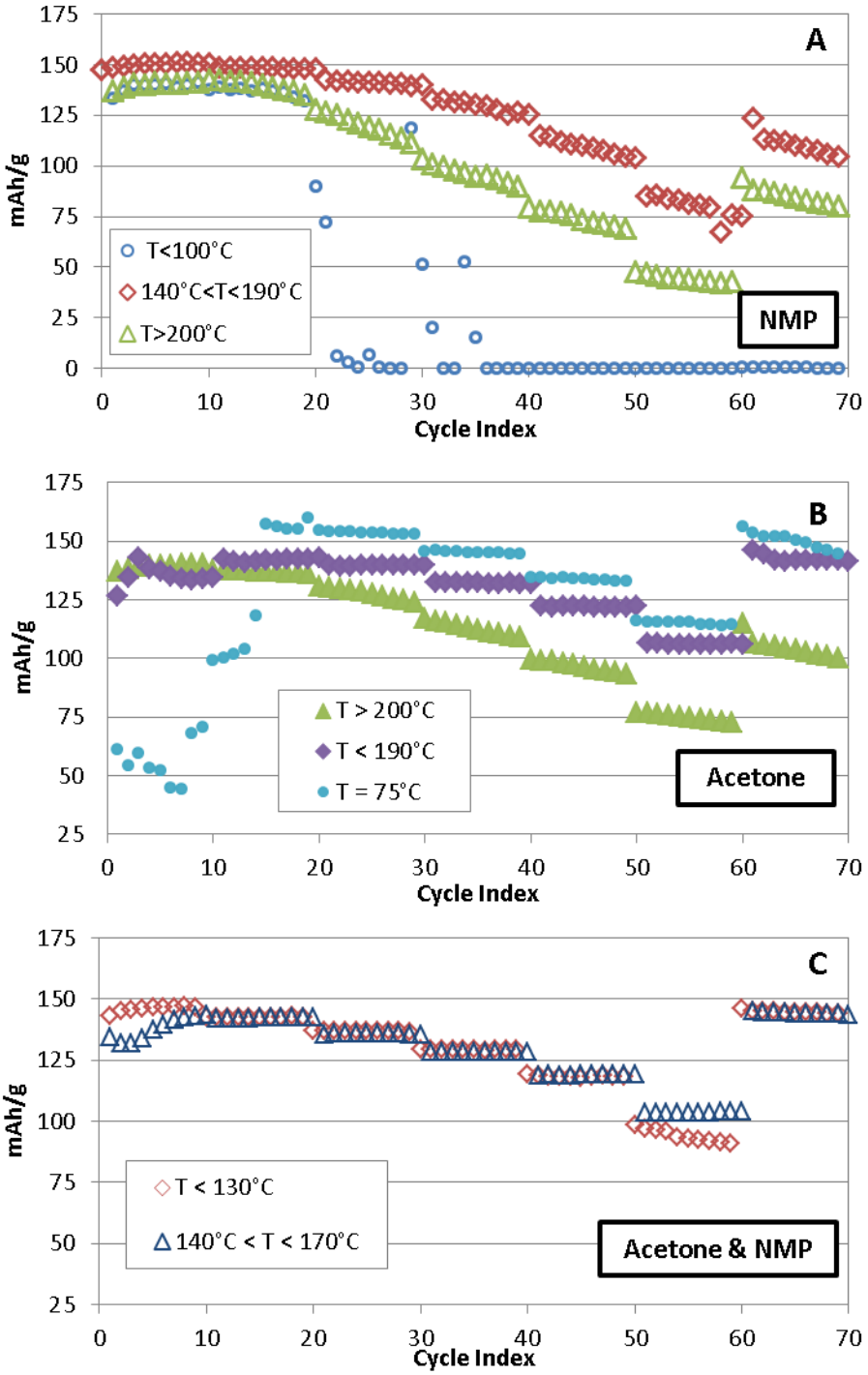

Figure 4.8. Capacity of batteries made by aerosol spray deposition (a) with NMP as the only suspention solvent, (b) with acetone added to NMP before spraying, and (c) with acetone and NMP mixed during sonication step. Depositions were done over a range of temperatures: 130°C(diamond), 140°C and 190°C (triangle), and above 200°C (triable). Acetone was mixed in at 1:1 vol/vol.

a b

Figure 4.9. Mixing of PVdF in Acetone, 2-Propanol, Ethylene, and Water (a) after mixing and (b) after one hour.

4.7 Hot Pressing, Punching, and Assembly

All cathode films were pressed for two minutes at 5,000 kg between Kapton® at 200°C. Films with low PVdF content were much more likely to crack or exhibit delamination issues. Furthermore, any area where the backing was not clean would delaminate in this step as well.

All samples were subsequently punched into ½" disks and dried in a vacuum oven at 120°C for 12 hours before being stored and assembled in a dry box. The films were packaged in 2032 coin cells (Pred Materials Inc.) with a Celgard 2400 separator, versus a Lithium anode, and with 1M $LiPF_6$ in EC:DMC (1:1 v/v) as the electrolyte. See Appendix B for a review of issues with packaging, identification, and the solutions.

Ultra-thin areas of the sample were avoided. It was found that samples with less than 2 mg of material would exhibit higher than reasonable capacity due to the ultra-thin film present. All samples measured should have at least 2 mg of active material.

4.8 Temperature

Although under anaerobic conditions (or reducing conditions) the $LiFePO_4$ is stable up to high temperature (500 to 900°C) with oxygen present it was found that LFP undergoes a phase change above 300°C. Due to the long drying rates at low hot plate temperature, it is tempting to drive off the solvents with high temperature hot plate or hot air flows.

After discovering films that were heated to 300°C in air had poor cycling capacities (2 mAh/g) we investigated a film with XPS, Figure 4.10. Since the Lithium peak is hard to resolve with XPS it was ignored in this analysis. The ratio of the concentration of each element in $FePO_4$ should be 1:1:4 (Fe, P, O). Since iron and phosphor should be present in equal concentrations, the lack of phosphor in Table 4.1 relative to iron indicated that the surface had evolved. Either the film had lost Phosphate and Oxygen content or Fe had migrated to the surface. In either case, the interface is no longer $LiFePO_4$.

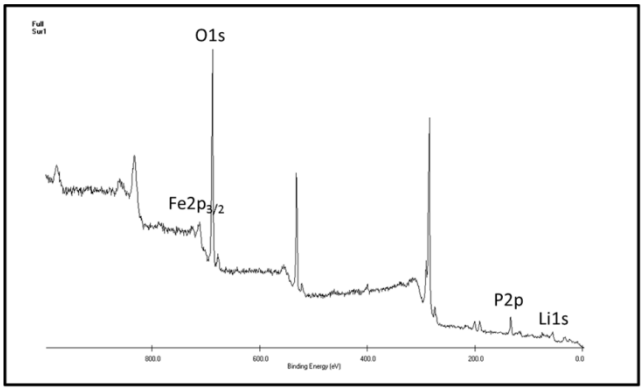

Figure 4.10. XPS of source $LiFePO_4$ and a film calcined at 200°C.

Table 4.1 Atomic Concentration as measured by XPS of source $LiFePO_4$ and a film calcined at 200°C.

element	Li	Fe	P	O
Untouched $LiFePO_4$	69.77	4.30	4.00	21.93
High Temp. Aerosol Spray	68.56	3.66	3.60	24.17

4.9 Summary

We have optimized the deposition conditions for producing composites with CNTs as the conductive additive. The initial efforts used CNT pastes with PVdF already mixed with the CNTs, Figure 4.11(a). These cathodes exhibited very poor capacity due to the bundles formed by the CNTs and the lack of dispersion of CNTs across the cathode. A ultrasonicated mixture of CNTs in the slurry produces a much higher capacity cell, Figure 4.11(b). Dispersion of the CNTs is essential to create cathodes with high capacity.

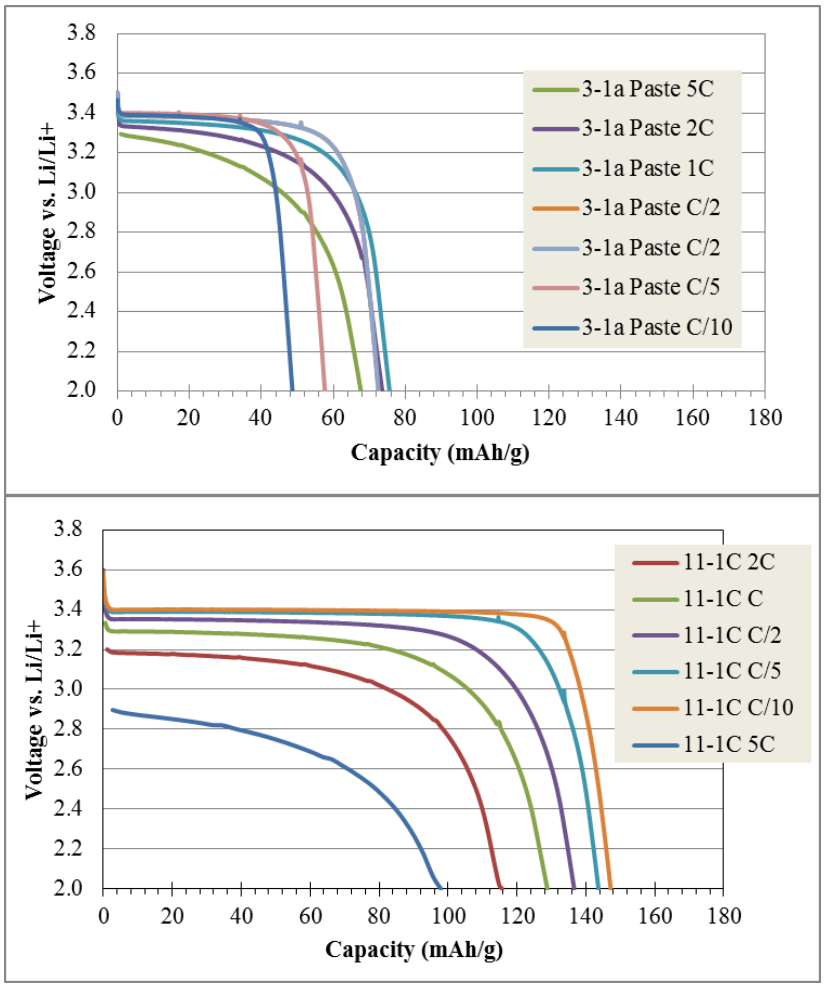

Figure 4.11. Voltage vs. Capacity at different C-rates using (a) CNT paste (series 3), (b) CNT mixed slurry (series 11) made with commercial $LiFePO_4$ and 5% CNTs and 5% PVdF.

We found that optimization of the cathode composite by aerosol spray deposition would further improve the charge capacity and cell potential during discharge, Figure 4.12(a). We have further optimized these parameters including: formulation, dispersion method, dispersion solvents, and deposition hot plate temperature. The optimal formulation was 5% CNTs and 5% PVdF. The optimal dispersion method was continuous ultrasonication for 20 minutes with all materials present in a NMP and Acetone mix. The optimal dispersion solvent was found to be NMP and Acetone with at least 50% Acetone. The optimal hot plate deposition temperature was found to be between 150 and 190°C.

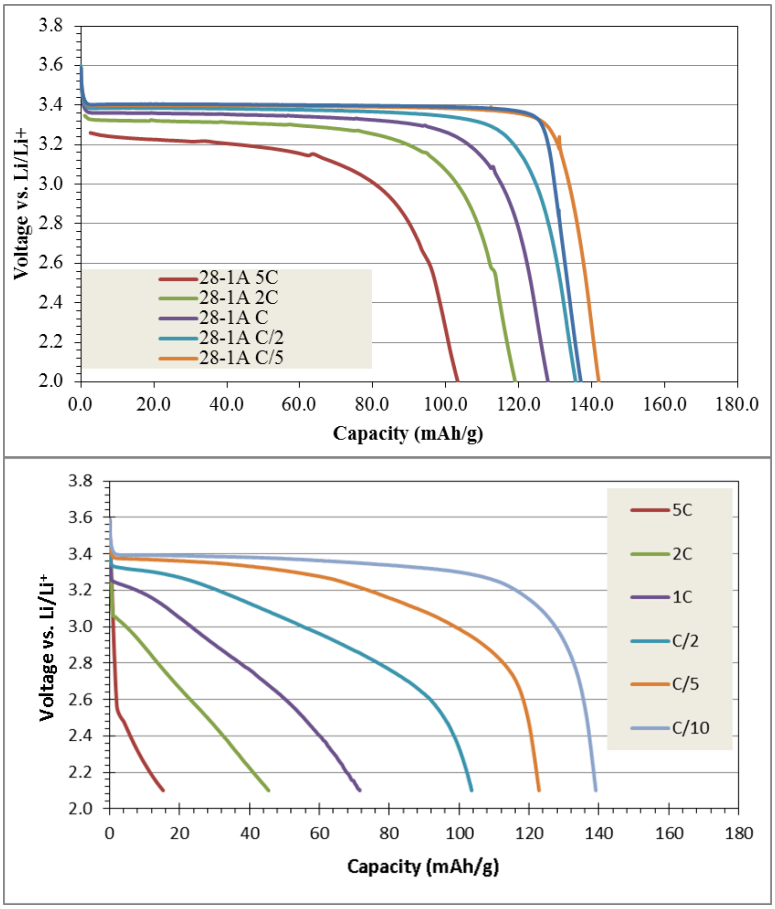

Figure 4.12. Voltage vs. Capacity at different C-rates using (a) Commercial $LiFePO_4$ made with 5% CNTs and 5% PVdF (series 28) and (b) 20% carbon black both made by aerosol spray deposition (series 51).

We investigated the benefit of the CNTs vs carbon black and compared the deposition methods using EIS. In Figure 4.13 the semi-circle crossing point for the aerosol spray is at 100Ω, nearly half that of the drawn-down method and one fifth of the carbon black mixture. This represents a significant decrease in the CPE resistance. If the porous surface model is used this represents a much more effective surface contact.

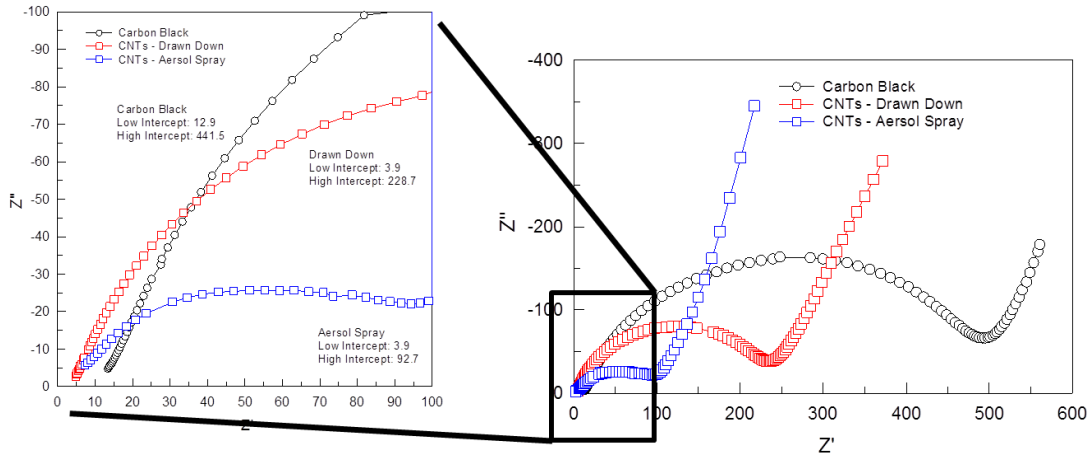

Figure 4.13. Electrode Impedance Spectroscopy of cathodes (blue square) aerosol sprayed with CNTs, (red square) drawn down with CNTs, and (circle) aerosol sprayed with carbon black.

The initial resistance crossing point with both the drawn down and the aerosol spray are reduced to 3.9Ω. This is the most direct measure of the electrode resistance.

The slope of the Warburg, the increasing tail, in all these samples is the same. This is to be expected as the cathode material is identical and thus the rate of phase change after polarization due to the electrode contact is accounted for should be the same.

Chapter 5. Embedding CNTs into Lithium Iron Phosphate

5.1 Motivation

The best batteries have high energy density, can discharge and charge fast, and will do so for thousands of cycles. The primary limitation to high current densities in $LiFePO_4$ is the diffusion of lithium in and out of the crystal.[58]. Since $LiFePO_4$ is also not particularly conductive, the electrode contact should be as near as possible in order to enable the fastest diffusion pathways. Here we investigate the formation of $LiFePO_4$ with CNTs that can form an internal distributed network, thus shorten the path length for diffusion. Growth was achieved using a Polyol synthesis.

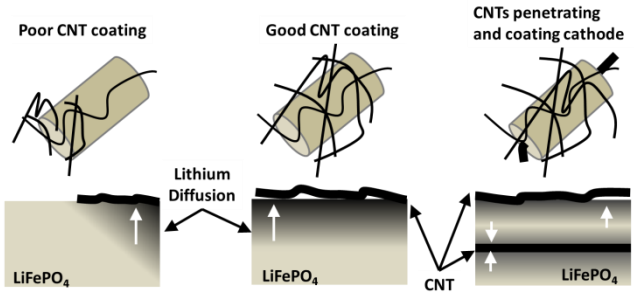

Figure 5.1. A Representation of films with poor (left) and good (center) dispersion of the CNTs. Lithium Iron Phosphate grown onto CNTs would have an even shorter diffusion length (right).

Highly conductive few walled carbon nanotubes were used in this work for their durability and high aspect ratio. Based on the analysis of the conductivity of CNT dry powders and 5% CNT composite, (see Figure 5.1) we selected the SMW-200. The SMW-200 from Southwest Nanotechnologies was the most highly conductive and produced the highest conductivity in the composite.

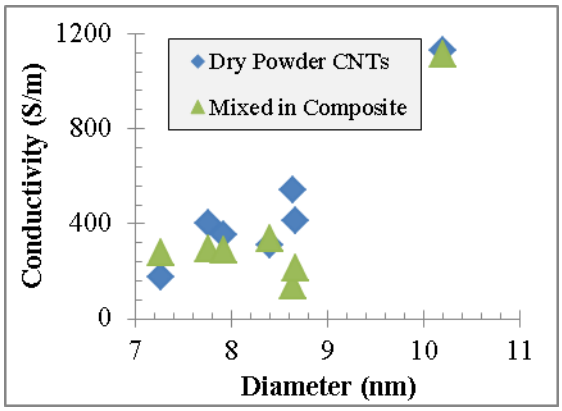

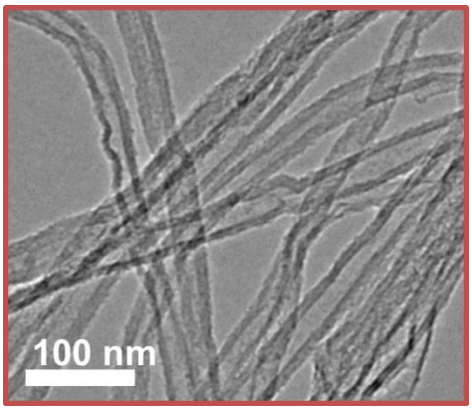

Figure 5.2. Multi-walled CNTs were evaluated as dry powders and in composites (left). Under TEM, the selected CNT appears highly crystalline with few bends or defects (right).

5.2 Initial Material Formation

$LiFePO_4$ was synthesized by reducing iron acetate, lithium acetate, and ammonium dihydrogen phosphate with ethylene glycol as the reducing medium, Table 5.1. The reaction is allowed to run for 18 hours open to the air (without a vapor lock). The materials were then annealed at 550°C under Argon for 6 hours. Based on the SEM and XRD analysis $LiFePO_4$ was the only crystalline material formed. Nevertheless, the material did not have large domains. PVP and Gum Arabic were included in the reaction to increase the dispersion of the CNTs. The formation of the crystalline LFP was further limited as can be observed in the XRD of the samples, Figure 5.3.

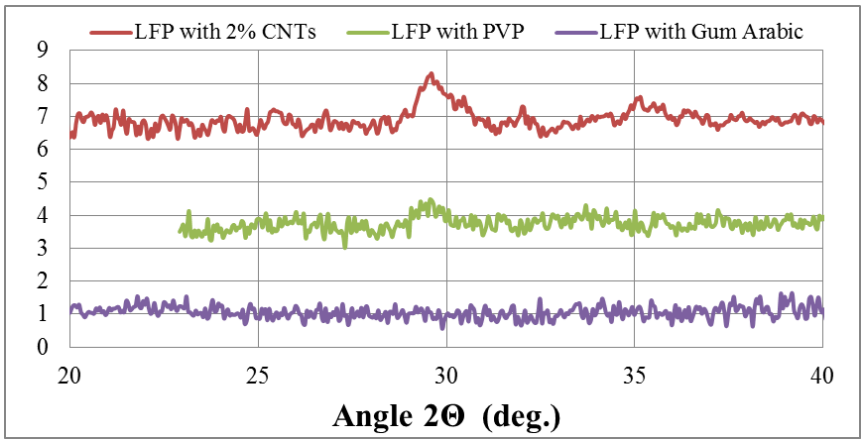

Figure 5.3. XRD analysis of polyol grown $LiFePO_4$ with 2% CNTs, CNTs and PVP in water, and CNTs and Gum Arabic in water.

Table 5.1. Precursors to Lithium Iron Phosphate Growth.

Name	Properties	Role
Ethylene glycol	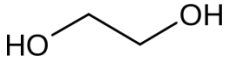	Supporting Solvent & Reducing medium Boiling point: 197.3°C
Triethylene glycol	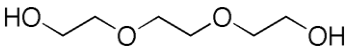	Supporting Solvent & Reducing medium Boiling point: 285°C
N-Methyl-2-pyrrolidon	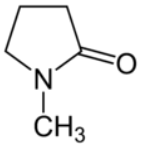	Dispersing Solvent Boiling point: 202°C
Dihydrogen Oxide	H_2O	Dispersing Solvent Boling point: 100°C
Lithium Acetate	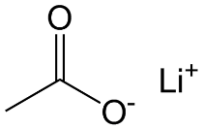	Lithium Source
Iron Acetate	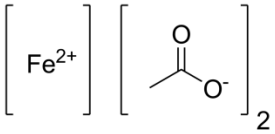	Iron Source
Ammonium Dihydrogen Phosphate	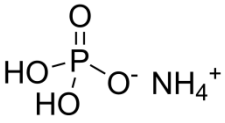	Phosphate Source

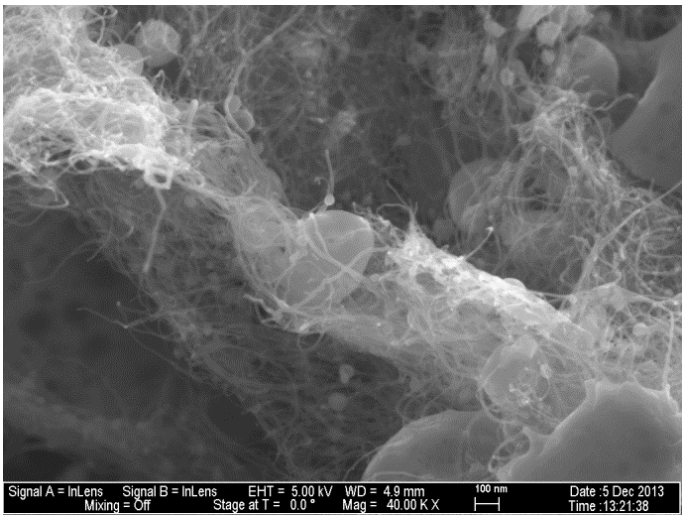

a

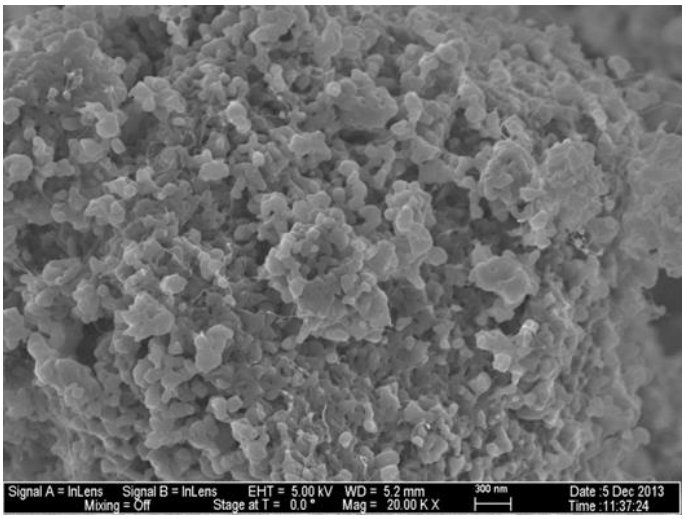

b

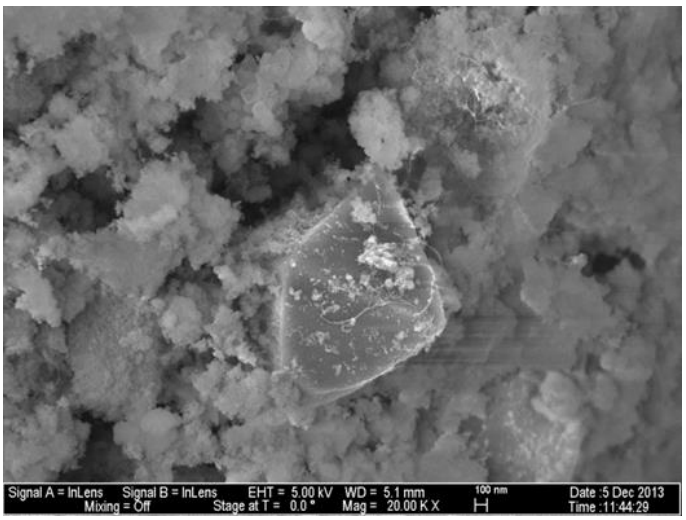

c

Figure 5.4. SEM micrographs of $LiFePO_4$ formed at 160°C with 2% CNTs without a vapor lock (a), with CNTs dispersed in PVP in water (b), with CNTs dispersed in water with Gum Arabic (c).

By including PVP, the particle size was drastically reduced but so was the crystallinity. It appears that the introduction of water inhibited the growth reaction. Based on these results this suggests an anaerobic reaction might be required.

5.3 Anaerobic LFP Growth

The above reactions were repeated with a vapor lock and nitrogen bubbler to ensure an anaerobic growth condition at a series of temperatures. The improved conditions have increased the crystallinity compared to the previous 160°C reaction, Figure 5.4.

The reaction temperatures 160°C, 180°C, and 190°C were investigated. The morphology of $LiFePO_4$ formed at 180°C is strikingly different from anything obtained at 160°C where the CNTs did not appear to impact the $LiFePO_4$ growth, Figure 5.6(c). At 180°C, the produced material appears to coat the CNTs to forms cylinder, Figure 5.7(c). Furthermore, nearer the ethylene glycol boiling point (190°C) the $LiFePO_4$ forms crystallites that are attached along the CNTs, Figure 5.8(c). We also observed a large fraction of the material forming larger crystals as well. XRD analysis demonstrates that the domains of these materials are much smaller than the solid state reaction produced $LiFePO_4$. Based on the relative heights of the peaks it appears the lithium uptake was not complete, the [121] peak should dominate with full lithium uptake instead of the [211] peak. This is reflected in the discharge capacity with rather unremarkable performance, see Figure 5.9, although the EIS spectra do demonstrate a reduction in impedance with increasing reaction temperature. To test these films we packed them in a half cell versus a lithium anode, $LiPF_6$ electrolyte, and cycled them with the standard cycling reaction.

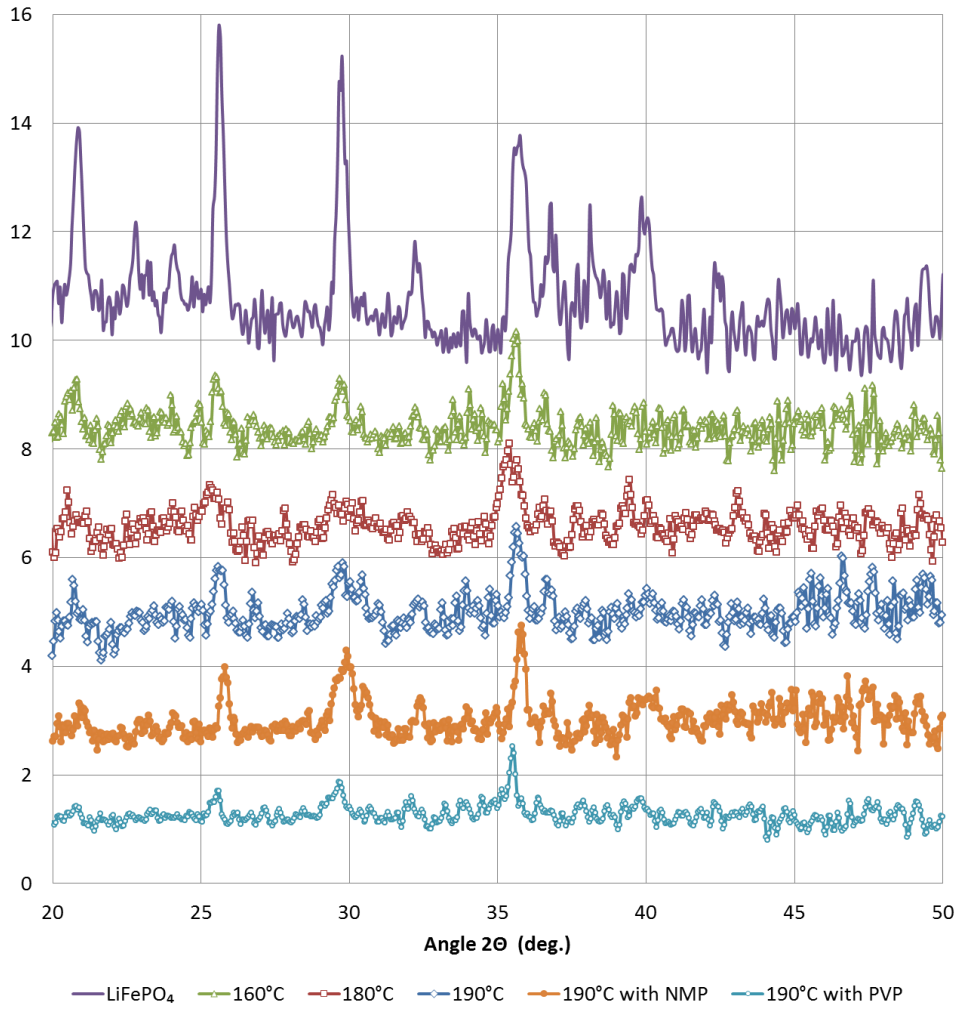

Figure 5.5. XRD diffractogram for $LiFePO_4$ solid state reaction reference and polyol formed at 160°C, 180°C, 190°C, 190°C with NMP, and 190°C with PVP and NMP.

Table 5.2. Diffraction peak angles, plane indices, and relative intensity.[59]

Angle 2θ	hkl	Intensity
17.348	[020]	34
20.768	[011]	76
22.666	[120]	26
24.019	[101]	10
25.545	[111]	70
29.700	[121]	100
32.187	[031]	34
35.554	[211]	81
36.496	[140]	25
36.886	[221]	15
39.597	[112]	19
42.189	[112]	15

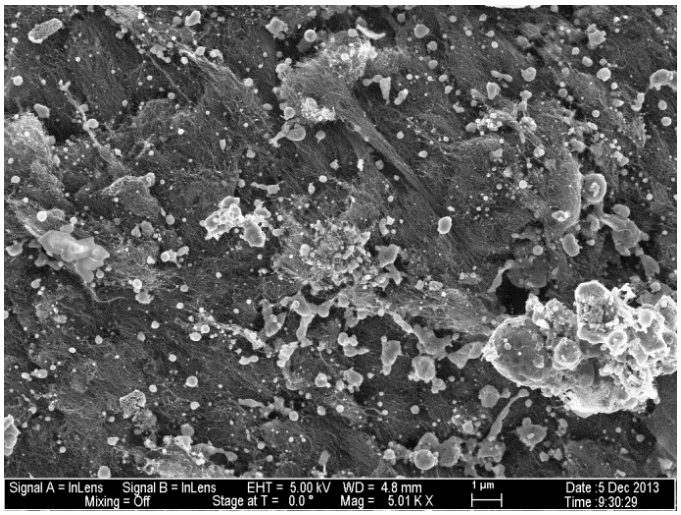

a

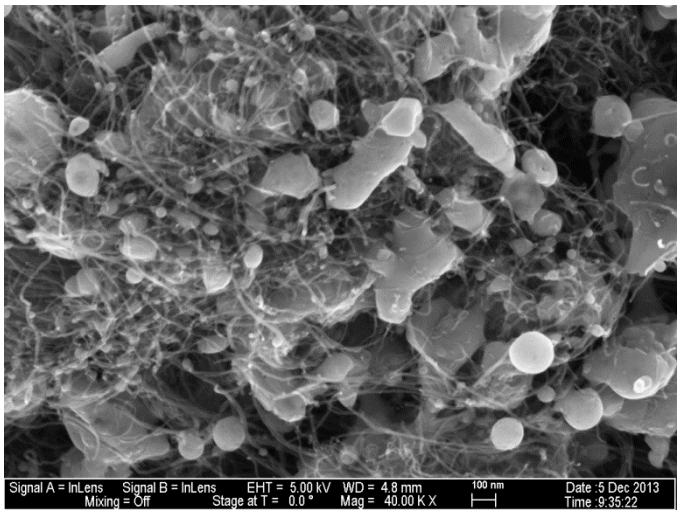

b

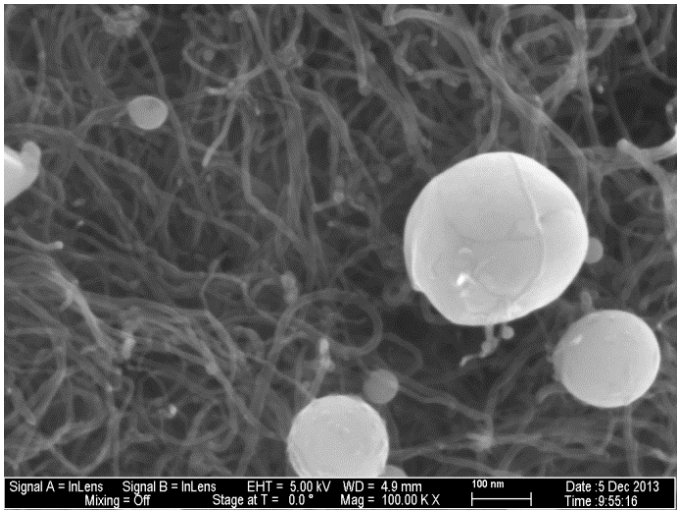

c

Figure 5.6. SEM micrograph of $LiFePO_4$ grown by polyol in ethylene glycol at 160°C under anaerobic conditions.

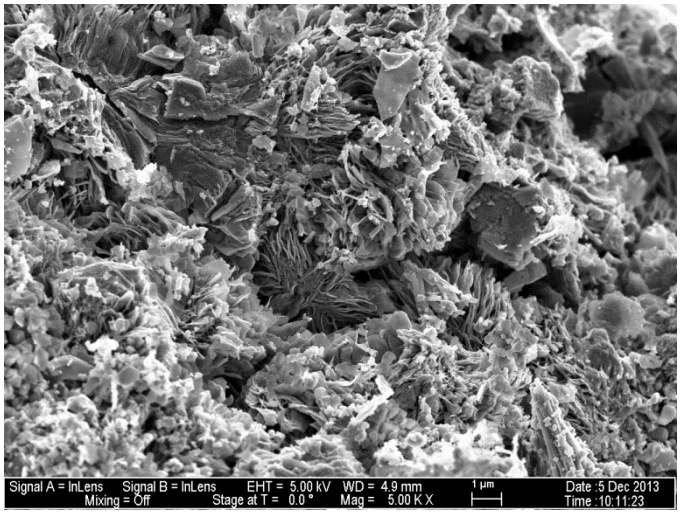

a

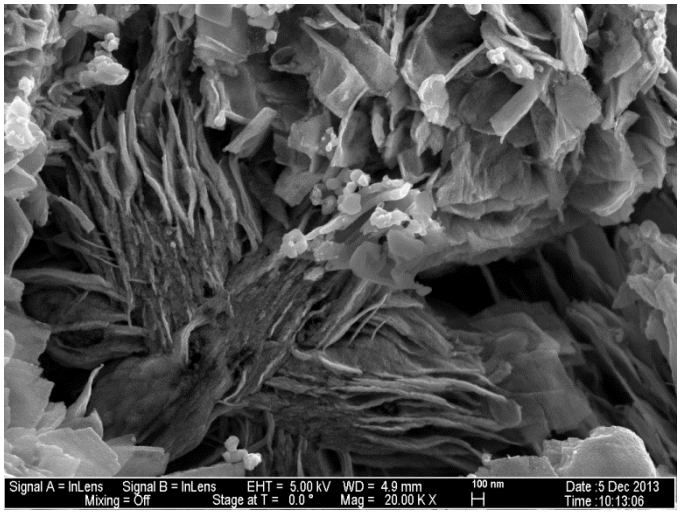

b

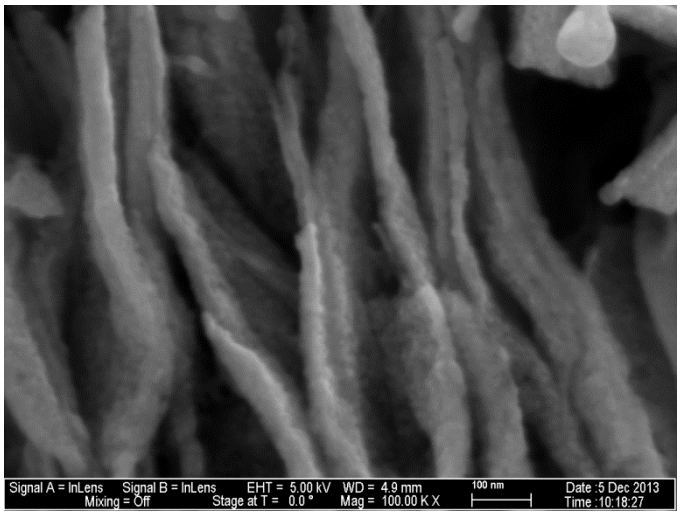

c

Figure 5.7. SEM micrograph of $LiFePO_4$ grown by polyol in ethylene glycol at 180°C under anaerobic conditions.

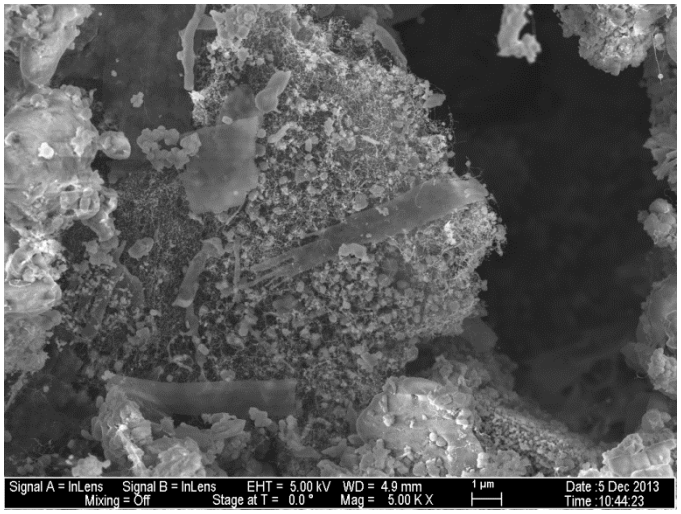

a

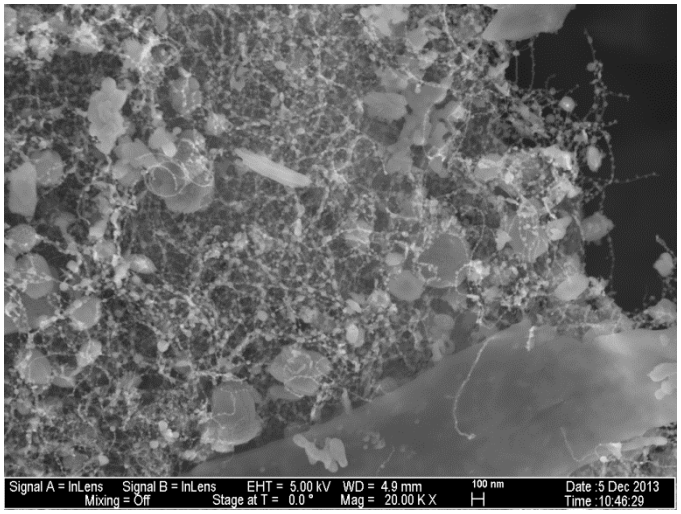

b

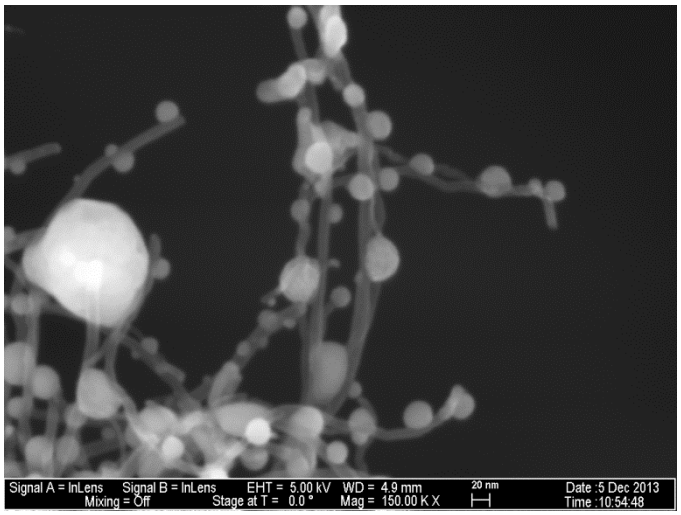

c

Figure 5.8. SEM micrograph of $LiFePO_4$ grown by polyol in ethylene glycol at 190°C under anaerobic conditions.

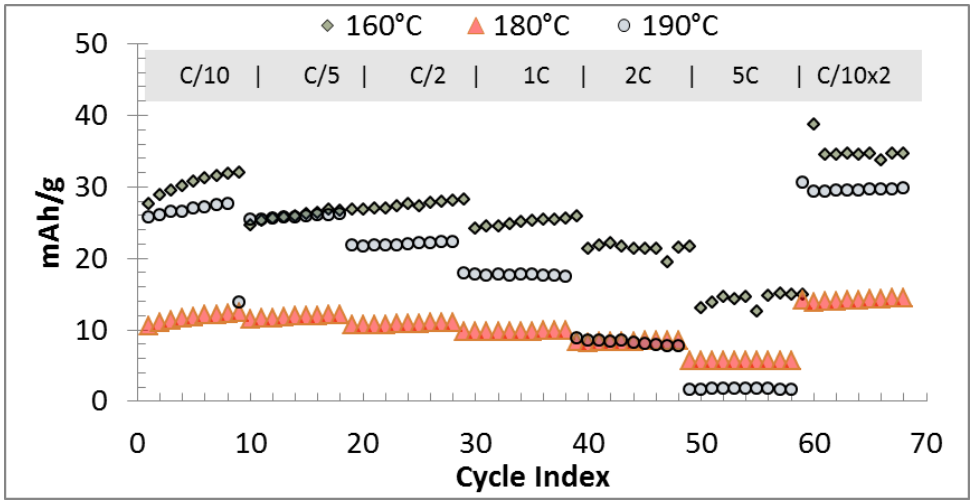

Figure 5.9. Electrochemical Performance of polyol (ethylene glycol) grown LFP with a vapor lock at different reaction temperatures.

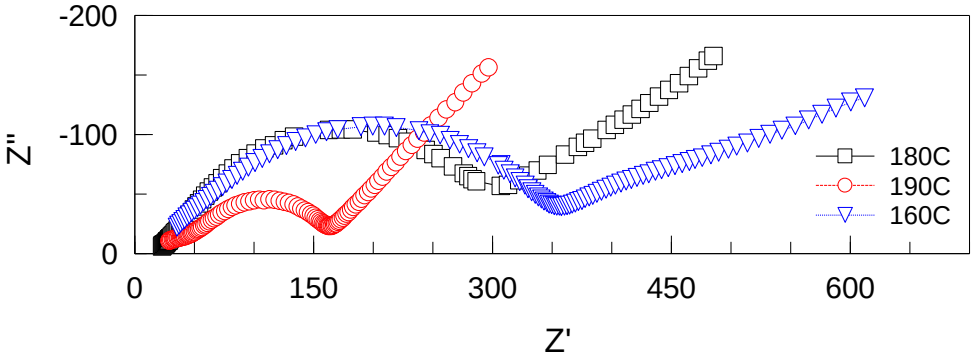

Figure 5.10. Electrochemical Impedance of $LiFePO_4$ grown by polyol in ethylene glycol under anaerobic conditions, cells held at 3.4V vs open circuit.

Although the relative intensities of the XRD diffractogram do not match the reference material, there were no other discernable peaks observed in the diffractogram. Additional peaks would be present if other possible crystallites were formed, Figure 5.5. Since these peaks were not present, only $FePO_4$ and $LiFePO_4$ were formed.

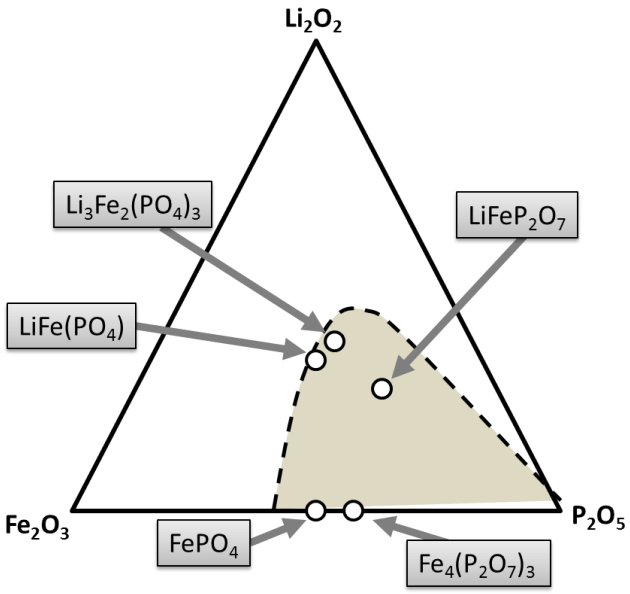

Figure 5.11. Crystal phases with Li-Fe-P and the glass-phase area.[60]

5.4 Growth with Dispersion

The formation of large particles in the matrix suggested that there might have been bundles of CNTs still present in the growth reaction thus limiting effectively utilizing all the surface area. We ultrasonicated the CNTs in N-Methyl-2-pyrrolidone (NMP) to ensure that they were well dispersed. The $LiFePO_4$ formed (190°C) in this reaction produced larger and extended structures that were interconnected (Figure 5.12). The $LiFePO_4$ did not coat the CNTs as it did in previous reactions. We also utilized polyvinylpyrrolidone (PVP) in NMP to disperse the CNTs. The $LiFePO_4$ (190°C) reaction produced much smaller particles with PVP introduced as compared to the above reaction (Figure 5.13).

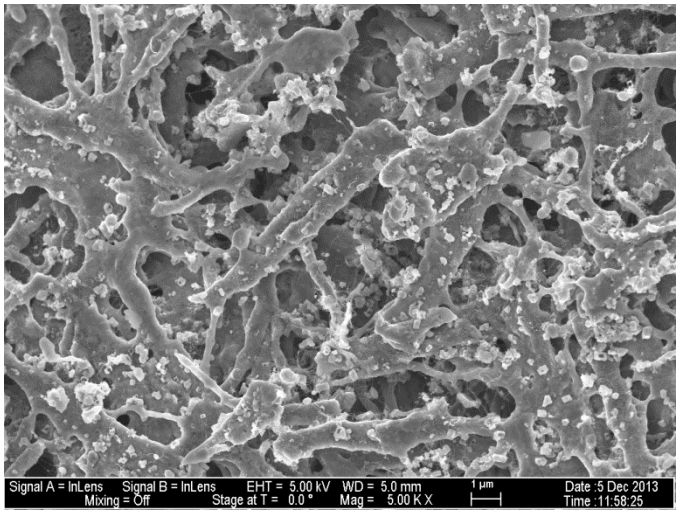

a

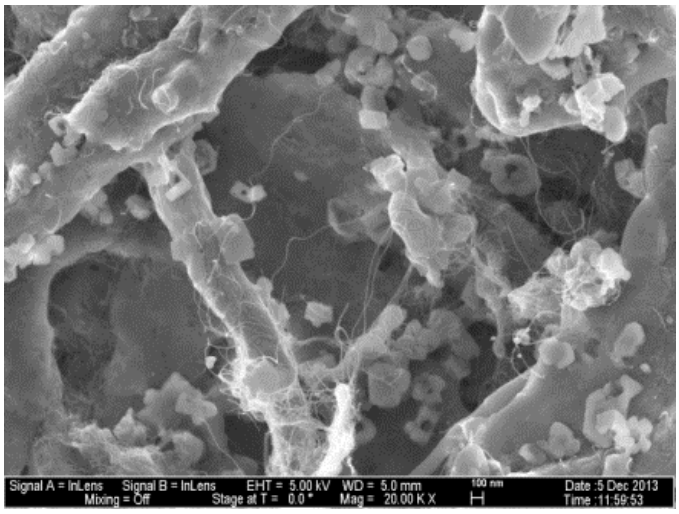

b

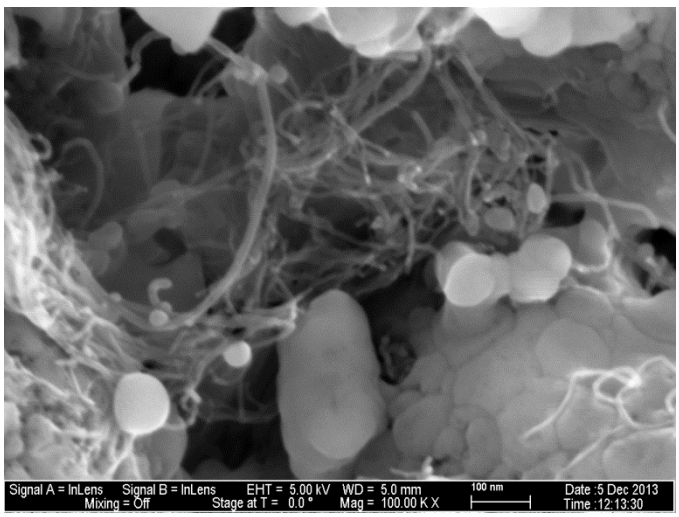

c

Figure 5.12. SEM micrograph of $LiFePO_4$ grown at 190°C with 2% CNTs dispersed with NMP.

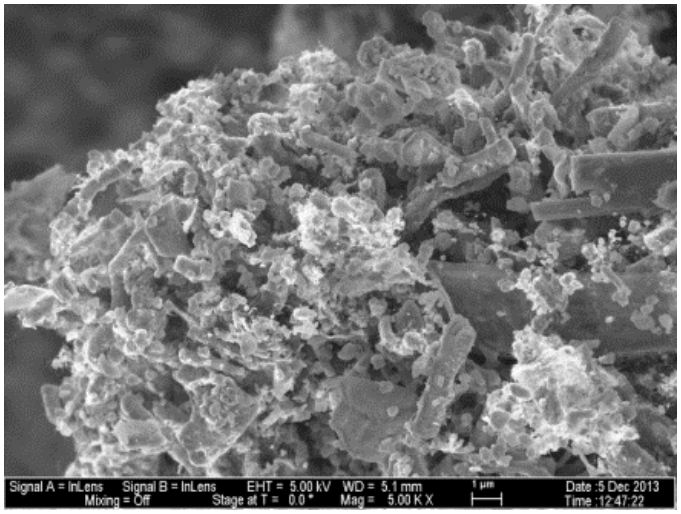

a

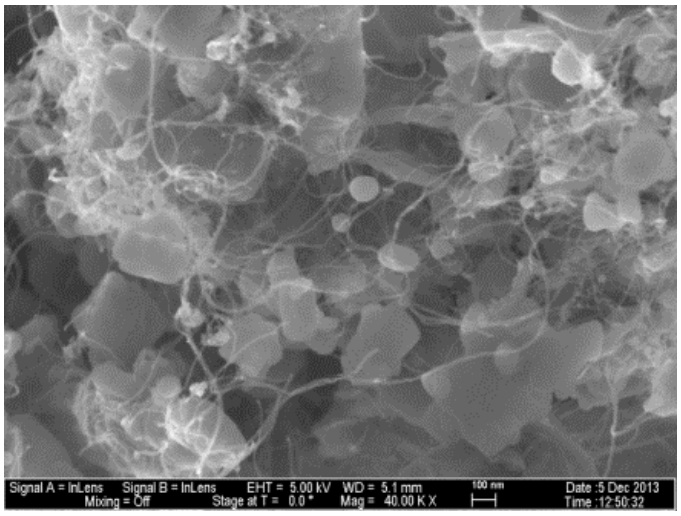

b

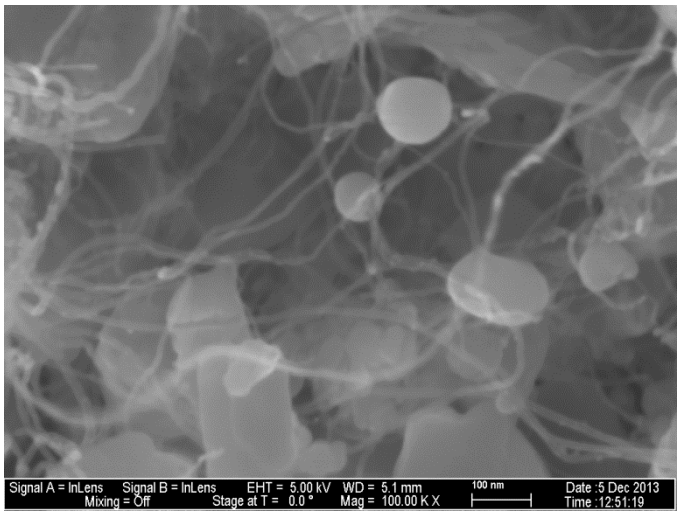

c

Figure 5.13. SEM micrograph of $LiFePO_4$ grown at 190°C with 2% CNTs dispersed with PVP in NMP.

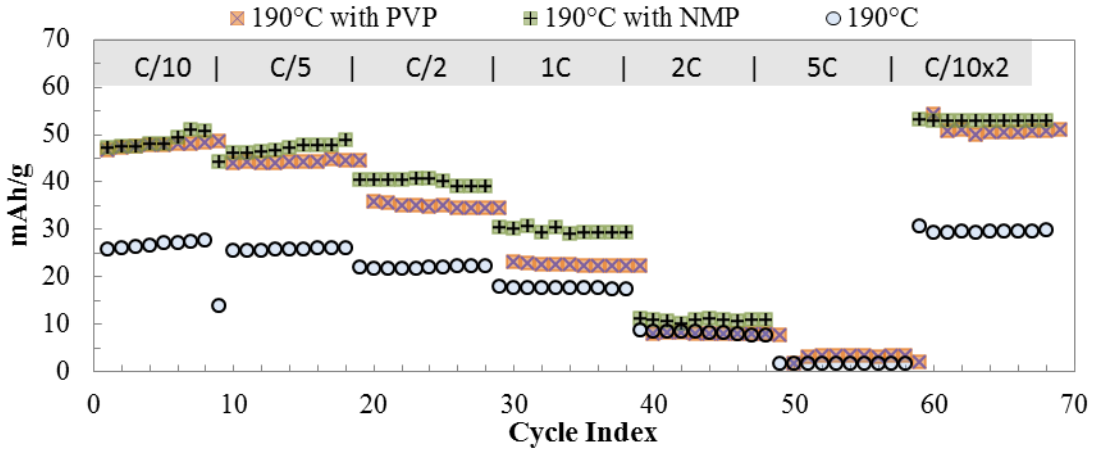

Figure 5.14. Discharge capacities of $LiFePO_4$ grown at 190°C with 2% CNTs dispersed with NMP and CNTs dispersed with PVP in NMP.

Although the capacity at low C-rates is increased for cathodes made with NMP and PVP, the capacity at higher currents does not change. This suggests a diffusion limitation at the particles. Based on stable capacity at low C-rates and the small domains as determined by XRD it is most likely that defects in the battery particles are the primary constraint.

5.5 Summary on Growth of $LiFePO_4$ with embedded CNT

We investigated methods to incorporate CNTs into battery particle formation. Specifically growing $LiFePO_4$ on the CNTs . The LFP precursors were placed in an ethylene glycol a bath medium with CNTs dispersed in combinations of water, n-methyl-2-pyrrolidone, and surfactants and heated to the reaction temperature for 18 hours. We have demonstrated the formation of battery material on CNTs using the polyol process is viable. The initiation of growth on CNTs is highly dependent on the temperature of the reaction. Common CNT dispersing agents reduced the contact with LFP particles and impacted the crystal particle size. Where crystal growth with NMP alone inhibits the interaction of CNTs and increases the crystal agglomerate size and

crystal growth with both PVP & NMP results in materials with reduced particle size. Neither dispersing agent increased the capacity at high C-rates. As noted before, in the XRD peak [121] or the [111] should be higher than the [211] if full Lithiation has occurred. In Figure 5.4, we observed that the sample with the CNTs dispersed with NMP only has the closest ratio to the desired peak intensities, and in addition, this series had slightly higher capacity than the other cells. The domain size in this sample appears to be larger, as the XRD peaks are narrower and well defined. This may be due to the larger particles formed in this reaction. The insertion of Lithium into the structure is difficult to do after the particles are formed. it appears now that excess Lithium acetate should have been used to ensure full uptake during crystal formation.

Some mechanical optimization could have assisted in the material formation, specifically, ultrasonication during the reaction to ensure CNT dispersion. Higher CNT content to meet the full conductivity needs of the composite without further added carbons. Mechanical milling of the produced materials before annealing could have reduced particle size and ensured complete mixing. Although mechanical mixing (ball milling) will reduce CNT aspect ratio. CNTs already encased in LFP should be able to withstand the milling action. Further optimization is required to increase the domain size to enhance the lithium uptake and thus the capacity of these materials.

Chapter 6. Technology Implications

6.1 Motivation—Electric Vehicles

This work was originally motivated for the purpose of increasing the power capacity of Li-ion cells with the eventual goal of making cathodes for use in electric vehicles. Unfortunately the main limitation to high power rates is the Lithium diffusion (since the activation barrier for Lithium diffusion is much larger than the electrons, Table 2.3), not the electronic conduction, though the conductivity does have some small impact on the Lithium diffusion as the driving force moving the ions. We found that by using carbon nanotubes we could replace 20% carbon black with 5% CNTs. This represents a large increase in specific capacity and specific power.

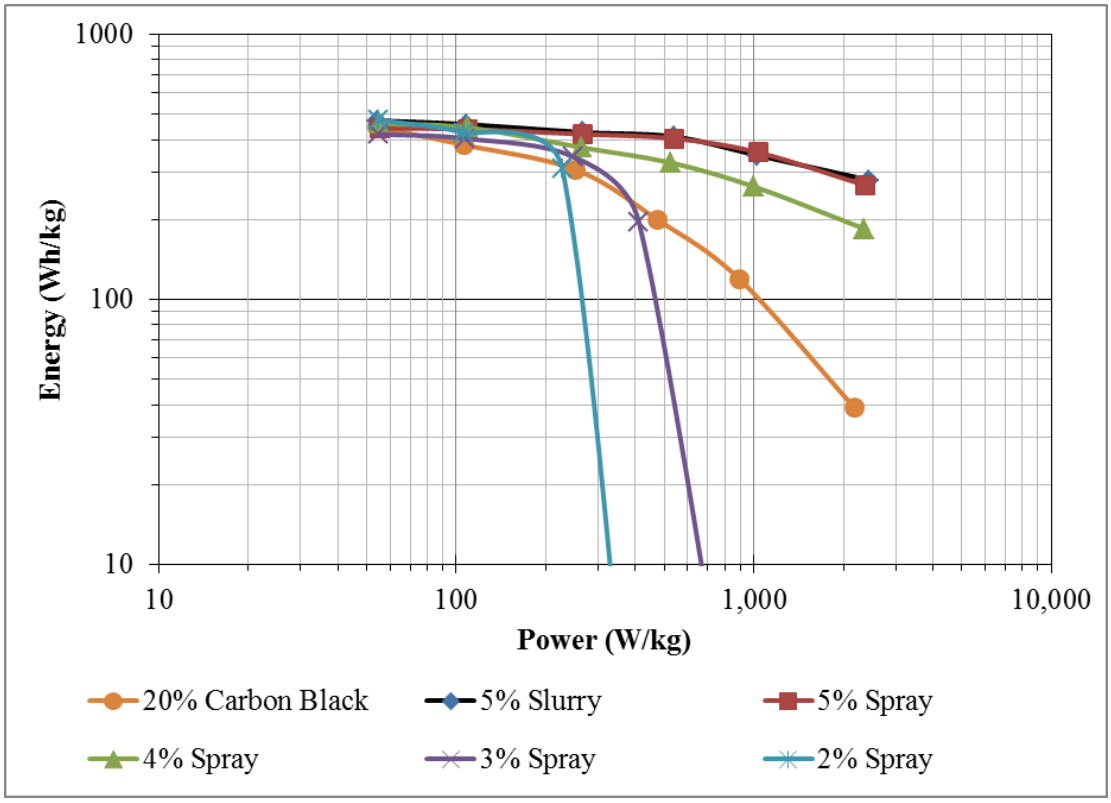

Figure 6.1. Average Performance of Batteries across the Surface Threshold.

Furthermore, we found that the carbon nanotubes networks, when made well, are more resilient than carbon black. The electrode contact decay that is typical of batteries with amorphous conductive additives is resolved by having a net of CNTs that coat the battery particles. The material will swell and crack, it will evolve, as the battery is uses. Nevertheless, the electrode contact will be maintained due to the high aspect ratio of the CNTs, their high strength, and their resilience in the high chemical potential environment.

We would very much like batteries that were long lasting, that carried enough capacity, at a high enough potential to move our cars 300 miles per charge. It would additionally be great if these materials were inexpensive, sustainable, and easy to make. The DOE has developed guidelines for hybrid and fully electric vehicle battery systems that could power our transportation fleet, Table 6.1. These are ambitious and demanding goals and yet no battery system to date has achieved all of them.

Table 6.1. Summary Requirements of PHEV Batteries from the DOE.[61]

Characteristics at the End of Life		**High Power/Energy Ratio Battery**	**High Energy/Power Ratio Battery**
Reference Equivalent Electric Range	miles	**10**	**40**
Peak Pulse Discharge Power (2 sec/10 sec)	kW	**50/45**	**46/38**
Peak Regen Pulse Power (10 sec)	kW	**30**	**25**
Available Energy for CD (Charge Depleting) Mode, 10 kW Rate	kWh	**3.4**	**11.6**
Available Energy in Charge Sustaining (CS) Mode	kWh	**0.5**	**0.3**
CD Life	Cycles	**5,000**	**5,000**
CS HEV Cycle Life, 50 Wh Profile	Cycles	**300,000**	**300,000**
Calendar Life, 35°C	year	**15**	**15**
Maximum System Weight	kg	**60**	**120**
Maximum System Volume	Liter	**40**	**80**
System Recharge Rate at 30°C	kW	**1.4 (120V/15A)**	**1.4 (120V/15A)**
Unassisted Operating & Charging Temperature	°C	**-30 to +52**	**-30 to +52**
Maximum System Price @ 100k units/yr	$	**$1,700**	**$3,400**

The energy and power density for vehicle batteries should be in terms of the whole mass of the battery, including: electrodes, separators, cathode, anode, electrolyte, and housing. Since power from these batteries is determined by the series and parallel combination of individual cells, parallel banks increase the capacity and series banks increase the voltage. As discussed in chapter 1, we can either increase the voltage or increase the current to produce more power. Until an electrolyte is found that is stable over a larger electrode potential than we currently have, we must look to reducing the electrode mass as the primary method to increase the energy and power densities.

Let us look at the requirements set by the DOE report. In particular, let us focus on durability requirements. Three hundred thousand cycles is a very large number for battery life. A cell must be resilient and must be able to recover from high current discharges and charging. This represents a maximum loss of 2×10^{-4} % per cycle, essentially no capacity loss. Both the interface and the electrode must be stabilized in order to meet this demand. In order to ensure this is the case, the charge efficiency should be nearly 100%. During the first cycles an SEI layer is formed. This layer should not continue to grow thicker and thicker as the battery is used. This would represent the formation of dendrites or a reaction that is depleting the electrolyte. The charge capacity should nearly match the discharge capacity on a stable cell.

We tested the CNT and carbon black cells at a 2C charge rate and 1C discharge rate. As expected the fast charge rate polarized the cathode material significantly, leading to low capacity from all the cells. The CNT stabilized cell

reproduced the charge capacity with high fidelity and with the highest capacity. Furthermore, the capacity produced under these strenuous conditions is stable from cycle to cycle. Only at every 50th cycle, when the batteries are charged slowly and discharged slowly again, is there a change disruption in this pattern. The carbon black batteries repeat this trend as well, meaning that the effect is likely due to the particles or interface and not the electrode.

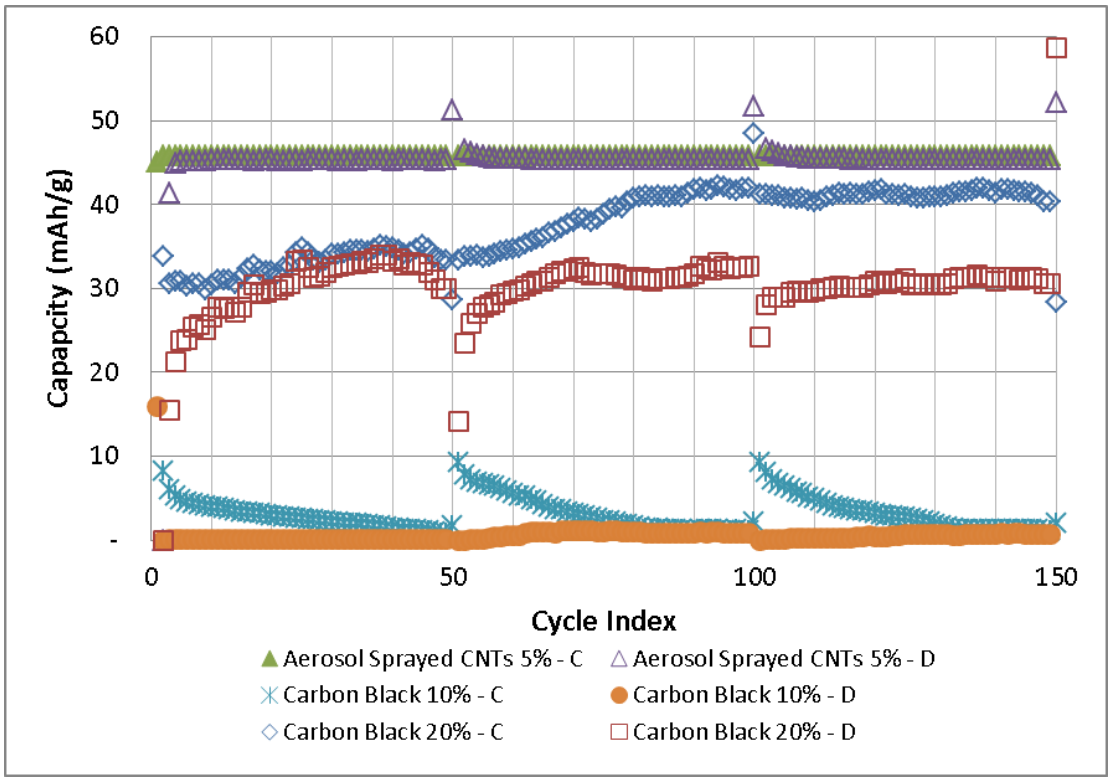

Figure 6.2. Battery Life Testing with 2C charge and 1C discharge on a cells with 5% CNTs or Carbon Black.

If we estimate the weight of the battery as no more than 40% of the anode and cathode then from Table 6.1 we can derive the expected capacity upon full discharge of the cell. The 10 kW rate on a 3.4 kWh energy cell is effectively a C/3 C-rate. With a mass of 60 kg for the entire battery, and using the potential of LFP vs. graphite the expected capacity is only 40 mAh/g. The cells we made have achieved a stable 35

mAh/g at a 2C charge rate. That is a half hour charge time, which is within reason for recharging an electric vehicle. We have achieved nearly this specific energy density with a current density three times the requirement. LFP with CNTs as the conductive additive alone meets the sustained power requirements for high power cells in hybrid electric vehicles. We have not established if it can meet the peak power requirements, which would be effectively a rate greater than 10C, or below the 3.6 s line in Figure 6.3. It seems clear that a capacitor system is better suited for peak power.

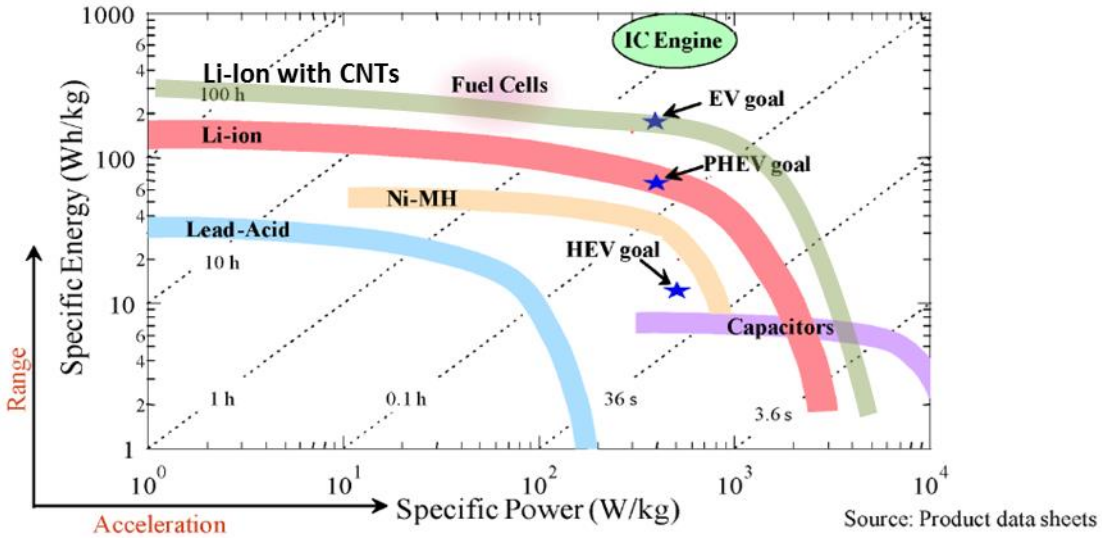

Figure 6.3. Energy and Power available with common battery technologies as of 2008 with the Energy density of this work added.[62]

6.2 CNT Enhanced Cathodes

In chapter 4, we examined in detail the optimization of CNT enhanced Li-Ion battery composites films, their processing, and formulation with PVdF as the binder and LFP as the active material. The conductive additives, dispersion steps, deposition methods, and drying conditions were all considered. Given that the LFP was purchased and made via solid state reaction with a wide distribution of particle sizes with 10% as large as 20 microns and a with a reported typical capacity of 150mAh/g at C/2, it is fair to say this material is considered fairly non-ideal. This material has no

advantage from surface coatings to bridge gaps in the conductive additive or small particle size to reduce the path length of the lithium or electron diffusion. The only way this material will perform well is by ensuring all of the battery material is connected to the electrode. Since the available capacity of LFP is highly dependent on the current density, reducing the local C-rate at each particle will increase the battery performance. We found that by optimizing the processing of the CNTs a 3-dimensional network that is both highly conductive and resilient can be formed that connects a large fraction of the total surface area. Ideally, each and every particle surface in the composite should be connected to the electrode.

The conductivity of multiwalled carbon nanotubes were evaluated as compressed powders and as additives in composites in chapter 3. Just as with single walled CNTs, multiwalled carbon nanotubes can have a range of properties based on their growth conditions. The physical differences may be in crystallinity, aspect ratio, or defect density, all of which can impact their conductivity. As previously stated and shown by others, the primary advantage of CNTs over acetylene black is the ability to make a highly conductive and resilient 3-D network with much less conductive additive. This means that the inactive material can be significantly reduced and replaced by only 5% CNTs and 5% PVdF instead of 20% CB and 10% PVdF. The energy density delivered at different C-rates with different contents of CNTs demonstrates that 5% CNTs is needed to reach the surface threshold.

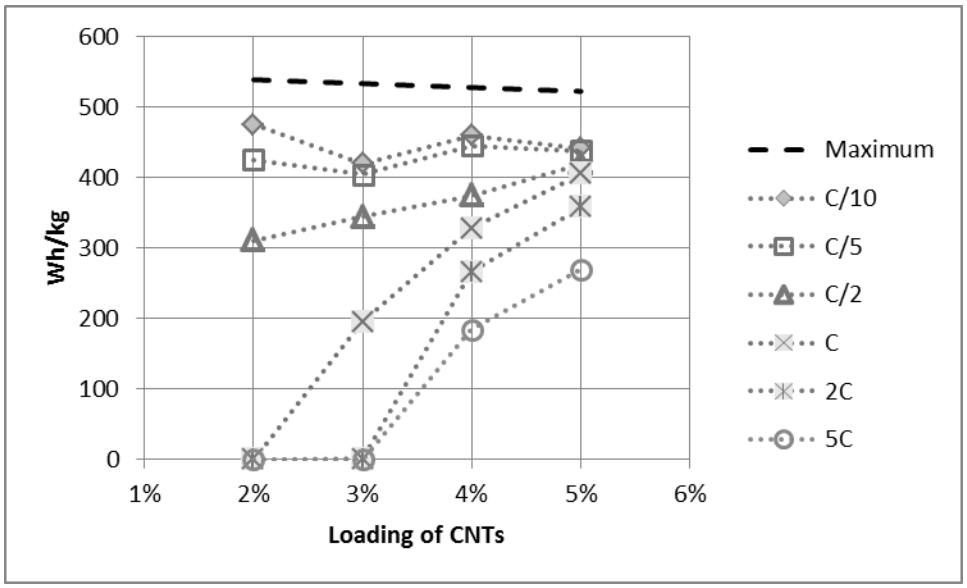

Figure 6.4. Energy density of MTI Corp. LFP made with aerosol spray method.

If proper attention is paid to the dispersion of the CNTs and an optimized deposition procedure is used, highly conductive and resilient networks can be formed with either the draw down method or the aerosol spray coating, Figure 6.5. The aerosol spray application may be most advantageous for studying new materials, as there is very little material loss as compared to the draw down method.

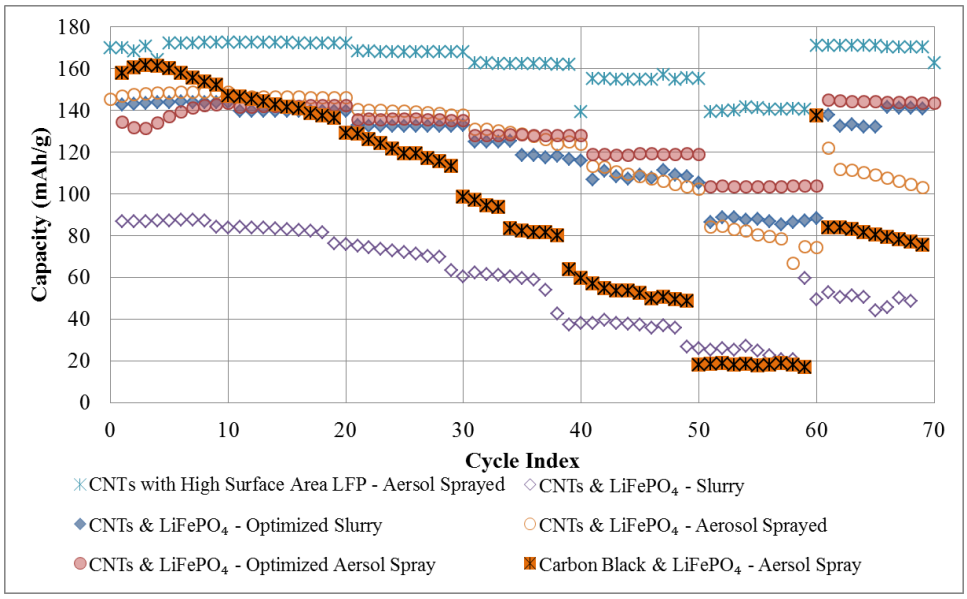

Figure 6.5. Charge and Discharge Capacity of $LiFePO_4$ cathodes with standard and optimized procedures and different deposition methods. Samples included 5% CNTs and 5% PVdF or 20% carbon black and 5% PVdF.

We also investigated high surface area cathode materials and found that, with a cathode material designed to deliver higher current densities, we were able to reproduce the high energy densities, and the high rate performance improved significantly over the commercial LFP. The rate limitation of LFP composites is primarily due to the diffusion of Lithium within the crystal. Particle size engineering to obtain small particle size or large crystals facets in the (010) direction could greatly increase the rate capability of these materials. Nevertheless, the stabilization of the electrode contact under high strain demonstrates the unique advantage of the CNTs incorporated as the conductive additive.

6.3 Competition

Lithium Iron Phosphate ($LiFePO_4$) is one among many battery cathodes that are commercially viable. It is helpful to review some of the benefits and problems of some of the most prominent competing systems to understand the full advantage of a particular system. These materials were first introduced in Table 1.2.

The Li-O_2 or Li-Air battery has a theoretical energy density that could rival that of the combustion engine. The Li-air battery is similar to a fuel cell in that gas or liquid is fed into the cell to drive the reaction. Unfortunately, Li-Air batteries have a problem with water and carbon dioxide passing through the separator and corroding the anode. There is also the problem of numerous side reactions that interrupt the Li-O_2 or Li-OH reactions on the cathode side. Needless to say, the full capacity of Li-Air has not been realized yet. If these problems can be worked out Li-Air could potentially replace the combustion engine as the predominate energy storage medium for personal transport.

Super capacitors are particularly advantageous for high power applications but suffer from poor energy density. The difference between batteries and capacitors is the relationship with the state of charge and the battery voltage. With capacitors, this is a linear relationship. This means the state of charge is straight forward to interpret merely based on the battery voltage. This advantage makes super capacitors much less expensive to implement in circuits since the capacity used does not have to be monitored to know the state of charge. These are usually materials with high surface areas to store large amounts of charge.

Another crystalline material is the NASICON structure. Although its capacity is less than $LiFePO_4$, it has a more open 3-D structure, which lends itself to higher diffusion rates. Unfortunately even with the high rate capability this material suffers from unrealized capacity, typically 140 mAh/g at C/10, clear capacity fade over time, and with the presence of two redox reactions during charge and discharge the potential for many other intermediate reactions is possible at high potentials. This of course is a problem all high voltage batteries have. Work with surface coatings, nano-directed growth, and conductive additives may reduce the severity of these problems.

For all of these systems the problem remains to deliver energy, power, and long life between two electrode contacts at an economically viable cost.

REFERENCES

1 R. Hiesgen, S. Sörgel, R. Costa, L. Carlé, I. Galm, N. Cañas, B. Pascucci, and K.A. Friedrich, *Beilstein J. Nanotechnol.*, **4**, 611 (2013).

2 W. Wei, J. Wang, L. Zhou, J. Yang, B. Schumann, Y. NuLi, *Electrochem. Commun.*,**13**, 399 (2011).

3 H. Wang, K. Huang, Y. Ren, X. Huang, S. Liu, and W. Wang, *J. Power Sources*, **196**, 9786 (2011).

4 M. Kerlau, M. Marcinek, V. Srinivasan, R.M. Kostecki, *Electrochimica Acta*, **52**, 5422 (2007).

---

5 Types of Battery Cells, (n.d.)., *Battery University*, Retrieved October 2013, from http://batteryuniversity.com/learn/article/types_of_battery_cells

6 S.V. Kalinin and N. Balke, *Advanced Energy Materials*, **22**, E193-E209 (2010).

7 Lide, D. R. Electrochemical Series, CRC handbook of chemistry and physics: a ready-reference book of chemical and physical data (75th ed.) 1994. Boca Raton, FL: CRC Press.

8 M.S. Islam, D. J. Driscoll, C.A. J. Fisher, and P.R. Slater, *Chem. Mater.* **17**, 5085–5092 (2005).

9 H. Gabrisch, R. Yazami, B. Fultz, *Electrochemical and Solid-State Letters*, **5–6**, A111-A114 (2002).

10 A. Miszczyk, K. Darowicki, *Anti-Corrosion Methods and Materials*, **58**, 13 – 21 (2011).

11 P. G. Bruce, S. A. Freunberger, L. J. Hardwick, and J.-M. Tarascon, *Nature* Materials, **11**, 19-29 (2012). DOI:10.1038/NMAT3191

12 Li-Xia Yuan,a Zhao-Hui Wang,a Wu-Xing Zhang,a Xian-Luo Hu,a Ji-Tao Chen,b Yun-Hui Huang*a and John B. Goodenough, *Energy Environ. Sci.*, 2011,4, 269-284, DOI: 10.1039/C0EE00029A

13 Lithium diffusion is limited by surface states [Keith Stevenson, U.T. Austin @ MRS meeting 2014]

14 K. Xu, A. von W. Cresce, *Materials Research Soc.*, **27**(18), 2327 (2011).

15 T.-Y. Hsieh, Y.-S. Duh, C.-S. Kao, *J Therm Anal Calorim*, **116**, 1491–1495 (2014). DOI 10.1007/s10973-014-3755-x

16 J. Wang and X. Sun, *Energy Environ. Sci.*, **5**, 5163 (2012).

17 U. Dettlaff-Weglikowska, J. Yoshida, N. Sato, and S. Roth, *J. Electrochem. Soc.*, **158**(2), A174 (2011).

18 M. Baibarac, M. Lira-Cantú, J. Oró-Solé, N. Casan-Pastor, and P. Gomez-Romero, *Small*, **2**(8), 1075 (2006).

19 M. J. Ganter, R. A. DiLeo, C. M. Schauerman, R. E. Rogers, R. P. Raffaelle, B. J. Landi, *Electrochimica Acta*, **56**, 7272 (2011).

20 X.-M. Liu, Z. D. Huang, S. W. Oh, B. Zhang, P.-C.Ma, M. M.F. Yuen, and J.-K. Kim, *Composites Science and Tech.*, **72**, 121 (2012).

21 M. Kerlau, M. Marcinek, V. Srinivasan, and R. M. Kostechi, *ElectrochimicaActa*, **52**, 5422 (2007).

22 J. Hilding, E.A. Grulke, Z.G. Zhang, and F. Lockwood, **24**(1), 1 (2003).

23 S. W. Kim, T. Kim, Y. S. Kim, H. S. Choi, H. J. Lim, S. J. Yang, and C. R. Park, *Carbon*, **50**(1), 3 (2012).

24 D. H. Sing, H. C. Shim, J.-W.Song, S. Kim, and C.-S.Han, *ScriptaMaterialia*, **60**, 607 (2009).

25 Y. Zhang, X.G. Zhang, H.L. Zhang, Z.G. Zhao, F. Li, C. Liu, H.M. Cheng, *ElectrochimicaActa*, **51**, 4994-5000 (2006).

26 R.H. Woodman, B.R. Klotz, R.J. Dowding, *Ceram. Int.*, **31**, 765-768 (2005).

27 J. Li, P. C. Ma, W. S. Chow, C. K. To, B. Z. Tang, and J.-K. Kim, *Adv. Funct. Mater.*, **17**, 3207 (2007).

28 Q.-C. Zhuang, X.-Y. Qiu, S.-D. Xu, Y.-H. Qiang and S.-G. Sun, *"*Diagnosis of Electrochemical Impedance Spectroscopy in Lithium-Ion Batteries*" Lithium Ion Batteries - New Developments*. Ed. Ilias Belharouak . InTech. 2012. DOI: 10.5772/26749.

29 M. Parka, X. Zhanga, M. Chunga, G. B. Lessa, A. Marie Sastrya, M. Park, *J. Power Sources*, **195**, 7904-7929 (2010). DOI:10.1016/j.jpowsour.2010.06.060

30 Y. Zhao, L.Peng, B. Liu, and G. Yu, *Nano Lett.*, **14**(5), 2849–2853, (2014). DOI:10.1021/nl5008568

31 M. D Levi and D. Aurbach, *J. Phys. Chem. B*, **108** (31), 11693–11703 (2004). DOI:10.1021/jp0486402

32 G. Paasch, K. Micka, and P. Gersdorf, *Electrochimica Acta*, **38**(18), 2653-2663 (1993).

33 M. Kerlau, M. Marcinek, V. Srinivasan, R. M. Kostecki, *Electrochimica Acta*, **52**, 5422–5429 (2007). DOI:10.1016/j.electacta.2007.02.085

34 L. Y. Beaulieu, V. K. Cumyn, K. W. Eberman, L. J. Gaberscek, J. Jamnik, *J. of Power Sources*, **184**, 593-597 (2008). DOI:10.1016/j.jpowsour.2008.02.046

35 L.-X. Yuan, Z.-H. Wang, W.-X. Zhang, *Energy & Environmental Science*, **4**(2), 269-284 (2011). DOI: 10.1039/c0ee00029a

36 *VLSI fabrication principles: silicon and gallium arsenide*, Ed. S. K. Ghandhi, 150-257 (1994).

37 M. Milovic, D. Jugovic, N. Cvjeticaninb, D. Uskokovic, A. S. Milo, Z. S. Popovicc, F. R. Vukajlovic, *Journal of Power Sources*, **241**, 70-79, (2013). DOI: 10.1016/j.jpowsour.2013.04.109

38 P. Tang and N. A. W. Holzwarth, *Physical Review B*, **68**, 165107 (2003). DOI: 10.1103/PhysRevB.68.165107

39 A. A. Griffith, *Philosophical Transactions of the Royal Society of London. Series A, Containing Papers of a Mathematical or Physical Character*, **221**, 163-198 (1921). http://www.jstor.org/stable/91192

40 K. Zhao, M. Pharr, J. J. Vlassak, and Z. Suoa, *Journal of Applied Physics*, **108**, 073517 (2010). DOI:10.1063/1.3492617

41 P. Bai, D. A. Cogswell, and M. Z. Bazant, *Nano Letters*, 11(11), 4890-4896 (2011). DOI: 10.1021/nl202764f

42 A. J. Bard, L. R. Faulkner, "Chapters 5 & 6" *Electrochemical Methods: Fundamentals* and *Applications*, *2nd ed.*, John Wiley & Sons, New York. (2001).

43 M. Takahashi, S. Tobishima, K. Takei, Y. Sakurai, *Solid State Ionics*, **148**, 283-289 (2002).

44 E. Barsoukov, J. Hy. Kim, J. Hu. Kim, C. O. Yoon, H. Lee, *Solid State Ionics*, **116**, 249–261 (1999).

45 Z. Chen, H. Zhu, W. Zhu, J. Zhang, Q. Li, *Trans. Nonferrous Met. Soc. China*, **20**, 614 (2010).

46 J. Li, P. C. Ma, W. S. Chow, C. K. To, B. Z. Tang, J.-K. Kim, *Adv. Funct. Mater.*, **17**, 3207 (2007).

47 G. Wang, H. Li, Q. Zhang, Z. Yu, M. Qu, *J. Solid State Electrochem.*, **15**, 759 (2011).

48 C.C. Chen, Y. C. Chou, *Physical Review Letters*, **54**(23), 2529 (1985).

49 H. Wang, K. Huang, Y. Ren, X. Huang, S. Liu, and W. Wang, *J. Power Sources*, **196**, 9786 (2011).

50 M. Gnanavel, Manu U. M. Patel, A. K. Sood, Aninda J. Bhattacharyya, *Journal of The Electrochemical Society*, **159**(4), A336-A341 (2012).

51 X.-M. Liu, Z. D. Huang, S. W. Oh, B. Zhang, P.-C. Ma, M. M.F. Yuen, and J.-K. Kim, *Composites Science and Tech.*, **72**, 121 (2012).

52 R.H. Woodman, B.R. Klotz, R.J. Dowding, *Ceram. Int.*, **31**, 765-768 (2005).

53 X. Li, F. Kang, X. Bai, and W. Shen, *Electrochem. Commun.*, **9**, 663 (2007).

54 J. A. Isaacs, A. Tanwani, M. L. Healy, and L. J. Dahlben, *J. Nanopart. Res.*, **12**, 551 (2010).

55 S. Hu, Y. Li, J. Yin, H. Wang, X. Yuan, Q. Li, *Chemical Engineering Journal*, **237**, 497 (2014).

56 J. K. Beddow, *Particulate Science and Technology*, Chemical Publishing Co. Inc. New York, N.Y. (1980).

57 N. Singh, C. Galande, A.Miranda, A. Mathkar, W. Gao, A. L. M. Reddy, A. Vlad, and P. M. Ajayan, *Scientific Reports*, **2**, 481 (2012).

58 R.H. Woodman, B.R. Klotz, R.J. Dowding, Ceram. Int., 31, 765-768 (2005).

59 PDF #00-040-1499, International Centre for Diffraction Data, (2005).

60 X. Yuan, *Lithium-ion batteries advanced materials and technologies*, (2012). Boca Raton, FL: CRC Press.

61 David Howell, Progress Report for Energy Storage Research and Development, U.S. Department of Energy Office of Vehicle Technologies (2008).

62 Venkat Srinivasan, *AIP Conf. Proc*. **1044**, 283 (2008). DOI:10.1063/1.2993726

Appendix A. Summary of Samples Made

Table 8.1. All Cells made with Commercial LFP.

Series #	$LiFePO_4$	SMW 200	PVdF	CNT : $LiFePO_4$ (%)	Sonication Solvent	Deposition method	Sonication	Deposition temperature (^0C)
5	94.67	4.73	0.6	5	NMP	Drawdown	Intermittent	Used heat gun
7	91.43	4.57	4	5	NMP	Drawdown	Intermittent	Used heat gun
8	93.33	4.67	2	5	NMP	Drawdown	Intermittent	Used heat gun
9	91.43	4.57	4	5	NMP	Drawdown	Continuous	Used heat gun
11	89.52	4.48	6	5	NMP	Drawdown	Intermittent	Used heat gun
12	86.95	4.35	8.7	5	NMP	Drawdown	Intermittent	Used heat gun
14	91.5	4.5	4	5	NMP	Spraying	Continuous	
22	90.5	4.5	5	5	Acetone ONLY	-	-	
23	90.5	4.5	5	5	NMP : Acetone (1:3)	Spraying	Continuous	
24	90.5	4.5	5	5		Spraying	Continuous	80C
26	90.5	4.5	5	5	PVP in DI water	Spraying	Continuous	-
27	90.5	4.5	5	5	NMP	Spraying with Acetone & NMP	Continuous	170-200
28	90.5	4.5	5	5	NMP:Acetone =50:50	Spraying	Continuous	160-180
29	90.5	4.5	5	5	NMP:Acetone =25:75	Spraying	Continuous	130
31	93.14	1.86	5	2	NMP	Spraying with Acetone & NMP	Continuous	~130
32	92.23	2.77	5	3	NMP	Spraying with Acetone & NMP	Continuous	~130
33	91.35	3.65	5	4	NMP	Spraying with Acetone & NMP	Continuous	~130
34	90.5	4.5	5	5	NMP	Spraying with Acetone & NMP	Continuous	140
35	90.5	4.5	5	5	NMP	Spraying with Acetone & NMP	Interupted	200
36	90.5	4.5	5	5	NMP	Spraying with Acetone 3x & NMP	Interupted	80-100
37	90.5	4.5	5	5	NMP	Spraying with Acetone & NMP	Continuous	80-90
39	90.5	4.5	5	5	NMP	Spraying	Continuous	70-80
40	90.5	4.5	5	5	NMP	Spraying	Continuous	130
41	90.5	4.5	5	5	NMP	Spraying	Continuous	160-180
50	90.5	CB 5%	5	-	NMP	Spraying with Acetone & NMP	Continuous	120
51	75	CB 20%	5	-	NMP	Spraying with Acetone & NMP	Continuous	120
52	85	CB 10%	5	-	NMP	Spraying with Acetone & NMP	Continuous	120
67	90.5	4.5	5	5	Ball Milled	Spraying with Acetone & NMP	Continuous	120

Table 8.2. All Series made with High Surface Area LFP.

Series #	$LiFePO_4$	SMW 200	PVdF	CNT : $LiFePO_4$ (%)	Sonication Solvent	Deposition method	Sonication	Deposition temperature (^0C)
15	90.5	4.5	5	5	LFP-BASF	NMP	Spraying	Continuous, D=1/2', 20 min, 25%
16	90.5	4.5	5	5	NCM - BASF	NMP	Spraying	Continuous, D=1/2', 20 min, 25%
17	75	CB 20%	5		LFP-BASF	NMP	Spraying	Continuous, D=1/2', 20 min, 25%
18	75	CB 20%	5		NCM - BASF	NMP	Spraying	Continuous, D=1/2', 20 min, 25%
19	90.5	4.5	5	5	LFP-BASF	THF	Spraying	Continuous, D=1/2', 20 min, 25%
20	90.5	4.5	5	5	NCM - BASF	THF	Spraying	Continuous, D=1/2', 20 min, 25%
21	90.5	4.5	5	5	LFP-BASF	Acetone, NMP	-	Continuous, D=1/2', 20 min, 25%

Table 8.3. All $LiFePO_4$ Series Synthesized with a 18 hour reaction time and NMP bubbler air lock.

Series #	Precursors	CNTs & Carbon Coating	Solvent, vol	Dispersion	Reaction Temp
60	Fe-Acetate, H_2-PO_4, Li-acetate	2%	Ethlene Glycol, 500mL	No bubbler	HP 230C -> 170C
61	Fe-Acetate, H_2-PO_4, Li-acetate	2%	Ethlene Glycol, 500mL	No bubbler	HP 230C -> 170C
62	Fe-Acetate, H_2-PO_4, Li-acetate	4%, PVP 4%	EG and Water	CNTs w/ PVP in water & No bubbler	HP 230C -> 170C
63	Fe-Acetate, H_2-PO_4, Li-acetate	2%, Gumm Arabic 6%	EG and Water	CNTs w/ GA in water & No bubbler	HP 230C -> 170C
61.b	Fe-Acetate, H_2-PO_4, Li-acetate	2%	Ethlene Glycol, 500mL	CNTs in EG	Set Temp: 160C
61.d	Fe-Acetate, H_2-PO_4, Li-acetate	2%	Ethlene Glycol, 500mL	CNTs in EG	Set Temp: 180C
61.f	Fe-Acetate, H_2-PO_4, Li-acetate	2%	Ethlene Glycol, 500mL	CNTs in EG	Set Temp: 190C
64.a	Fe-Acetate, H_2-PO_4, Li-acetate	2%	EG and NMP	CNTs in NMP	Set Temp: 190C
64.b	Fe-Acetate, H_2-PO_4, Li-acetate	2%, PVP 4%	EG and NMP	CNTs w/ PVP in NMP	Set Temp: 190C
65	Fe-Acetate, H_2-PO_4, Li-acetate	2%	EG	CNTs in EG	Vacuum Run: 146C
66	Fe-Acetate, H_2-PO_4, Li-acetate	2%	TTEG, 500mL	CNTs in TTEG	
68	$FePO_4$, Li-acetate	2%	EG	CNTs in EG	

Appendix B. Battery Failure

9.1 Introduction

Our goal here is to introduce battery failure mechanisms and their characterizes. This is a practical guide and not meant to be a review of the physical mechanisms. I hope that this will give the reader some idea as to what kinds of problems one might encounter when making battery cells.

9.2 Packaging

Ironically, the battery packaging is the most essential part of the battery. Battery packages can fail by either unsealing or by shorting. If a battery is not sealed, the electrolyte will escape and more often than not, the water content will increase within the cell. A battery short can be a simple stacking fault, a dendrite, or a hole in the separator. Any path that allows electrons to complete the circuit within the battery behaves as a short. These problems should have the following characteristics:

1. Unsealed
    - Battery exterior corrodes in air.
    - Overcapacity observed when discharging, due to water in cell
    - Corrosion on the electrode surfaces will confirm a leaky package
2. Short
    - Low potential on cell after packaging (less than 2 Volts)
    - Battery does not maintain a potential after charging
    - Battery can be charged beyond their nominal capacity
    - An ultra-low potential and a low reactance confirm a short

9.3 Electrolyte

Whenever you are working with Lithium water is a problem. With water alone it reacts and forms Lithium hydroxide quite readily. In electrolytes, HF is the prime product, which can then reduce the electrolyte further and produce more water thus propagating the reaction. This reaction is kinetically limited thus, heightened temperatures can exacerbate the problem. Thus using battery at high current rates can produce power at the cost of the battery surfaces. This is one of the mechanisms that will foul Li-Ion interfaces if water is in the cell. A dry box, as in Figure 9.1, with an active drying system is essential to avoid the most basic contamination problems.

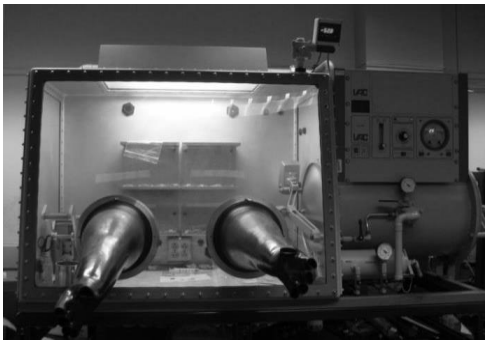

Figure 9.1. Dry box for working with water sensitive materials and battery assembly.

9.4 Separators

Transport is the name of the game for separators. Any separator that does not allow conduction of the electrolyte is doing too good of a job. The PVdF material these separators are usually made of does not conduct electricity well and are not (generally) good ionic conductors either. In liquid cells, the electrolyte travels through pores in the film. Aging and heat can reduce the pore volume, which can be severe enough to cut off electrolyte flow. A battery with a bad separator (that is not a

short) will behave as a capacitor with a very small capacitance, charging and discharging reliable but with extremely small capacitance.